

MASTER

Identifying the support conditions of a monopile in a 2D setup with varying soil stiffness conditions

Towards a Structural Health Monitoring framework for offshore monopile structures

Jaeger, Yonne C.C.

Award date:
2023

[Link to publication](#)

Disclaimer

This document contains a student thesis (bachelor's or master's), as authored by a student at Eindhoven University of Technology. Student theses are made available in the TU/e repository upon obtaining the required degree. The grade received is not published on the document as presented in the repository. The required complexity or quality of research of student theses may vary by program, and the required minimum study period may vary in duration.

General rights

Copyright and moral rights for the publications made accessible in the public portal are retained by the authors and/or other copyright owners and it is a condition of accessing publications that users recognise and abide by the legal requirements associated with these rights.

- Users may download and print one copy of any publication from the public portal for the purpose of private study or research.
- You may not further distribute the material or use it for any profit-making activity or commercial gain



Department the Built Environment
Structural Engineering and Design

Identifying the support conditions of a monopile in a 2D setup with varying soil stiffness conditions

*Towards a Structural Health Monitoring
framework for offshore monopile structures*

Supervisors:

Prof. Ir. B. Snijder
Dr. Ir. D. Leonetti
Ir. M. Orlando

Y.C.C. Jaeger
1578308

Eindhoven, March 2023

General information

University: Eindhoven University of Technology
Department: Built Environment
Master Program: Architecture, Building and Planning
Master Track: Structural Engineering and Design

Course information

Course Name: Graduation Project Structural Engineering and Design (SED)
Course Code: 7K45M0
Study Load: 45ECTS
Master Track: Structural Engineering and Design

Author

Name: Y.C.C. (Yonne) Jaeger
Student Number: 1578308
Student Email: y.c.c.jaeger@student.tue.nl
Deadline thesis: 02-03-2023

Graduation committee

Committee member 1: Prof. ir. H.H. (Bert) Snijder
Professor Steel Structures
Eindhoven University of Technology
Committee member 2: Dr. ir. D. (Davide) Leonetti
Assistant professor Steel and Aluminum Structures
Committee member 3: ir. M. (Michele) Orlando
Lead Engineer Strength and Fatigue
HVR-Engineering

Final Colloquium

March 2, 2023

This thesis has been carried out in accordance with the rules of the TU/e Code of Scientific Integrity.

Public information

Abstract

In this research project the relation between a change in soil stiffness and the dynamic response in steady state of offshore monopile foundations is investigated, in order to contribute to the structural health monitoring framework of offshore wind turbines. To that extent, an experimental setup, representative of planar geometry and loading conditions, is designed where the soil-structure interaction is represented by a flexible support made by spring and aluminum block supports. To investigate the possibility of characterizing the support stiffness in terms of springs stiffness and amount of aluminum block supports, based on output-only measurements such as accelerations and strains, a numerical model is built. It is shown by means of experimental modal analysis, based on "Peak-Picking" method, after the application of an impact test on the experimental setup that as the stiffness of the support decreases, also the natural frequencies of the setup decrease. The same holds when applying a modal analysis to the numerical model.

Also a harmonic analysis is performed using both the experimental data and the numerical data to compare the numerical and experimental fatigue life of the structure. However, further research is required in order to create correlate a change in soil/support stiffness with a change in fatigue performances of a real structure.

Based on the results of the experimental and numerical modal analysis, an algorithm is suggested to infer data of the experimental boundary conditions of the soil/structure support from the numerical model. This algorithm solves an optimization problem, where the cost function yields the norm of the difference between the experimental and numerical natural frequencies for each of the investigated natural modes. The algorithm aims to minimize this norm over the stiffness parameters of the support required in the numerical model such as the amount of aluminum block supports, the distance between the blocks, the stiffness of the springs and the length of the support structure. The validation of the algorithm solving the optimization problem results in the methodology for characterizing the support conditions of the experimental setup. This methodology contributes to the development of the Structural Health Monitoring framework for fatigue assessment for a monopile of an offshore wind turbine.

Preface

This document forms the the graduation thesis "*Identifying the support conditions of a monopile in a 2D setup with varying soil stiffness conditions*". The thesis has been written to complete the graduation project of the master program "*Architecture, Building and Planning*", at the TU Eindhoven. This graduation project is a co-orporation between TU Eindhoven and HVR Engineering. The graduation project has been supervised by Prof. Ir. H.H. Snijder, Dr. D. Leonetti and M. Orlando. The research started in April 2022 and is finalized in March 2023.

Due to the interest in gaining a better understanding on fatigue analysis for structures subjected to dynamic loading, I have selected this research project for finalizing the master program. The process of conducting this research has been a challenging experience, yet also very educational.

I would like to thank the supervising committee for the guidance throughout the graduation project. Next to the supervising committee, I would also like to thank John, Jeroen and Jan from HVR Engineering, for always make time to answer my questions and helping me with the experimental setup. I would also like to thank Hans and Theo from the Structures Laboratory Eindhoven of the TU Eindhoven, for providing the elements for the experimental setup. Also a special thanks to ATV Springs for sponsoring the springs used in the experimental setup. Last but not least, I would like to thank my grandfather for being a great inspiration as the only other engineer in the family.

Yonne Jaeger

Eindhoven 2023

Table of Content

Table of Content	vii
List of Figures	xi
List of Tables	xv
Nomenclature	xvii
1 Introduction	1
1.1 Motivation	1
1.2 Problem statement	3
1.3 Research objective	4
1.4 Methodology	4
1.5 Report outline	6
2 Literature review	7
2.1 Fatigue	7
2.1.1 S-N curve	8
2.1.2 Fatigue of offshore steel structures	8
2.2 Monopiles	10
2.2.1 Structural properties	10
2.2.2 Dynamic loading on OWTs	10
2.2.3 Influence of alternating soil stiffness	11
2.3 Modal analysis	12
2.3.1 Analytical modal analysis	12
2.3.2 Numerical modal analysis	14
2.3.3 Experimental and Operational Modal Analysis	16
2.4 Experimental testing	18
2.4.1 Impact test	18
2.4.2 Forced vibration test	19
2.4.3 Measurement system settings	19
2.5 Structural Health Monitoring	20
3 Experimental Setup	21
3.1 Design of Setup	21

3.1.1	Elements of experimental setup	22
3.1.2	Justification of setup	24
3.2	Sensors	25
3.2.1	Accelerometers	26
3.2.2	Strain gauges	27
3.3	Performed tests	27
3.3.1	Impact test	28
3.3.2	Forced vibration test	30
3.4	Visual representation of setup	32
4	Numerical Model	33
4.1	Pre-processor	33
4.1.1	Keypoints and lines	33
4.1.2	Elements and material properties	34
4.1.3	Parameters	35
4.2	Solution	36
4.2.1	Boundary conditions	36
4.2.2	Modal analysis	37
4.2.3	Harmonic analysis	38
4.3	Post-processor	38
5	Results	41
5.1	Modal analysis	41
5.1.1	Experimental setup	41
5.1.2	Numerical model	43
5.1.3	Discussion	46
5.2	Harmonic analysis	47
5.2.1	Discussion	51
6	Characterization of support structure	53
6.1	Cost function	53
6.2	ANSYS and Matlab scripting	54
6.3	Validation	56
7	Conclusions and future research	59
7.1	Conclusions	59
7.2	Future Research	60
	Bibliography	61
	Appendix	65
	A Flowchart	65
	B Drawings of Experimental test setup	68
	C Numerical Justification of Experimental Setup	70
C.1	Boundary conditions	70
C.2	Springs	71
C.3	Results of modal analysis	72
C.4	Preliminary numerical analysis script	73
	D Hand calculations	75
D.1	Stability of experimental setup	76
D.2	Harmonic load	77

TABLE OF CONTENT

D.3	Loads on support	78
D.4	Analytical Modal Analysis	78
E	Spring specifications	79
F	FE-model script	81
F.1	Numerical model script	81
F.2	Script for parameters	84
F.3	Modal analysis script	84
F.4	Harmonic analysis script	84
G	Post processing of output signals	86
G.1	Three aluminum supports attached to the beam	86
G.2	Two aluminum supports attached to the beam	88
G.3	One aluminum support attached to the beam	90
H	Harmonic analysis data	92
H.1	Experimental setup	92
H.2	Numerical model	94
I	MatLab script	100
I.1	Optimization-script-ANSYS.m	101
I.2	ParameterAnsys.m	102
I.3	Ansys.m	102
I.4	LAUNCH.BAT	103
I.5	Export.mac	103

List of Figures

1.1	(a) Dynamic loading on an OWT and (b) a vibrating oscillator when the forcing frequencies (f_f) come close to the natural frequencies (f_n) of the structure [1] . . .	3
1.2	An offshore monopile (a) modeled as a lumped parameter model with springs (b) .	4
1.3	Three different stiffness cases for analysis: (a) Case 1 has three blocks attached to the beam, (b) Case 2 has two blocks attached to the beam, and (c) Case 3 has one block attached to the beam	5
2.1	Schematic representation of different phases of fatigue life [2]	8
2.2	S-N curve from Eurocode 3 [3]	9
2.3	Visual explanation of fatigue failure modes at stress concentrators[4]	9
2.4	Forcing frequencies regarding PSD [5]	11
2.5	p-y curve of for sand [6]	12
2.6	(a) Cantilever beam, fixed on one end and free on the other end [7], (b) Cantilever beam subjected by a point load P [7]	12
2.7	First three mode shapes of a cantilever beam [8]	14
2.8	(a) Strain gauge applied to a steel surface, (b) Circuit of a strain gauge known as the Wheatstone Bridge [9]	17
2.9	Applicable filters to reduce the contribution of noise to the output signal [10] . . .	18
2.10	Representation of sampling frequency in a signal [11]	20
3.1	(a) Top-view of experimental setup and (b) Sections of experimental setup	23
3.2	(a) Cross section of steel beam (b) Sections of aluminum support attached to strengthened IPE300 profile	23
3.3	(a) Schenk 100kN electromechanical compression test and (b) result of the compression test for springs used in the experimental setup	24
3.4	(a) Load-scheme of load-case self-weight and (b) load-scheme of load-case dynamic	25
3.5	Experimental setup including sensors and eccentric motor	26
3.6	(a) Accelerometer 1 and (b) Strain gauge 4	27
3.7	The first three mode shapes of a cantilever beam and the locations of accelerometers on the line $y = 0$	27
3.8	The three different stiffness cases schematically presented	28
3.9	(a) Wired accelerometers to the hardware system and (b) Wired strain gauges to the hardware system	28

3.10	Schematic overview of post processing of measurement from impact test. The first step is to reduce the offset of the output signal. The second step is to apply a time window and a low-pass filter frequency. The third step is to apply an FFT with a Hamming window	29
3.11	The eccentric motor with dimensions used for vibration testing [12]	31
3.12	A visual representation of the experimental setup where (a) is a front view (b) is the support structure (c) is the aluminum support and (d) is a side view of the experimental test setup	32
4.1	Generating keypoints in APDL macro code	34
4.2	Cross section of BEAM188 element with local coordinate system	35
4.3	(a) Aluminum blocks supporting the steel strip in the experimental test setup; (b) Schematic representation of the aluminum blocks and steel rods; (c) Schematic representation of the calculation for the spring stiffness of the COMBIN14 element; (d) COMBIN14 element in the numerical model	36
4.4	parameter.inp file APDL macro code	36
4.5	Boundary conditions visualised in the experimental setup	37
4.6	Commands for the application of boundary conditions	37
4.7	Commands for the application of modal analysis	38
4.8	Commands for the application of harmonic analysis	38
4.9	Harmonic analysis for strains in (a) numerical model and (b) at location of strain gauge 3 and strain gauge 4 of experimental setup	39
4.10	Commands for post-processing of the harmonic analysis	39
5.1	Modal analysis Case 1	42
5.2	Modal analysis Case 2	42
5.3	Modal analysis Case 3	42
5.4	Mode shapes for Case 1 of state of the support structure [m/m]	43
5.5	Mode shapes for Case 2 of state of the support structure [m/m]	44
5.6	Mode shapes for Case 3 of state of the support structure [m/m]	45
5.7	Harmonic analysis on experimental setup and numerical model for Case 1	48
5.8	Harmonic analysis on experimental setup and numerical model for Case 2	49
5.9	Harmonic analysis on experimental setup and numerical model for Case 3	50
6.1	Flowchart of the optimization problem	56
7.1	An example of an output signal of accelerations in the frequency domain during forced vibration testing on the experimental setup	60
C.1	Location of rigid boundary conditions shown by the means of the experimental test setup section	71
C.2	(a) Deflection of the beam in the third mode when a spring constant of $0N/m$ is applied and (b) the deflection of the beam in the third mode when a spring constant of $1000000N/m$	71
E.1	Spring specifications from ATV-Springs [13]	80
G.1	Output signal of accelerometers during impact test with three aluminum blocks attached to the steel beam	86
G.2	Signal correction for output signal of impact test for three aluminum supports attached to steel beam	87
G.3	Application of a time window on output signal for impact test for three aluminum supports attached to steel beam	87
G.4	Output signal in frequency domain for three aluminum supports attached to steel beam	87

LIST OF FIGURES

G.5	Output signal of accelerometers during impact test with two aluminum blocks attached to the steel beam	88
G.6	Signal correction for output signal of impact test for two aluminum supports attached to steel beam	88
G.7	Application of a time window on output signal for impact test for two aluminum supports attached to steel beam	89
G.8	Output signal in frequency domain for two aluminum supports attached to steel beam	89
G.9	Output signal of accelerometers during impact test with one aluminum blocks attached to the steel beam	90
G.10	Signal correction for output signal of impact test for one aluminum supports attached to steel beam	90
G.11	Application of a time window on output signal for impact test for one aluminum supports attached to steel beam	91
G.12	Output signal in frequency domain for one aluminum supports attached to steel beam	91

List of Tables

1.1	Used Computer Software	6
2.1	Peak frequencies of internal and external loading on an OWT considering a 3 bladed 3MW turbine	10
2.2	Loading at mud-line of monopile foundation supporting a 5-MW OWT [14]	11
2.3	The first three values for $K_n L$ [7]	13
3.1	Specifications experimental test setup	22
3.2	Results of hand calculations for steel beam due to self-weight	25
3.3	Results of hand calculations for the support of the experimental setup due to dynamical loading	25
3.4	Results of hand calculations for determining loads inside the support of the experimental setup	25
3.5	Specifications of used sensors	26
3.6	System settings for impact test	29
3.7	Post processing settings for impact test	30
3.8	System settings for forced vibration test	30
5.1	First three natural frequencies of experimental model for different states of support structure	42
5.2	First three natural frequencies of numerical model for different states of support structure	43
5.3	Comparison of modal analysis for Case 1	46
5.4	Comparison of modal analysis for Case 2	47
5.5	Comparison of modal analysis for Case 3	47
5.6	Comparison of harmonic analysis of strain gauge 3 for Case 1 in terms of strain (ϵ)	51
6.1	Parameters for the support structure of the input and output of the optimization script	57
D.1	Comparison between first three natural frequencies based on analytical and numerical calculations	78
H.1	Output measurement of stresses for forced vibration testing for case 1	92
H.2	Output measurement of stresses for forced vibration testing for case 2	93

H.3	Output measurement of stresses for forced vibration testing for case 3	93
H.4	Harmonic analysis for numerical model for case 1	94
H.5	Harmonic analysis for numerical model for case 2	96
H.6	Harmonic analysis for numerical model for case 3	98

Nomenclature

Abbreviations

APDL ANSYS Parametric Design Language

CMA Classical modal analysis

DOF Degrees of freedom

FE Finite element

FEA Finite element analysis

LPM Lumped parameter model

OMA Operational modal analysis

OWT Offshore wind turbine

SHM Structural health monitoring

FFT Fast Fourier Transform

n.f.f.t. Number of Fast Fourier data points

PSD Power Spectral Density

Terms and definitions

Fatigue limit The stress amplitude resulting from the applied cyclic loading below which a fatigue failure does not occur

BEAM188 A two node element which is suitable for analyzing slender and thick beam structures

COMBIN14 nonlinear spring element

Symbols

ϵ Strain

$\omega_{dynamic}$ Displacement due to dynamic loading (mm)

$\omega_{self-weight}$ Displacement due to self-weight (mm)

$\sigma_{allowable}$ Allowable stress considering S235 steel (N/mm^2)

$\sigma_{max,dynamic}$ Maximum stress in section due to dynamic loading (N/mm^2)

σ_{max} Maximum stress in section due to self-weight (N/mm^2)

f_f Forcing frequency (Hz)

f_n Natural frequency (Hz)

$F_{max,dynamic}$ Maximum allowable dynamic load (N)

F_{spring} Maximum amount of force on a spring (N)

F_{tot} Total amount of force on the support due to self-weight and dynamic loading (N)

I Moment of inertia (mm^4)

$M_{support}$ Reaction moment in support (Nm)

M_{tot} Total amount of moment in the support due to self-weight and dynamic loading (Nm)

$q_{self-weight}$ Evenly distributed load (N/m)

$R_{support}$ Reaction force in support (N)

S_f Fatigue limit

Due to the growing shift from fossil fuels to renewable energy resources, the offshore wind market is developing rapidly and the offshore wind turbines (OWTs) are expanding in number and size. Offshore wind power stations as a renewable energy source are composed to play a significant role in providing energy for the future global gross energy consumption [15]. A part of the rapidly developing offshore wind market is the expanding of OWTs in size. To ensure safe and sustainable development of the OWTs, wind turbine and foundation designers must provide light and reliable structural and mechanical components of OWTs. In order to provide light and reliable structural and mechanical components, understanding of the OWTs dynamics on a fundamental level is required.

Reliable real-time estimations of the current condition of these components, in terms of loading and damages are necessary to ensure safe and sustainable developments in the offshore wind turbine market. The aim of this thesis is to assess the dynamic response of OWTs, in relation to the change in soil conditions due to the cyclic loading acting at interface between the OWT foundation and the soil. The influence of soil relaxation on the dynamic response of the foundation of an OWT is currently not well defined and therefore requires thorough investigation.

1.1 Motivation

A potential development that would result in economical and ecological benefits, is the extension of the service life of an OWT. Foundations of an OWT contribute for 30% to the total cost of the OWT [16]. Furthermore, the design life of an OWT is bounded by the design life of the foundation. Approximately 75% of the currently installed OWTs have a monopile foundation [6], due to the huge benefits in terms of costs and installations compared to more complex layouts such as tripods or jackets. Monopile foundations are long and slender structures, and are therefore very flexible compared to other structures. The monopiles are exposed to cyclic loading due to wind and waves. The frequency of the cyclic loading can be close to the resonance frequencies of the monopile structure, which makes the structure sensitive to resonance effects and thus deflection amplifications [17]. Due to the sensitivity of the monopiles with respect to these resonance effects and cyclic loading, the monopile is expected to suffer from fatigue. Nowadays an OWT is designed to have an operation life of 20 to 25 years. This relatively short service life is a consequence of the

unknown factors in the fatigue life prediction, such as "pseudo-random" loading conditions, of an offshore monopile structure [18].

Around 90% of the steel structures fail due to fatigue [2]. Therefore, to be able to extend the service life of an offshore monopile it is important to make an accurate fatigue life prediction. By increasing the reliability and accuracy of the estimations of *e.g.*, loading, stress, strains and damage conditions, the fatigue life predictions can be improved, which potentially results in an extension of the service life of an offshore monopile structure. Besides a potential life time extension of OWTs, a thorough understanding of the conditions, in terms of loading, stresses, strains and damage, is necessary for the development of correct management of the offshore wind power stations. A reliable fatigue life prediction is important in order to establish a correct maintenance program of a structure. By improving the decision making process, the monopile foundation is more likely to continue a safe service life.

Due to displacements of the monopile caused by the dynamic loading, there is an interaction between the soil and the foundation. Specifically, vibrations of the monopile structure will alter the stiffness of the soil around it. The changes in soil conditions around the structure will result in small changes in the soil support stiffness. Which may lead to negative effects on the fatigue life of the monopile structure. The changes in soil stiffness and the influence on the monopile's dynamic response characteristics are difficult to measure or estimate, due to the effects of many different parameters, *e.g.* the soil type, the depth and size of the foundation, the loading magnitude, etc. For this reason it is difficult to make an accurate prediction of the fatigue life of a monopile that is exposed to cyclic loading since, during its service life, the natural frequencies of the structure can become closer to the excitation frequencies of the structure [17].

The long term performance of the foundation of an OWT is one of the main uncertainties during the design process. This is mainly caused by the effects of dynamic loading during service life on the foundation [1]. For this reason it is important to build a good structural health management system. A promising method for structural health management, and therefore for the avoidance of catastrophic failure, is structural health monitoring (SHM). A SHM system can be used to monitor the structural health state and update the state of the system of a foundation based on only output measurements. A SHM system for offshore monopile structures implies a vibration monitoring system which permanently monitors vibrations, for example in terms of accelerations and strains. In other words, the effect of loading and unloading is measured [19]. This health monitoring system is used to determine the current health state of a structure, in terms of loading and stresses. For this reason SHM is a good method for health management and maintenance management of OWT structures. A good SHM system can result in safe and sustainable development of OWTs.

However, as previously mentioned, there are many uncertainties regarding the long term dynamic response of such a structure. One of the uncertainties regarding the dynamic response, is the influence of a change in soil stiffness around the structure on the dynamic characteristics of the structure. Figure 1.1 shows the dynamic effect of 1P, 3P, wind and wave load on an offshore monopile foundation when the forcing frequencies (f_f) become close to the structures natural frequencies (f_n). The 1P load represents the load caused by the vibrations of the rotating rotor on top the wind turbine, and 3P presents the aerodynamic loading caused by the passing of the wind turbine blades by the monopile structure. An offshore monopile structure is founded in many layers of soil and therefore supported by these layers. As shown in Figure 1.1, the vibrating oscillator causes movement in the soil layers around the structure [1]. Due to movement in the soil, the stiffness of the support of the foundation changes. In order to develop a SHM system it is of crucial importance to be able to model the potential effects of the change in stiffness of the support on the structure's dynamic characteristics.

1.2 Problem statement

This research aims to investigate the influence of soil stiffness on the dynamic response of offshore monopile structures by proposing a modeling framework in a 2D setup. As previously mentioned, approximately 75% of the currently installed OWTs are monopiles. Due to this high percentage this thesis only focuses on offshore monopile foundations. In this section the modeling approach of the soil-structure interaction of an offshore monopile foundation is further elaborated on.

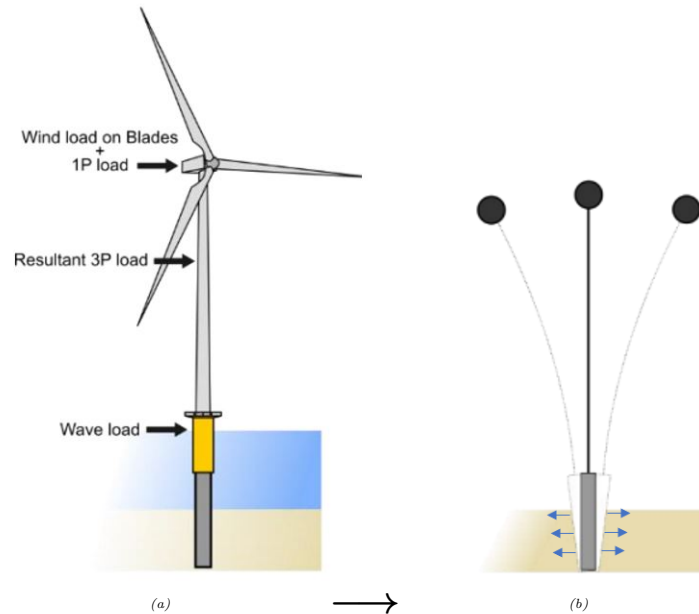


Figure 1.1: (a) Dynamic loading on an OWT and (b) a vibrating oscillator when the forcing frequencies (f_f) come close to the natural frequencies (f_n) of the structure [1]

The stiffness of the soil varies non-linearly yet continuously over the depth of the installed monopile foundation. Consequently, the soil can be regarded as infinite number of springs attached to infinitesimally small sections of the monopile foundation lying under the mud-line. Each of these springs has a (possibly) different spring stiffness. To approximate the behavior of the soil-structure interaction discretely, the length of the monopile foundation is divided into a finite number of segments and to each segment one spring is attached. By doing so, the soil structure interaction is thus approximated as a finite number of springs supporting the structure non-linearly against cyclic loading [20]. Figure 1.2 shows the discretization of the soil-structure interaction in a lumped parameter model (LPM).

When the monopile is initially placed into the soil it is assumed that the soil acts as simple supports in the lateral direction and one simple support in the longitudinal direction. This case corresponds to all springs having an infinite stiffness in the model. However, it is also assumed that due to the dynamic loading on the monopile, the support stiffness decreases over time, which causes the soil not to act as a simple support in the lateral direction, and rather as a spring. This phenomenon of a decrease in support stiffness corresponds to a decrease in the support stiffness in the model. However the stiffness of the support around an offshore monopile can not be measured directly, therefore it needs to be inferred from measurement data, such as monopile accelerations and strains.

Accelerations and strains on an offshore monopile can be measured by the means of accelerometers and strain gauges over time. The output of these measurements allows for the identification of dynamic characteristics, such as natural frequencies, of the structure. The goal of this project is to develop a method to infer the stiffness of the supporting soil from only the output measurements

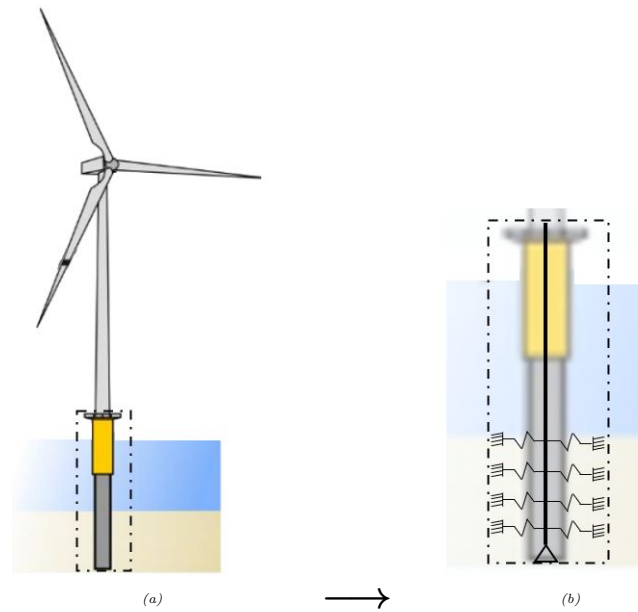


Figure 1.2: An offshore monopile (a) modeled as a lumped parameter model with springs (b)

of accelerometers and strain gauges during a steady-state response in the presence of a single harmonic load.

1.3 Research objective

The aim of this project is to contribute to the development of a structural health monitoring framework for fatigue assessment of a monopile of an OWT. The goal of this research is to characterize the stiffness of the support structure, based on only output measurements on the acceleration and the strain, during the steady-state response in the presence of a single harmonic load.

1.4 Methodology

This research focuses on the identification of the soil stiffness influence on the dynamic response of monopile structures. The research is split into two parts. The first part contains an experimental analysis on a slender steel structure with varying stiffness of the support structure, representing the soil, and the second part consist of a numerical approach to the experimental setup. The numerical approach consist of the development of a numerical model which aims to mimic the dynamic characteristics of the experimental setup. In order to reach the above described goal, the two parts of the research are conducted in an iterative way. A flowchart of the different aspects of the thesis is shown in Appendix A.

The experimental setup represents a 2D small-scale simplified offshore monopile. The monopile structure is modeled as a slender solid beam, with strain gauges and accelerometers attached. The experimental setup incorporates the modeling approach of the soil-structure interaction as described in Section 1.2. The soil support around the monopile foundation is modeled in the experimental test setup by the means of aluminum block supports and steel springs. The aluminum blocks aim to have an infinite stiffness which results in a rigidly supported monopile for the lateral direction. In order to model soil relaxation, i.e. a decrease in stiffness of the support structure, three different stiffness cases of the support structure are analyzed. The three different cases are

schematically shown in Figure 1.3. This figure shows that the aluminum block supports, with infinite stiffness in the lateral direction, can be released from the beam for which the springs will become active. Releasing the blocks from the steel beam results in a reduction of the stiffness of the support structure. Case 1 has three blocks attached to the steel beam, case 2 has two blocks attached to the steel beam and case 3 has one block attached to the beam.

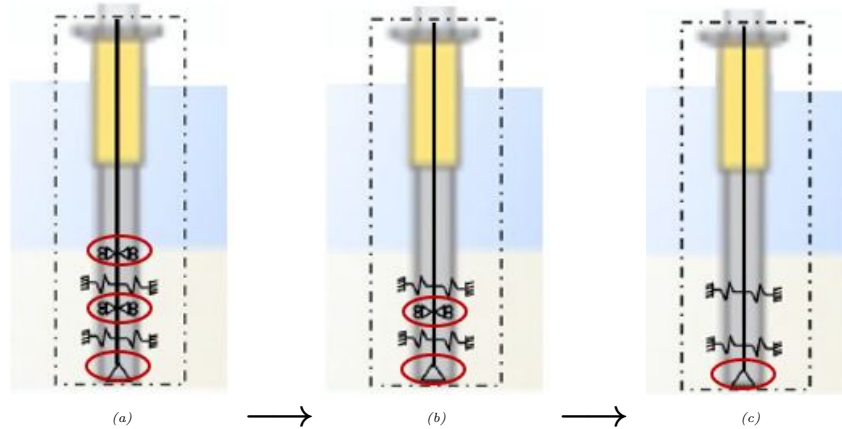


Figure 1.3: Three different stiffness cases for analysis: (a) Case 1 has three blocks attached to the beam, (b) Case 2 has two blocks attached to the beam, and (c) Case 3 has one block attached to the beam

Two different tests will be performed on the designed experimental setup. The first testing phase is done to identify the natural modes to a reduction of the supporting stiffness, representing a reduction in the soil stiffness. The test done to identify the structural dynamic response of the test setup is an impact test. An impact test is done by the means of applying a small impulse load to the end of the slender beam, to excite all modes of vibration with equal energy. The impact to the end of the slender beam is induced by a hammer strike. Due to the deformation of the structure, caused by the hammer strike, the accelerometers and strain gauges will measure respectively accelerations and strains on the beam over a certain time period. The identification of the natural frequencies is done by the means of a modal analysis. During post-processing the Peak Picking method is used to extract the natural frequencies of the experimental setup. The second phase of testing consist of a harmonic analysis by means of a forced vibration test on the experimental setup, with the forced vibration test it is possible to investigate the structural response of the structure under different boundary conditions. The harmonic analysis is done by using the output measurements of stresses occurring in the structure when a harmonic load is applied. The harmonic load applied to the structure is induced by an eccentric motor which can vary in vibration speed. The harmonic analysis is used as a tool to get more insight in the relation between the fatigue life of the experimental setup and the numerical model. The measurements obtained from these tests are analysed for the stresses occurring in the structure. Details of the design of the experimental setup, and the performed tests are given in Chapter 3.

The second part is a numerical linear finite element analysis (FEA) of the problem using the FE software ANSYS. A script is written in the ANSYS parametric design language (APDL), and is used to build, solve and post process the results of the finite element model. The numerical analysis is used to perform a FEA to investigate the influence of the change in soil stiffness on the structure's dynamic response. The model is a representation of the experimental test setup which is developed in the first part of the research. The 2D FE model includes a beam modeled with BEAM188 elements and springs, representing the soil, modeled with COMBIN14 elements. In order to enhance model flexibility several parameters are used regarding the dimensions of the structure and the stiffness of the support, *e.g.* the amount of aluminum blocks attached to the beam and spring stiffness, etc. The 2D FE model is used to validate the results of the experimental test setup, therefore both a modal analysis and a harmonic analysis are conducted using the numerical model. A detailed description of the numerical model is given in Chapter 4.

The modal analysis of the numerical model allows the comparison of the natural frequencies of the numerical model to the natural frequencies of the experimental setup. Therefore, an optimization code in Matlab is written which looks for the set of parameters in the numerical model, in order to find the minimum difference between the natural frequencies of the numerical model and the natural frequencies of the experimental model. The set of parameters for which Matlab finds an optimal value for are the amount of aluminum block supports attached to the steel beam and the stiffness of the springs attached to the steel beam. With the optimized values for the amount of aluminum blocks and the spring stiffness, it is possible to make realistic estimations about the state of the supports of the experimental setup.

The ability to compare the numerical model and the experimental model results in a methodology for characterizing the state of the support conditions of the experimental setup, in terms of amount of aluminum block supports and spring stiffness, based on only output of accelerations and strain measurements. This methodology contributes to the SHM system of an offshore monopile structure.

1.5 Report outline

The remaining of this report describes in detail the conducted research. Table 1.1 shows the software used during this research. Primarily a literature review is done on fatigue, monopile structures, modal analysis and SHM. In Chapter 3 the design of the experimental setup and the performed tests are discussed in detail. The numerical model is elaborated on in Chapter 4. The results of the modal analysis and harmonic analysis, for both the experimental model and the numerical model, are presented and discussed in Chapter 5. Chapter 6 shows a methodology that contributes to the SHM framework of an offshore monopile, presenting an automatic model updating model. A conclusion along with recommendations for further research is given in Chapter 7. The appendices are used for clarification on the methodology of the research by the means of a flowchart, for scaled drawings of the experimental setup, for numerical and analytical justification of the experimental setup, for the presentation of all scripting codes and for presenting all data of the performed analysis during this research.

Table 1.1: Used Computer Software

Software	Application	Version
MatLab	Calculations	R2021 a
AutoCAD	Drawings of experimental setup	2020 Student version
ANSYS	FE-modelling	2021 R1
Excel	Calculations	2202
Overleaf	Documentation	Web-version

In this chapter the literature on fatigue and dynamic behavior of offshore monopiles is reviewed. First the concept of fatigue and the notion of S-N curves is discussed. Secondly, offshore monopiles are treated regarding their structural properties, dynamic loading, soil stiffness and lastly fatigue of offshore monopiles. The literature research continues with an elaboration on modal analysis, experimental testing and is concluded with a discussion on structural health monitoring (SHM).

2.1 Fatigue

Fatigue failures have first been researched in the 19th century. It was found that a single load application far below the static strength of the material did not do any damage. However when the same load was applied many times it would induce severe damage and eventually failure to the material. During this time fatigue could not be seen and failure would occur without any warning, therefore fatigue was a mysterious phenomenon. In the 20th century the fatigue failure mechanism was found. The repeated load cycles cause nucleation of cracks which will initiate micro crack growth. Micro cracks will propagate and they will ultimately lead to macro cracks and complete failure. Laboratory research and accident investigation on fatigue failures have highly contributed to the present knowledge on fatigue failures and that fatigue must be considered as a serious problem for structures which are exposed to dynamic loading [2].

In general, fatigue life is a surface phenomenon which is understood as a micro crack initiation period followed by a macro crack growth period. The initiation of cracks is caused by cyclic loading, this period is influenced by the technical conditions such as material surface quality, residual stress, and environmental conditions. Immediately after a cyclic loading above the fatigue limit is applied the nucleation of micro cracks starts. These fatigue cracks are initially too small to be visible, however after repeated cycling, the crack growth period starts and macro cracks are formed. Depending on the magnitude of the load, the initiation period will roughly take $N < 10^8 - 10^9$ cycles of loading. Fatigue will transform into fracture when the micro cracks propagate into macro cracks. The macro cracks will eventually result into failure of the structure. The propagation of macro cracks are not longer a surface phenomenon [21]. Figure 2.1 is a schematic representation of the different phases of fatigue life described above. This research focuses on the fatigue of monopile structures before fracture occurs, therefore fracture mechanics is out of the scope of this research. For this reason fracture will not be further discussed in this research.

Around 90% of failed metal structures, failed due to fatigue. For this reason it is important to design metal structures that are robust with respect to fatigue. In order to do so, a prediction of the fatigue life of the structure is required. When all design aspects are known (structural concept, joints, material selection, material surface condition and production variables), the fatigue limit, fatigue life, crack growth and final failure can be estimated by means of the S-N curve. The S-N curve is used to relate the applied stress range to the number of cycles to be applied until failure for a certain stress ratio (R) [2]. In the following section the S-N curve is discussed.

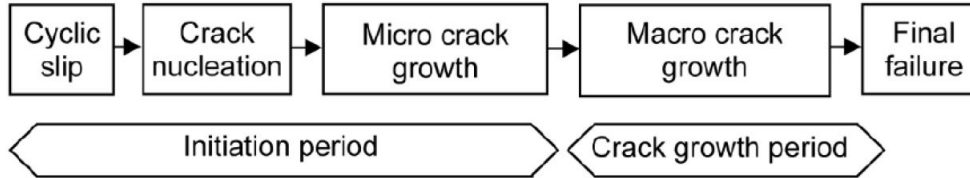


Figure 2.1: Schematic representation of different phases of fatigue life [2]

2.1.1 S-N curve

The S-N curve, also known as the Whöler curve, is obtained from laboratory testing. Such a curve is fitted over a scatter plot, where the data points are obtained from results of fatigue testing on failed and non-failed specimens at different stress levels. An example of an S-N curve presented in Eurocode 3 is given in Figure 2.2 [3]. The curve depends on the material, surface conditions and environmental conditions of the structure. The S-N curve is a curve with stress amplitudes or ranges on the y-axis (scaled linearly) and the number of cycles on the x-axis (logarithmic scale). Given a stress spectrum the number of cycles which can be applied before failure is within the area below the S-N curve [21]. However, it is important to note that stresses below the fatigue limit are not associated with an infinite life. It is assumed that only non-propagating cracks will occur and therefore the fatigue cracks initiated remain to be a surface phenomenon [2].

For stresses above the fatigue limit, $\Delta\sigma > \Delta\sigma_0$, the Basquin law is used to determine the fatigue life of the structure, given by

$$\log_{10} N = m_i \log_{10} \Delta\sigma + C, \quad (2.1)$$

In Equation 2.1, m_i is the gradient of the S-N curve, N is the number of cycles to failure for each specimen, and C provides information about the endurance, in other words the curve intercept. The gradient of the Basquin relation depends on the material of the evaluated specimen [21]. For steel $m_1 = 3$ and $m_2 = 5$ [21].

2.1.2 Fatigue of offshore steel structures

As previously mentioned, 75% of the OWTs are founded on slender monopile structures. These structures are flexible and very sensitive to resonance effects. For this reason the design of a monopile structure is driven by the fatigue limit state of the structure. Offshore steel structures are exposed to severe dynamic loading, including wind, wave and current loads. The fatigue life prediction of a monopile depends on the load cycles applied (amplitude and frequencies) and the structural properties (depth of foundation, length of pile, thickness of pile, production etc.), the average fatigue life prediction is between 20-25 years.

The initiation of cracks often occurs at stress concentrators like notches and welds along the monopile structure. For the design of an offshore monopile the following main fatigue failure modes are considered and shown in Figure 2.3 [4]:

- a) **From weld toe into the base material:** Due to the weld notch geometry the stress levels are the highest at the weld toe. This causes the initiation of fatigue cracks at small defects

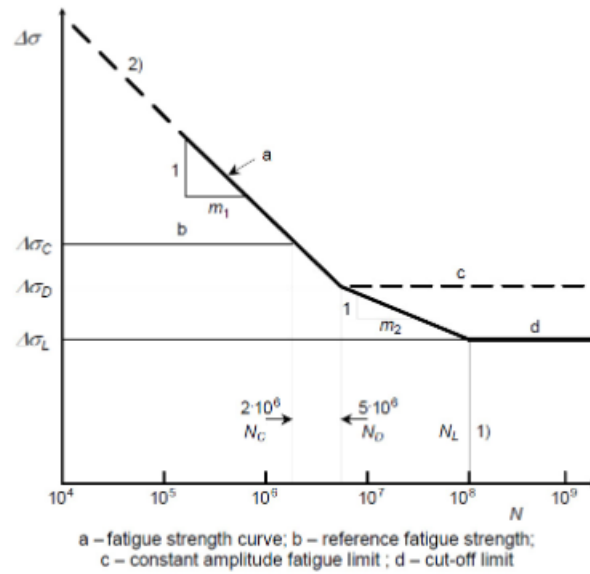


Figure 2.2: S-N curve from Eurocode 3 [3]

or undercuts at the weld toe. The fatigue crack growth from the weld toe into the base material is a frequent failure mode.

- b) **From weld root through the fillet weld:** The use of fillet welds should be avoided in connections, because the crack growth from the root of a fillet weld through the weld can lead to significant consequences.
- c) **From weld root into the section under the weld:** during the service life, fatigue crack growth is observed of the structures and in laboratory fatigue testing. The fatigue life for this failure mode is of a similar magnitude of the fatigue life of a weld toe in an as-welded state¹ condition.
- d) **From a surface irregularity or notch into the base material:** Components with high stress-cycles cause fatigue cracking in the base material. These fatigue cracks are often initiated from small surface defects/irregularities.

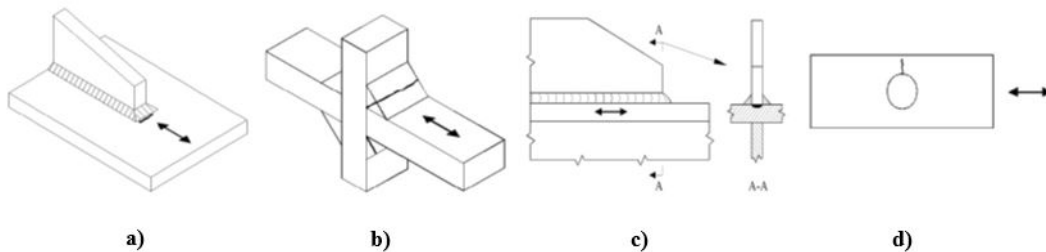


Figure 2.3: Visual explanation of fatigue failure modes at stress concentrators[4]

¹As-welded state is the final state of a weld, but before thermal, chemical, or mechanical processes have been applied as treatment of the weld

2.2 Monopiles

The choice of foundation for OWTs depends mainly on water depth, seabed characteristics, economic costs, available construction technologies and applied loading [22]. However 75% of the installed offshore foundations are hollow pipe monopiles, therefore this research focuses solely on the monopile structures. Monopiles are typically used for water depths between 20-40m. The structures are relatively flexible due to their slender design. This section elaborates on the structural properties of the structure, on the dynamic loading to which the structure is exposed to and finally an elaboration on the influence of the alternating soil stiffness around the foundation structure.

2.2.1 Structural properties

As mentioned previously, monopile structures are very slender hollow pipe structures. The structures have an outer diameter between 4-8m with a wall thickness ranging from 0.055-0.150m and penetration depth between 20-40m. The ratio between effective length and diameter of the structure usually ranges from 5 to 6. Due to the slenderness ratio being less than 10, the structure is considered to be rigid. Rigid implies that the rotation of the structure is prominent over the bending of the structure, *i.e.*, the rotation as a rigid body defines the structures lateral loading behavior. This means that the soil around the structure fails in bearing capacity before the structure would fail over its embedded length by plastic hinges [22].

2.2.2 Dynamic loading on OWTs

OWT are exposed to static and dynamic loads, which makes the design of an OWT very complex. There are several loading, acting on the foundation, effects regarding the OWT which cause these loads on its monopile foundation. The external loading is due to the motion of wind and wave. The internal loading is due to the vibration at hub level due to mass and aerodynamic in-balance of the motor, and the dynamic load is caused by the vibration of blade passing effects. The loading caused by mass and aerodynamic in-balance of the motor is often referred to as 1P and blade passing is referred to as 3P [5]. The peak frequencies at which these loads occur lay within 1Hz. Table 2.1 shows the peak frequencies of the external and internal loads to which the OWT is exposed. Figure 2.4 shows a schematic representation of the frequencies regarding a power spectral density (PSD), later on in this chapter PSD will be further discussed. The designer of an OWT should select a system frequency outside of the range of forcing frequencies in order to avoid resonance of the structure and eventually catastrophic failure [5]. Figure 2.4 shows the complexity of designing an OWT structure regarding its natural frequencies.

Table 2.1: Peak frequencies of internal and external loading on an OWT considering a 3 bladed 3MW turbine

Wind and wave	0.12Hz
Vibration due to motor (1P)	0.135Hz – 0.316Hz
Blade passing (3P)	0.405Hz – 0.948Hz

An example of loading conditions and values on an offshore monopile foundation for a 5-MW OWT installed in the North Sea, with a hub height of 95m above sea level and a rotor diameter of 125m, is shown in Table 2.2 [14]. The example of load scenarios given in Table 2.2 are quasi static loads caused by wind, wave and rotating blades of an OWT. According to this table, the wind and wave motion cause a very high bending moment which needs to be resisted by lateral compression of the surrounding soil. In the next subsection the interaction between the soil and the monopile structure is discussed.

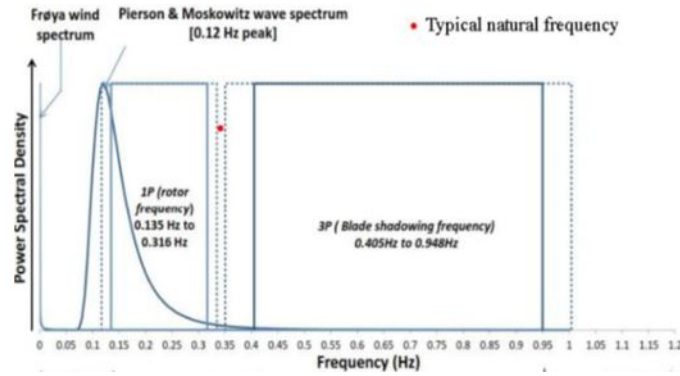


Figure 2.4: Forcing frequencies regarding PSD [5]

Table 2.2: Loading at mud-line of monopile foundation supporting a 5-MW OWT [14]

Axial load	35MN
Horizontal load	16MN
Bending moment	562MNm
Torsional moment	4MNm

2.2.3 Influence of alternating soil stiffness

Cyclic loading causes a gathering of pile displacements and stiffening or softening of the soils around the pile, this leads to a varying supporting stiffness for the monopile. The influence of loading, unloading and reloading on the behavior of the soil stiffness has been reported in cyclic large- and small-scale pile testing by Little and Briaud (1988) and by Roesen et al. (2013). Next to the cyclic large- and small-scale tests, some centrifuge tests are performed by e.g. Klinkvort et al. (2010) in order to identify the soil behavior when it is subjected to cyclic loading [20]. The varying soil stiffness evidently leads to a changing structural dynamic behavior of the monopile, the changed support stiffness of the monopile can lead to changes in the structure's natural frequencies. It is possible that the change in support stiffness causes the natural frequencies to be closer to the excitation frequencies, which results in an increased dynamic amplification of the response of the OWT. This amplification leads to an intensification of fatigue damage and thus a reduction in the estimated fatigue life of the OWT [6]. Several studies have been carried out to investigate the effect of soil stiffness on the structural dynamical response of a monopiles.

In previous studies the effect of the change in soil stiffness on the structure's dynamic response in sand is assessed by using $p - y$ curves. An example of a $p - y$ curve is shown in Figure 2.5. This figure shows the $p - y$ curve for sand with p presenting the soil reaction of sand due to the pile deflection y . The observation of the study suggests that a 50% reduction of the soil stiffness leads to an increase of 7% of the equivalent damage at mud-line [6]. Another study has investigated the change in soil stiffness and damping of the soil. They found that decreasing the soil stiffness with 50% causes an increase in the equivalent fatigue damage at mud-line by approximately 12% [17]. Among other contributions these studies highlight the impact of soil stiffness on the structural dynamic behavior of a monopile.

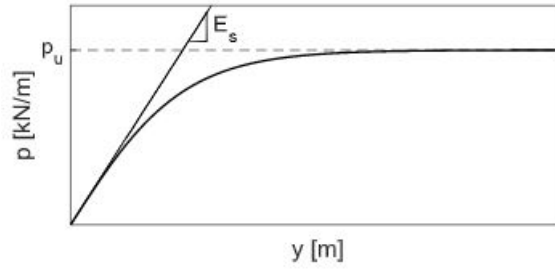


Figure 2.5: p - y curve of for sand [6]

2.3 Modal analysis

Modal analysis is used to characterize the dynamic properties of a system in the frequency domain. The dynamic properties of such a system includes the natural characteristics of frequency, damping and mode shapes. Modal analysis finds the dynamic characteristics of a structure, these characteristics are independent of time and external loading. For this reason modal analysis is also known as "free" vibration analysis [23]. Modal analysis is used to avoid designing a structure with natural frequencies close to the structure's excitation frequencies. With this analysis resonance, and thus catastrophic failure, can be avoided. The following subsections will discuss the theory of modal analysis and the analytical, numerical and experimental modal analysis considering a cantilever beam. A cantilever beam is known to be fixed at one end and free at the other end, such a beam is shown in Figure 2.6.



Figure 2.6: (a) Cantilever beam, fixed on one end and free on the other end [7], (b) Cantilever beam subjected by a point load P [7]

2.3.1 Analytical modal analysis

This section presents a theoretical modal analysis using Euler-Bernoulli beam theory of a cantilever beam subjected to a point load P . It is assumed that the beam undergoes a small deflection within the linear elastic region and the beam is considered to be uniform [7]. The Euler-Bernoulli theory is often used because it provides simple yet realistic engineering approximations for many problems. The theory neglects shear deformations and rotatory inertia effects. Euler-Bernoulli beam theory identifies the relationship between a beams deflection and the applied loads, and it gives an accurate result for long slender beams with a solid cross-section [24]. This relationship is shown in Equation 2.2 [7]. In this equation presents the curvature of the beam due to the bending moment at each section of the beam. Obtaining this equation it is assumed that the material is homogeneous, isotropic and is consistent with Hooke's law [7].

$$M = EI \frac{\partial^2 y}{\partial x^2} \quad (2.2)$$

Where E is the Young's Modulus and I the moment of inertia of the beam element. When the beam is subjected to a point load P , the beam will deform according to a certain curve. This is shown in Figure 2.6b. When the load P is removed from the end of the beam, the beam will try to return to its original shape. However, in order to return to its original shape, the beam starts

to vibrate around its neutral axis [7]. This equation of motion is given as follows

$$\frac{\partial^4 y}{\partial x^4} + \frac{\rho A}{EI} \frac{\partial^2 y}{\partial t^2} = 0 \quad (2.3)$$

Where ρ is the mass density of the material of the beam and A is the cross sectional area of the beam. When the variables are separated into variables depending on time and variables depending on location, the equation can be written as follows [7]

$$y = X(x)f(t) \quad (2.4)$$

The above equation can be substituted in Equation 2.3, which yields

$$\frac{EI}{A\rho X(x)} \frac{\partial^4 X(x)}{\partial x^4} = \frac{-1}{f(t)} \frac{\partial^2 f(t)}{\partial t^2} \quad (2.5)$$

This equation can be written into two differential equations

$$\frac{\partial^4 X}{\partial x^4} - K_n^4 X = 0 \quad (2.6)$$

$$\frac{\partial f}{\partial t^2} + \omega_n^2 f = 0 \quad (2.7)$$

With

$$K_n^4 = \frac{\omega_n^2 A \rho}{EI} \quad (2.8)$$

In order to find the solutions to Equation 2.6, the following form of equation is used

$$X = A(\cos K_n x + \cosh K_n x) + B(\cos K_n x - \cosh K_n x) + C(\sin K_n x + \sinh K_n x) + D(\sin K_n x - \sinh K_n x) \quad (2.9)$$

In order to be able to solving Equation 2.9, boundary conditions are needed. The four boundary conditions for a cantilever beam are as follows

1. at $x = 0 \rightarrow X = 0$
2. at $x = 0 \rightarrow X' = 0$
3. at $x = L \rightarrow X'' = 0$
4. at $x = L \rightarrow X''' = 0$

When the boundary conditions are substituted into Equation 2.9, the differential equation can be solved. The following equation is the result of the solved differential equation

$$\cos K_n L \times \cosh K_n L = -1 \quad (2.10)$$

This equation shows that the system has a result for infinite frequencies, because $K_n L$ and ω_n both have infinite values. Table 2.3 shows the results of solving Equation 2.10 [7].

Table 2.3: The first three values for $K_n L$ [7]

n	$K_n L$
1	1.87510
2	4.69409
3	7.85475

When equation 2.8 is rewritten in Equation 2.11, then the natural frequencies can be obtained when it is related to the circular natural frequency as shown in Equation 2.12.

$$\omega_n = K_n^2 \sqrt{\frac{EI}{\rho AL^4}} \quad (2.11)$$

$$f_n = \frac{\omega_n}{2\pi} Hz \quad (2.12)$$

The mode-shapes of the first three frequencies are shown in Figure 2.7.

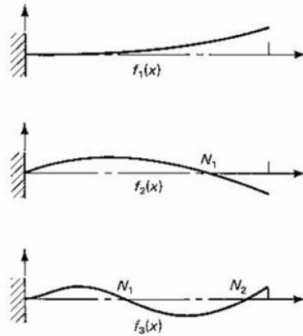


Figure 2.7: First three mode shapes of a cantilever beam [8]

Next to Euler-Bernoulli beam theory, it is also possible to analyse a beam according to Timoshenko-Ehrenfest beam theory. This beam theory takes shear deformation and rotational bending effects into account, which makes the theory suitable for thick beams. For large length/thickness ratios, the Euler-Bernoulli beam theory and the Timoshenko beam theory show, using finite element analysis, the same deflection results. However when the length/thickness ratio becomes smaller, Timoshenko beam theory is known to give more accurate results for the deflections of the beam. For this reason Timoshenko beam theory is known to be a superior method for analyzing beams with a smaller length/thickness ratio [25].

2.3.2 Numerical modal analysis

As mentioned in the previous section, a modal analysis can be applied to determine the vibration characteristics of linear elastic structures. Modal analysis helps to avoid designing a structure which has its natural frequencies close to the subjected excitation frequencies of the structure, this is important to avoid resonance. The analysis is a common root for dynamic simulations and it is commonly used to analyse advanced simulations, *e.g.* harmonic vibration and response spectrum analysis. From the equations used to do the modal analysis it is observed that a modal analysis is an eigenvalue problem, where the results of the problem can be obtained for simple and complex structures [26].

Modal analysis finds the dynamic characteristics of a structure, these characteristics are independent of time and external loading. For this reason modal analysis is also known as "free" vibration analysis. The main concept is to find the natural frequencies and mode shapes, to analyse the vibration behavior of the structure as a frequency domain problem instead of a time domain problem [27].

In order to go from a time domain problem to a frequency problem, it is assumed that every point experiences a harmonic motion. A periodic motion is observed as a function of the amplitude (A), the angular frequency (ω) and the phase angle (θ). Equation 2.13 shows that every point in the structure vibrates at the same frequency, however with different amplitudes and magnitude of

phase angle, which is observed to be timing of the vibration. The phase angle (θ) describes if the points in the structure are moving within phase or out of phase [28].

$$x = A \sin(\omega t + \theta) \quad (2.13)$$

ANSYS is a finite element software and consequently uses the finite element method to perform a modal analysis. The finite element method cuts the structure into a discrete amount of elements and then reconnects these elements. The connections of the elements are called nodes, and at each node a set of algebraic equations. These algebraic equations consist of equilibrium equations, strain-displacement relations, constitutive relations and boundary conditions [29]. The finite element method is used to perform a modal analysis, which is an eigenvalue problem presented as a function of displacement and acceleration, as can be seen in Equation 2.14 [30]

$$[\mathbf{M}]\{\ddot{\mathbf{u}}\} + [\mathbf{K}]\{\mathbf{u}\} = \{0\} \quad (2.14a)$$

Where \mathbf{M} is the mass matrix of the beam and \mathbf{K} is the stiffness matrix of the system. The displacement function \mathbf{u} is given by the following equation

$$\{\mathbf{u}\} = \{\phi\}_i \sin(\omega_i t + \theta_i) \quad (2.14b)$$

The acceleration function is obtained by taken the second derivative of the displacement function with respect to time

$$\{\ddot{\mathbf{u}}\} = -\omega_i^2 \{\phi\}_i \sin(\omega_i t + \theta_i) \quad (2.14c)$$

If the acceleration function $\ddot{\mathbf{u}}$, and the displacement function \mathbf{u} are substituted in the equation of motion given in Equation 2.14a, the following is obtained

$$([\mathbf{K}] - \omega_i^2 [\mathbf{M}])\{\phi\}_i = \{0\} \quad (2.15)$$

Where ω_i^2 are the eigenvalues and ϕ_i are the eigenvectors. It is observed that the equation of motion only depends on the angular frequency (ω) and the amplitude (ϕ). When solving the eigenvalue problem the determinant is set to 0.

$$\det([\mathbf{K}] - \omega_i^2 [\mathbf{M}]) = 0 \quad (2.16)$$

Where the angular frequency (ω_i) is related to the natural frequency as follows

$$f_i = \frac{\omega_i}{2\pi} \quad (2.17)$$

and the amplitude vector $\{\phi_i\}$ is the mode shape corresponding to the natural frequency $f_i(Hz)$. Depending on the dimensions of the stiffness and mass matrix, the amount of eigenvalues are found with corresponding eigenvectors [30].

In the solution step of modeling in ANSYS, the designer can choose the desired number of natural frequencies and modes. The designer can also visualize each mode shape corresponding to the natural frequencies. The maximum amount of modes that can be extracted numerically equals the number of DOFs. However, most often the number of modes that need to be extracted depends on the excitation frequencies. The number of modes is carefully chosen in order to capture the dynamic response of the structure. When the excitation frequency is low, the amount of relevant mode shapes is also low, however when the excitation frequency is high, the number of relevant mode shapes also increases. The mode shapes represent the relative deformation of the structure at the natural frequencies, which are the eigenvectors of the system that is analysed. For a realistic plot of the mode shape, the structure can be plotted with certain factors, but it will remain to present the same mode shape [30].

However, the lack of data for modeling real conditions a FE-analysis on a structure, causes an FE-analysis to not always be sufficient enough to characterize the dynamic behavior of a structure. For this reason experimental methods are necessary, especially for performing a correct modal analysis [31]. The next subsection elaborates on the two different methods of Experimental Modal Analysis and Operational Modal Analysis.

2.3.3 Experimental and Operational Modal Analysis

Modal analyses are done for understanding a structures dynamic behavior and investigate dynamic properties. The characterization of the dynamic behavior and the dynamic properties are used to improve the safety, reliability, and performance of a structure [19]. A modal analysis can be done with a mathematical model of the structure based on measurements and/or simulations of the dynamic behavior of the structure. The mathematical model includes calculations which are described in the previous sections, and the simulations are done by FE-analyses. The results of such a mathematical model are able to describe the modal parameters, such as natural frequencies, modal damping and modal shapes, of the evaluated structure [19]. The simulation and mathematical model of the dynamic behavior of the structure can then be compared to test results. According to the test results the mathematical model and the simulations of the structure can be updated in order to provide more reliable results of the dynamic behavior and/or dynamic properties of the structure.

Test results are obtained from measurements done on a scale model of the structure and/or on the structure itself. Using measurements from a structure with controlled DOFs for a modal analysis is classified as Classical Modal Analysis which is also known as experimental modal analysis [31]. For performing CMA measurements, the structure is exposed to measured applied forces in one or more points and directions. Forces are either applied by using a dedicated impact tool where the applied force can also be measured (for example an impact hammer), and/or using one or more modal exciters, *e.g.* a shaking table, and measuring the applied forces using force transducers. The results of the impact are typically measured in a number of response DOFs by *e.g.* accelerometers [19]. The provided excitation is also the main difference between CMA and Operational Modal Analysis (OMA). In the OMA the excitation forces are not measured, because they are caused by environmental or technological activities, *e.g.* wind, waves, motors etc. [31].

OMA implicates using measurements from a structure in the parked situation. The biggest advantage of using OMA is that the analysis represents real operating conditions, *e.g.* the true boundary conditions, real environmental conditions and true force, vibration and frequency ranges [19]. However, a limitation of OMA is that the excitation forces are difficult to measure and therefore modeling the structure becomes complicated. Secondly, it is not possible to excite at higher frequencies or exciting local modes with the energy inputs provided by the environment. In other words, the systems response to a measured load can not be calculated [31]. Both CMA and OMA are efficient ways to perform a modal analyses.

Sensors for modal analysis

As mentioned previously, sensors that are used to measure the dynamic response of a structure during experimental or operational analysis, are for example accelerometers and strain gauges. An accelerometer is a sensor that transfers vibrations of a physical object into voltage, and it measures accelerations [32]. The sensors works by directly installing it to the vibrating object. The accelerometer will convert the energy of the vibrations into an electric signal which corresponds to the acceleration of the object in time [32]. An example of an accelerometer is a piezoresistive accelerometer. This sensor measures the electrical resistance of the material when vibrations are applied to the object. When choosing an accelerometer it is important to consider the following specifications of the sensor:

1. *Analog or digital output*

Analog output signals a continuous voltage which corresponds to the accelerations. Digital output signals cause a square wave at certain frequencies and the amount of time the voltage is high corresponds to the amount of acceleration [32].

2. *Number of axes*

The number of axis the accelerometer needs to measure in

3. Maximum swing

Enough swing is needed to be able to measure at all motions necessary.

A strain gauge measures strain on any structure. This sensor measures a change in resistance on a certain location of the structure, due to forces, pressure, tension, weight, etc. The resistance of the strain gauge can be changed by external forces altering the shape and size of the sensor. The sensor is directly implemented to the object. The sensor measures strain by the principle of the conductors resistance given by Equation 2.18, where L is the length of the strain gauge and A is the cross-sectional area [9].

$$R = \frac{L}{A} \quad (2.18)$$

The resistance of the strain gauges conductors will lead to the Gauge Factor by the following equation

$$GF = \left[\frac{\Delta R}{(RG * \epsilon)} \right] \quad (2.19)$$

Where GF is the Gauge Factor, RG is the resistance in the undeformed shape of the gauge, ΔR is the change in resistance and ϵ is the measured strain. The strain in an object is measured by the Wheatstone Bridge. Figure 2.8b shows such a Wheatstone Bridge, where V_{ex} is the voltage that is applied across the bridge and R_1, R_2, R_3, R_4 are voltage dividers [9]. Figure 2.8a is a picture of a pre-wired strain gauge implanted on a steel surface. In order to protect the strain gauge from external factors, some putty can be applied on top of the sensor.

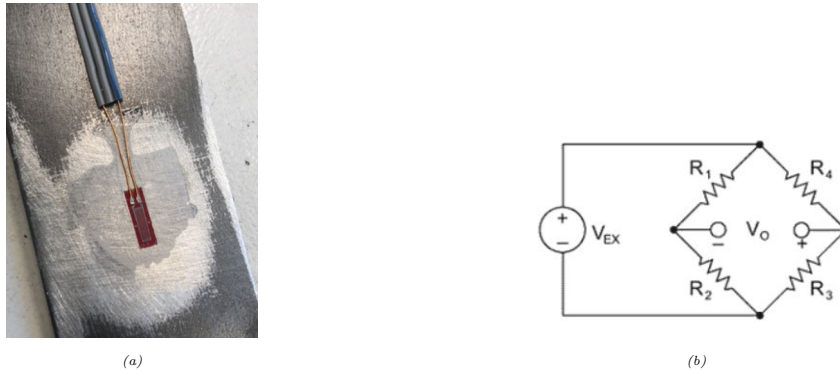


Figure 2.8: (a) Strain gauge applied to a steel surface, (b) Circuit of a strain gauge known as the Wheatstone Bridge [9]

Post processing of data for modal analysis

An identification technique for modal analysis on measurement data in the frequency domain is the Peak Picking method. This method is also known as the basic frequency domain technique, or the classical frequency domain approach. The Peak Picking method is based on the fact that the frequency response function of the system goes through extreme values around its natural frequencies [33]. This method is a simple post processing method, which makes use of the discrete Fourier transformation [34]. This transformation, referred to as a Fast Fourier Transformation (FFT), is a transformation of the data from the time domain to the frequency domain [23].

When the transformation from the time domain to the frequency domain is made, some leakage of the data can occur. For this reason it is important to apply a Hamming Window in order to reduce this leakage [23]. A Hamming Window is commonly used for closely spaced sine waves. Other windows can also be applied, *e.g.*, Hann, Flat Top, Uniform etc. [35].

When only output signal modal analysis is performed, the fact that well separated modes can be estimated directly from the frequency domain graph of the output signals, is used [34]. After the

data is transformed to the frequency domain, the peaks in the obtained graph are the frequencies measured in the system. When conducting an impact test on the structure, the natural frequencies of the system will follow from the peaks in the data in the frequency domain.

During post processing it is possible to reduce the contribution of noise to the obtained signal by filters. The following filters can be used

1. Low pass filter: Rejects high frequency components of a signal and passes the low frequency range.
2. High pass filter: Rejects the low frequency components of a signal and passes the high frequency range.
3. Band pass filter: Filters a particular band of frequency components.

Figure 2.9 is a graphical representation of the applicable frequency filters. It is important to note that $\pm 20\%$ needs to be added to the cutoff frequency in order to make sure the filters do not reject components of the desired frequency range [10].

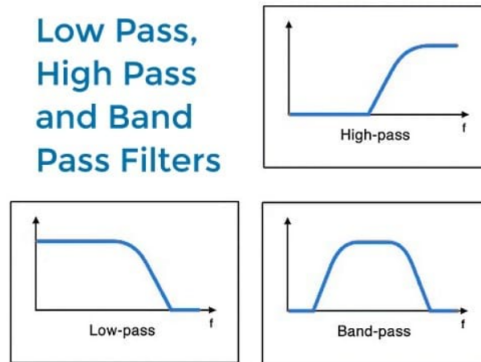


Figure 2.9: Applicable filters to reduce the contribution of noise to the output signal [10]

The above described methods can be used when doing an impact test, however conducting an operational modal analysis with these methods is more difficult. An operational modal analysis implicates a modal analysis done on an operating structure. Further elaboration on this subject is given in Chapter 7.

2.4 Experimental testing

In this section impact testing and forced vibration testing is discussed.

2.4.1 Impact test

An impact test is often done with an impact hammer, a hammer which measures the force via load cell. An impact test simply consists of applying an impact to a structure. During impact testing for modal analysis it is important to have accelerometers attached at fixed points and directions to the structure which is impacted, to measure the response accelerations. In order to analyse the data obtained from the impact test, a post-processing modal software is needed for identifying natural frequencies [36].

Several requirements are needed in order to be able to perform an impact test and obtaining correct data. One of the main requirements is a pre-trigger delay. In order to ensure that the entire signal is captured it is important to have a pre-trigger time prior to the applied impact. Another requirement is the possibility to apply windows in order to reduce leakage of the FFT, a

Force Window can also be applied in order to reduce noise of the signal. It is also important to repeat the test 3-5 times in order to ensure the measurements are conducted correctly [36].

2.4.2 Forced vibration test

In order to reproduce a structure during operation time, a structure that is subjected to cyclic loading, a forced vibration test can be conducted. The forced vibration test can be used to compare stresses of the structure to stresses obtained from a numerical model of the structure. The forcing vibration can be applied by an eccentric motor. The working principle of an eccentric motor is based on the unbalancing rotations of eccentric masses. The excitation force produced by this device depends on the eccentric placed mass (m), the radius of the rotations (r) and the velocity of the motor (ω). The frequency of the cyclic loading depends on the voltage of the power supply. Therefore, the frequency can easily be controlled [1].

2.4.3 Measurement system settings

As mentioned previously, the pre-triggering time is an important factor to consider when conducting an impact test. Other settings of the measurement system, like the filter frequency and the sample frequency, are important factors which need some attention when doing experimental testing.

Filter frequency

Before the measurements start it is important to assure that there is no aliasing of higher frequencies in the to be analyzed frequency range. For this reason a filter frequency is applied. When an insufficient large sampling rate is applied, it is possible that frequency components will overlap in the measurement. It causes frequencies in the amplitude-frequency spectrum, which do not belong to the original signal [37]. This phenomenon is called aliasing. To avoid aliasing it is also important to choose the correct sample frequency.

Sample frequency

The sample frequency is the amount of data points sent from the sensor to the measurement system in order to obtain a measurement. It is the frequency at which the data is captured by the sensor. The Shannon Sampling Theorem uses Equation 2.20 to find the correct sampling frequency. This equation shows that the sample frequency f_s is a multiplication of the amount of measured cycles f [11]. Figure 2.10 *C* represents the Shannon Sampling Theorem in an output signal. The theorem uses at least twice the maximum frequency component for the sampling frequency. Figure 2.10 *B* shows that not having an integer multiplication of the amount of cycles for the sampling rate also causes aliasing [11].

$$f_s = 2 * f_{max} \quad (2.20)$$

However it is favorable to increase the sampling frequency in order to increase the resolution of the signal.

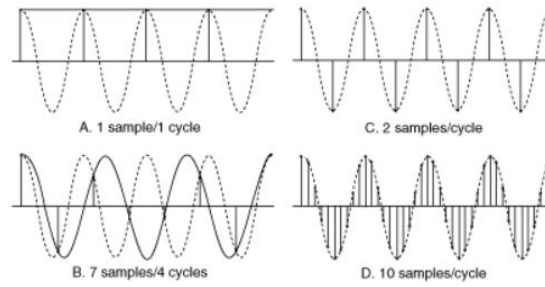


Figure 2.10: Representation of sampling frequency in a signal [11]

2.5 Structural Health Monitoring

Structural Health Monitoring is a detection strategy for detecting damage on a structure. Damage includes all changes to the material or the materials properties of a structure, which affects the performance of the structure. SHM includes measuring the structures displacements, strains, acceleration etc. The measurements are used to observe the structure. SHM can be applied for long term and short term events. Long term SHM includes continuous monitoring, interval monitoring and regular checks of the structure regarding degradation. Short term SHM simply concerns a full check, in terms of damage, after a short term event [38].

SHM proceeds in three different steps. The first step includes data acquisition, data normalization and a cleaning of the data regarding noise. Step two concerns a feature extraction, like a modal analysis, and information substantiation. The third step includes a development of a model, this includes developing a model and updating an existing model [38].

A SHM system is used to monitor the structural health state and update the state of the system of a structure based on only output measurements. The SHM is in the middle of its development, however it is a good method for health management and maintenance management of structures [19].

Experimental Setup

This research aims to develop a framework for identifying the influence of soil stiffness on the dynamic response of the offshore monopile structure. In particular, the aim is to characterize the state of the support of a monopile using only output measurements. To do so, an experimental tests setup is designed as well as a numerical model of the setup. By acquiring measurements on the experimental setup, it is possible to verify to what extent the numerical model predicts the behavior of the setup. The details of the numerical model are described in Chapter 4. In order to mimic the problem described in Section 1.2 an experimental test setup is designed. The design of the test setup is shown in Figure 3.1. Figure 3.1(*a*) shows the top-view of the experimental setup and Figure 3.1(*b*) shows the sections of the setup. Section A shows the springs attached to the steel strip, section B shows the aluminum supports attached to the steel strip, and section C shows the entire support structure of the steel strip. In Appendix B all drawings of the experimental setup are shown including scaled dimensions of the setup and a description of the elements.

In this chapter the experimental test setup and the tests performed on the setup will be discussed in detail. However, a numerical justification for the design of the setup is given in Appendix C. An analytical justification of the setup is given in Appendix D.

The remainder of this chapter is structured as follows. Section 3.1 describes in detail the design of the experimental test setup, Section 3.2 describes the applied sensors, and Section 3.3 elaborates of the tests performed on the setup including the measurement system settings and the post processing of the measurements. The results of the performed tests are shown in Chapter 5.

Materials used for the setup were made available at the Structures Laboratory at Eindhoven University of Technology. The four springs used in the setup are provided by ATV-springs. The sensors used for the measurements performed on the experimental test setup and the data acquisition system are available at the laboratory of HVR Engineering. The tests are also performed at the laboratory of HVR Engineering.

3.1 Design of Setup

As mentioned in Section 1.2, the experimental test setup is designed by means of a lumped parameter model representing the soil-structure interaction of an offshore monopile. The soil-structure interaction can be regarded as a continuous system with a varying nonlinear stiffness

over the depth of the monopile. The soil-structure interaction is approximated by dividing the soil into a finite number of segments which are represented by springs. The discretized soil-structure interaction of such a continuous system is shown as a lumped parameter model in Figure 1.2b. For simplicity the soil-structure interaction is referred to as 'the support of the structure'.

In this research the following is assumed. First, the support is assumed to have infinite stiffness in the lateral direction when the monopile is initially placed in the soil. Consequently, the support is modeled as a simple roller support. These supports are modeled with aluminum blocks in the experimental setup. The simple supports are attached to heavy IPE profiles with two steel M12 rods. Section B in Figure 3.1(b) and Figure 3.2(b) show the aluminum supports, with steel rods, attached to a strengthened IPE300 profile.

Secondly, the stiffness of the support for the slender beam structure is assumed to decrease over time due to the dynamic loading on the structure. The decrease in support stiffness of the structure is modeled by releasing the aluminum supports one by one. By releasing the first support (case 2), the first spring becomes active and by releasing the second support, both springs become active (case 3). The stiffness of the aluminum support is higher than the stiffness of the springs, therefore by releasing these supports the stiffness of the entire support structure of the steel strip is reduced. The lumped parameter models of the three different cases of support stiffness are shown in Figure 1.3 in Section 1.2.

A list with specifications of the elements used in the test setup is given in Table 3.1. The test setup exists of a steel beam and aluminum block supports, with several sensors attached to the beam element in order to measure strains and accelerations when the beam is subjected to impact or dynamic loading.

Table 3.1: Specifications experimental test setup

Element	From	Element specifications
Beam	Structures Laboratory TU/e	Material: Steel (S235) Dimensions $b \times h \times L = 0.0795m \times 0.0295m \times 3.1m$ Elastic modulus: $2.1 \times 10^{11} N/m^2$ Density (ρ): $7850kg/m^3$
Clamps	Structures Laboratory TU/e	Material: Aluminum Dimensions $b \times h \times L = 0.146m \times 0.03m \times 0.06m$ Depth of hole $d = 0.005m$ Elastic modulus: $7.0 \times 10^{10} N/m^2$ Density (ρ): $2710kg/m^3$
Springs	ATV-springs	Material: Steel (S235) Length $l_o = 0.23m$ Spring stiffness: $65.2N/m$ <i>More specifications are given in Appendix E</i>

3.1.1 Elements of experimental setup

The experimental setup consists of a steel beam, springs, aluminum supports and several sensors. Section 3.2 elaborates on the sensors used for measuring strain and accelerations of the steel beam when subjected to impact or dynamic loading. A steel beam with a length of $3.1m$ is used for the test setup. As can be seen in Figure 3.1, $0.3m$ of the steel beam hangs on the left side of support structure. The right side of the steel beam is used for measuring the dynamic response of the structure. The left part of the steel beam is used for lengthening the left part of the beam. In other words, the length of the analyzed steel beam can vary up to a length of $2.3m$.

The steel beam used for the test setup is a slender beam with a rectangular cross-section as shown in Figure 3.2(a). The dimensions of the steel beam are such that the beam is strong enough to withstand the applied loads, whereas the first three natural frequencies are low enough to be excited in the forced vibration testing. This means that the first three natural frequencies of the structure should range between $0Hz - 100Hz$. Furthermore it is necessary for the natural frequencies of the structure to be well separated in order to apply the Peak Picking method to perform a modal

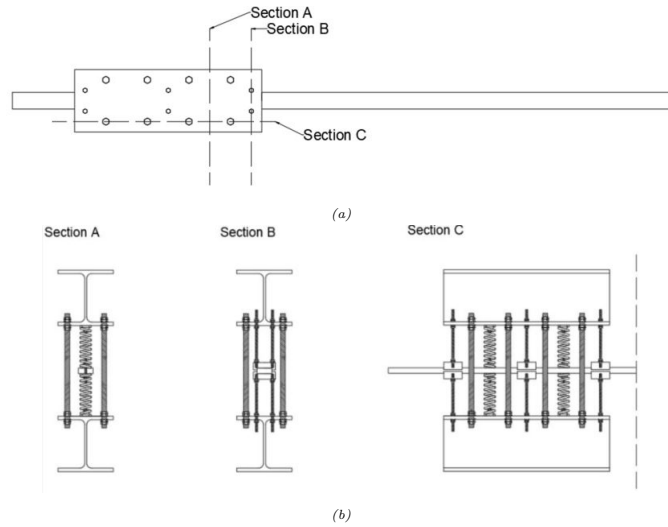


Figure 3.1: (a) Top-view of experimental setup and (b) Sections of experimental setup

analysis. The analytical justification of the strength and stability of the steel beam is given in Appendix D. Later on in this section the analytical justification is briefly discussed. For these reasons the slender beam with a cross section of $b \times h = 0.08m \times 0.03m$ is chosen, and in practice this results in the current beam with a measured cross section of $b \times h = 0.0795m \times 0.0295m$.

The aluminum blocks constraining the steel beam have a simple roller support function. At each support location the beam is constrained for displacements in the lateral (y -axis) and out of plane (z -axis) direction of the steel beam. It is important to note that the aluminum supports do not constrain the steel beam in its longitudinal direction (x -axis). Figure 3.2(b) is a schematic representation of the aluminum supports and the global axes of the structure. Other elements within the support of the steel beam are four springs. The choice of spring stiffness of the springs are justified by a simple numerical model which is further discussed in Appendix C.

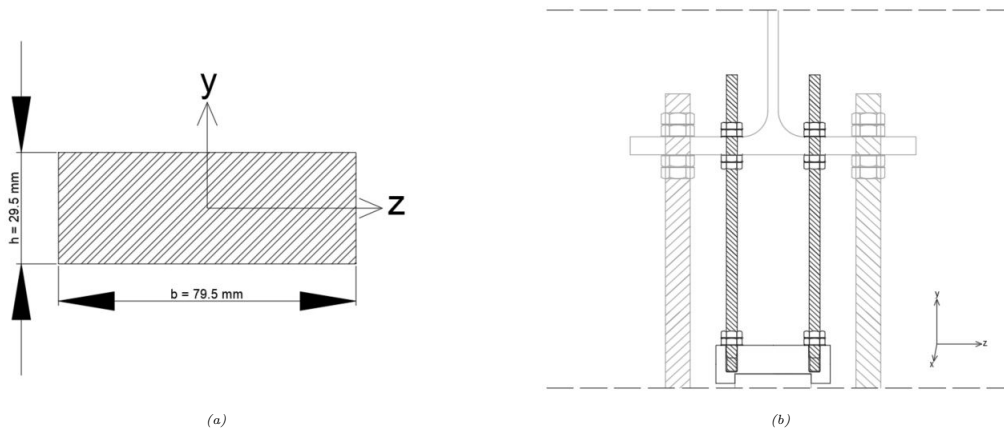


Figure 3.2: (a) Cross section of steel beam (b) Sections of aluminum support attached to strengthened IPE300 profile

Springs

According to the numerical model, described in Appendix C, and the hand calculations for the support of the test setup, given in Appendix D, a spring with a spring constant of $65600N/m$ is used. A list of specifications of the spring is given in Appendix E. The springs are tested in a Schenk 100kN electromechanical machine for static testing in order to obtain the spring

constant; this test is shown in Figure 3.3(a). The springs are tested in the compression mode of the electromechanical machine. Figure 3.3(b) shows the result of the compression test. The spring constant is obtained from the slope of the linear part of this graph. Equations 3.1 are used to determine the spring constant.

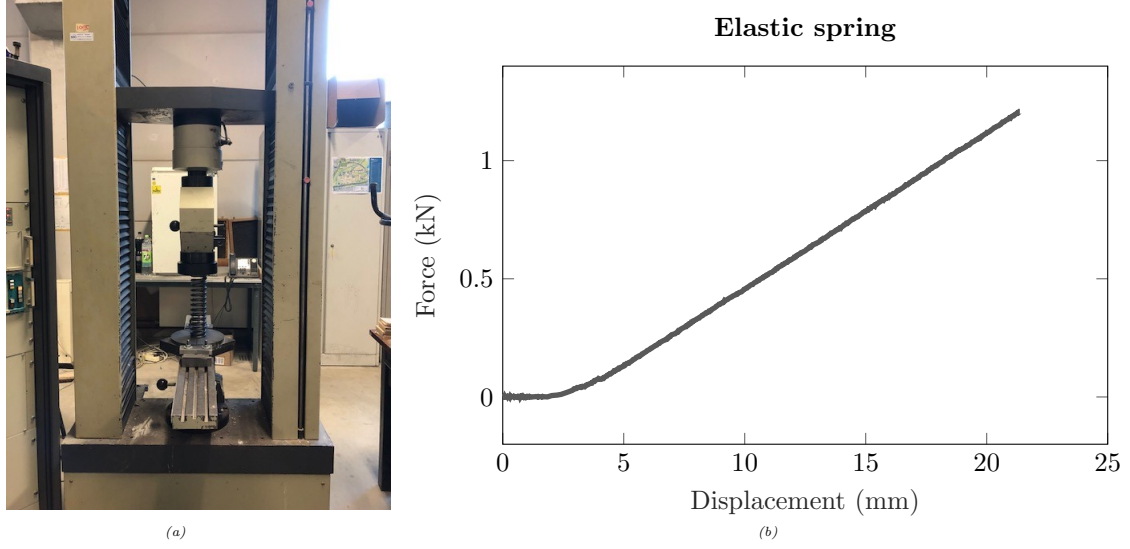


Figure 3.3: (a) Schenk 100kN electromechanical compression test and (b) result of the compression test for springs used in the experimental setup

$$\begin{aligned}
 \Delta d &= d_2 - d_1 \rightarrow 20\text{mm} - 10\text{mm} = 10\text{mm} \\
 \Delta F &= F_2 - F_1 \rightarrow 1.112\text{kN} - 0.456\text{kN} = 0.656\text{kN} \\
 \text{Slope} &= \frac{\Delta F}{\Delta d} \rightarrow \frac{0.656 \times 10^3 \text{N}}{10\text{mm}} = 65.6\text{N/mm}
 \end{aligned} \tag{3.1}$$

From the results of the compression test for the springs it is concluded that the springs need to have a compression displacement of 10mm in order for the springs to work linearly. For this reason the springs in the experimental setup are pre-stressed and have a length of $23\text{cm} - 1.5\text{cm} = 21.5\text{cm}$.

3.1.2 Justification of setup

In order to finalize the design of the experimental test setup, a preliminary numerical model is designed. Next to the numerical model, several hand-calculations are performed in order to create a well structured experimental test setup. The numerical model is used to justify specifications of structural elements of the experimental test setup, such as the spring constant, and to extract preliminary results of dynamic characteristics of the setup. This model is discussed in Appendix C.

Several hand calculations are performed on the designed setup in order to check the structure's stability. Hand calculations are made to determine the maximum allowable dynamic load to the end of the steel strip. The maximum applied load is calculated by the means of the following the FKM guidelines (*Rechnerischer Festigkeitsnachweis für Maschinenbauteile*): $S_f = 0.40 \times F_{y1}(\text{N/mm}^2)$. In other words, the fatigue limit is equal to 40% of the tensile strength of the steel beam [39]. Within this calculation the self-weight of the steel beam is incorporated. Table 3.2 shows the results of the calculations with the self-weight of the strip. Figure 3.4 presents the load scheme of both load cases (self-weight and dynamic loading). Furthermore, the forces in the support are determined assuming all maximum loads are applied. The results for the calculations for the support are shown in Table 3.4. These results shows the maximum applicable loads in

order to not exceed the structures strength. All calculations are given in Appendix D. Appendix D also includes an analytical approach to find the preliminary results of the modal analysis for the experimental setup using Matlab. The analytical results of modal analysis setup coincides with the the results of the numerical modal analysis given in Appendix C.

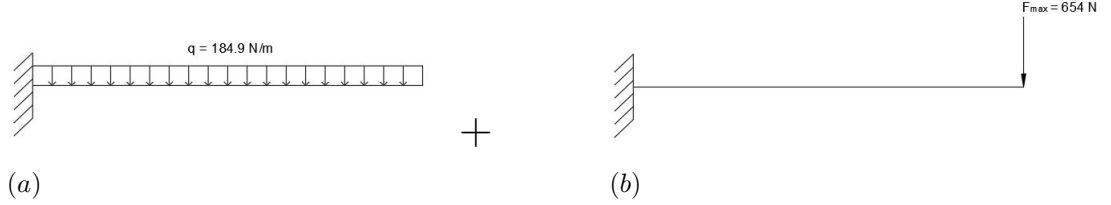


Figure 3.4: (a) Load-scheme of load-case self-weight and (b) load-scheme of load-case dynamic

Table 3.2: Results of hand calculations for steel beam due to self-weight

Load	Value	Unit
I	180000	mm^4
$q_{self-weight}$	184.9	N/m
$R_{support}$	369.8	N
$M_{support}$	369.8	Nm
$\omega_{self-weight}$	9.8	mm
$\sigma_{allowable}$	200	N/mm^2
σ_{max}	30.8	N/mm^2

Table 3.3: Results of hand calculations for the support of the experimental setup due to dynamical loading

Load	Value	Unit
S_f	144	N/mm^2
$\sigma_{max,dynamic}$	113.2	N/mm^2
$M_{support}$	1358.4	Nm
$F_{max,dynamic}$	679.2	N
$mass$	69.2	kg
$\omega_{dynamic}$	47.9	mm

Table 3.4: Results of hand calculations for determining loads inside the support of the experimental setup

Load	Value	Unit
F_{tot}	1049	N
M_{tot}	2716.8	Nm
F_{spring}	6792	N

3.2 Sensors

The sensors used for the experimental setup are accelerometers and strain gauges. Accelerometers are used to measure the accelerations of the steel beam and the strain gauges are used to measure the strains of the steel beam. The surface of the steel beam is sanded and cleaned before the sensors are glued to the beam. The glue used to attach the sensors to the steel surface is *M-Bond 200 Adhesive* glue. All sensors are wired to the hardware of the measurement system. Specifications of the sensors are shown in Table 3.5. Figure 3.6(a) shows Accelerometer 1 and Figure 3.6(b) shows Strain gauge 4 mounted to the steel beam.

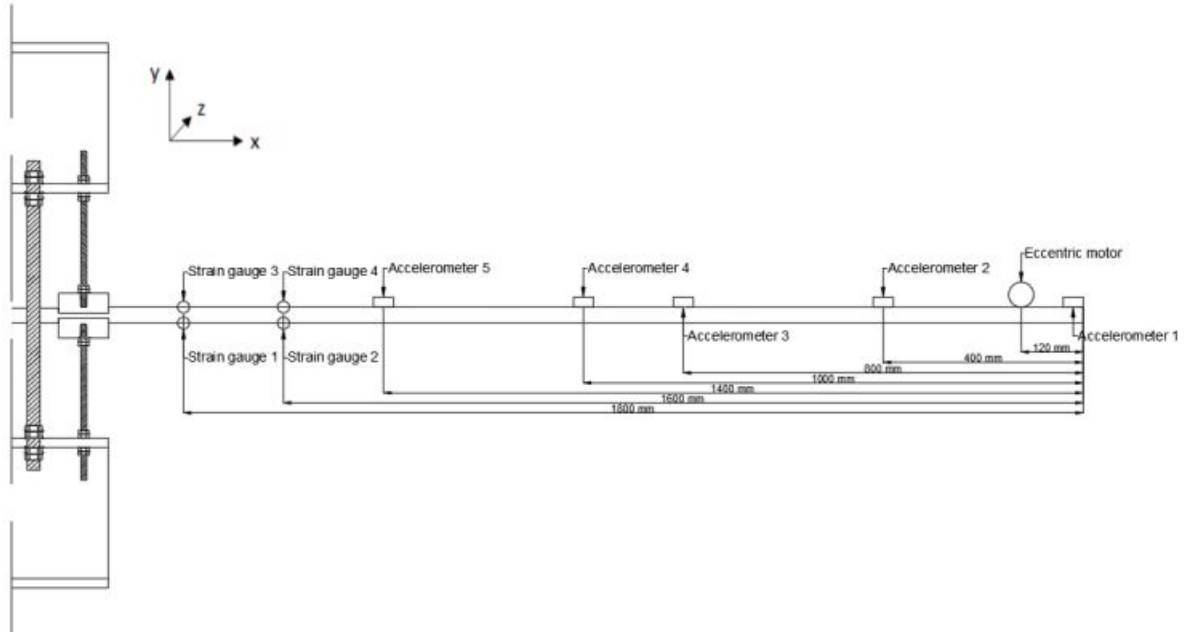


Figure 3.5: Experimental setup including sensors and eccentric motor

Table 3.5: Specifications of used sensors

Name	Maximum range	Measuring axis
Accelerometer 1 352014	5G ($50m/s^2$)	z-axis
Accelerometer 2 352003	5G ($50m/s^2$)	z-axis
Accelerometer 3 352000	5G ($50m/s^2$)	z-axis
Accelerometer 4 352015	5G ($50m/s^2$)	z-axis
Accelerometer 5 352002	5G ($50m/s^2$)	z-axis
Strain gauge 1 (350Ω)	$\pm 752MPa$	x-axis
Strain gauge 2 (350Ω)	$\pm 752MPa$	x-axis
Strain gauge 3 (350Ω)	$\pm 752MPa$	x-axis
Strain gauge 4 (350Ω)	$\pm 752MPa$	x-axis

3.2.1 Accelerometers

Piezoresistive accelerometers are used to measure accelerations on the beam. As the first three natural frequencies of the structure are analyzed, the accelerometers are placed such that the accelerations of the first three mode shapes of the structure are measured. It follows from analytical calculations performed in Matlab that the first three mode-shapes are given as in Figure 3.7. Figure 3.7 also shows the locations of the five accelerometers in squared boxes on the line $y = 0$ as placed on the beam. The accelerometers placed according to Figure 3.7 are schematically shown on the experimental setup in Figure 3.5 and a visualisation of the sensors applied to the experimental setup is shown in Figure 3.12 (a) and Figure 3.12 (d). The accelerometers are positioned where the deflection of the beam is maximal and hence the accelerations are maximal as well. For example, accelerometer 4 is placed at a node for mode-shape 3, for this reason accelerometer 4 will have less contribution to the measurement of the third natural frequency. However this accelerometer is also at the anti-node of mode shape two, and is therefore expected to contribute more to the measurement of the second natural frequency.

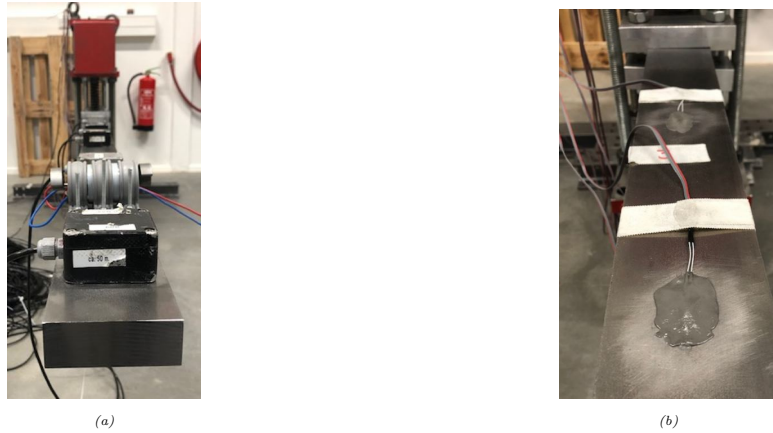


Figure 3.6: (a) Accelerometer 1 and (b) Strain gauge 4

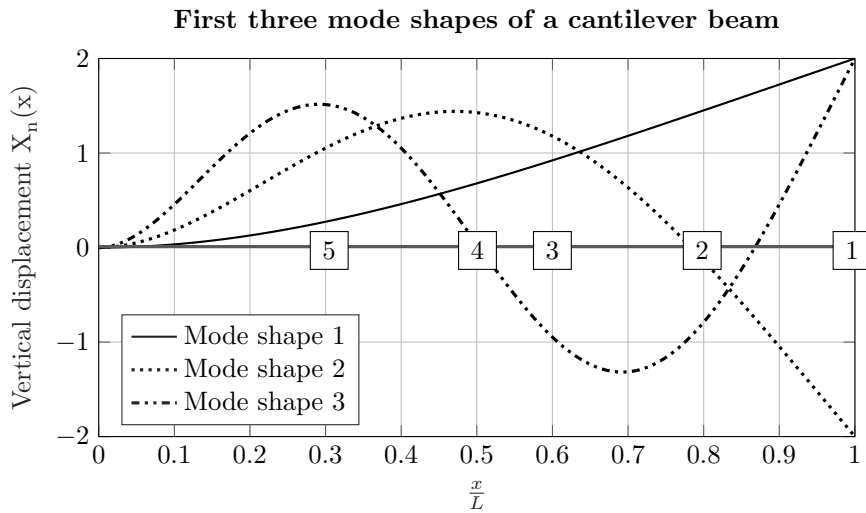


Figure 3.7: The first three mode shapes of a cantilever beam and the locations of accelerometers on the line $y = 0$

3.2.2 Strain gauges

Four pre-wired strain gauges are applied to the steel beam with an adhesive glue. The strain gauges have a gauge length of 10mm, a resistance of $350\Omega \pm 0.35\%$ and a gauge factor of $2.04 \pm 1.0\%$. The strain gauges are located close to the support of the strip, where the highest strains are expected to occur. The sensors are located such that one strain gauge measures the tension and another strain gauge measures the compression of the steel strip. Figure 3.5 shows the locations of the strain gauges. Specifications of the sensors are given in Table 3.5.

3.3 Performed tests

The experimental setup has three different cases at which the tests are performed. Case 1 is where three aluminum block supports are attached to the steel beam, case 2 is where two aluminum blocks are attached to the steel beam, and case 3 is where one aluminum block is attached to the steel beam. Figure 3.8 is a schematic representation of all cases analyzed for the experimental setup.

Two tests are performed in order to provide measurements for a modal analysis and a harmonic

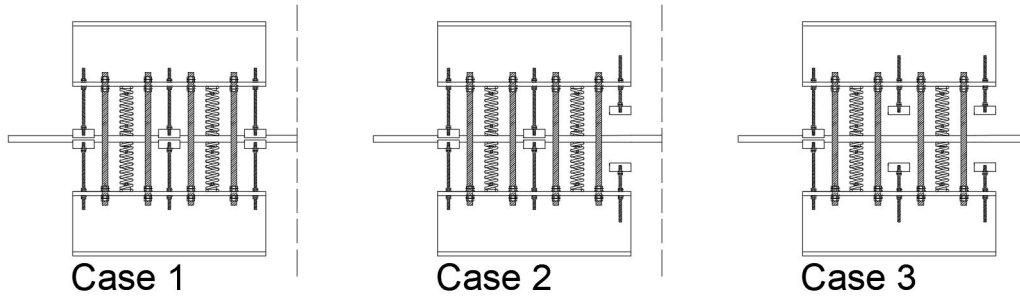
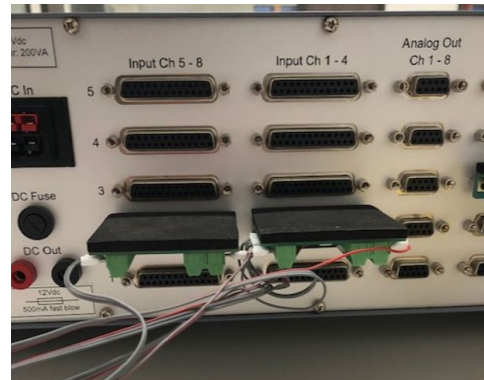


Figure 3.8: The three different stiffness cases schematically presented

analysis. An impact test is performed to obtain measurements for a modal analysis and a forced vibration test is performed to obtain measurements for a harmonic analysis. The measurement system used for the receiving signals from the applied sensors is the H&R Measurement System. This measurement system has an ethernet connection to the hardware to which the sensors are connected. The measurement system interprets the hardware and shows the output signals of the strain gauges and accelerometers. The accelerometers are wired to the hardware system as shown in Figure 3.9(a). Within the measurement system the strains are automatically transformed to stresses, therefore the output measurement from the strain gauges have the unit MPa . The output measurements of the accelerometers have the unit m/s^2 . The strain gauges are wired to the hardware system as shown in Figure 3.9(b).



(a)



(b)

Figure 3.9: (a) Wired accelerometers to the hardware system and (b) Wired strain gauges to the hardware system

3.3.1 Impact test

To identify the structural dynamic response of the test setup, regarding a reduction in support stiffness, an impact test is performed. An impact test is done by the means of applying a small impulse load to the end of the slender beam, to excite all modes of vibration with equal energy. The impact at the end of the slender beam is induced by a hammer strike. It is important to note that the currently performed impact test does not measure the impact given by the hammer strike, in other words, no input is measured. Due to the deformation of the structure, caused by the hammer strike, the accelerometers and strain gauges will measure accelerations and strains, respectively over a certain time period. Before every measurement starts the sensors are balanced in order to reduce external contributions to the accelerations and strains, such as gravity. Table 3.7 describes the measurement settings in order to obtain correct measurements. The sample frequency is chosen by the means of the theory explained in Chapter 2.

Table 3.6: System settings for impact test

Setting	Description	Value
Measurement length	Measuring time in seconds	300s
Filter frequency	Cut off frequency	500Hz
Sample frequency	How many data points measured per second	1000Hz

Post processing

The identification of the structures dynamic response is done by means of a modal analysis. The modal analysis can be performed with the Peak Picking method, assuming that the natural modes of the structure are well separated in their frequency domain. The output signal obtained from the acceleration sensors needs to be modified in order to be able to extract correct results for the natural frequencies with the Peak Picking method.

Primarily it is important to ensure that all sensors have a minimum offset. Therefore an averaging of the signal is applied to reduce the offset of certain accelerometers. It is also important to frame the measurement for the steady response time period, as a steady state of the structure is considered.

In order to reduce the noise contribution to the power spectral density a low pass filter is applied. This low pass filter is obtained following Equation 3.2. Where f_{filter} is the applied low pass filter and f_{max} the maximum frequency to be analyzed.

$$f_{\text{filter}} = 1.2 \times f_{\text{max}} \quad (3.2)$$

After the low pass filter is applied, a Fast Fourier Transformation is made in order to analyze the measurements in the frequency domain. The number of FFT points ($n.f.f.t.$) used are $nfft = f_s \times \text{time measured}(s)$, and a Hamming window is applied to reduce leakage of data. The measurement in the frequency domain is analyzed and the peaks of the results are found to be the natural frequencies of the structure. Figure 3.10 is a schematic representation of the post processing for the impact test measurements. The results of the impact test are given in Chapter 5.

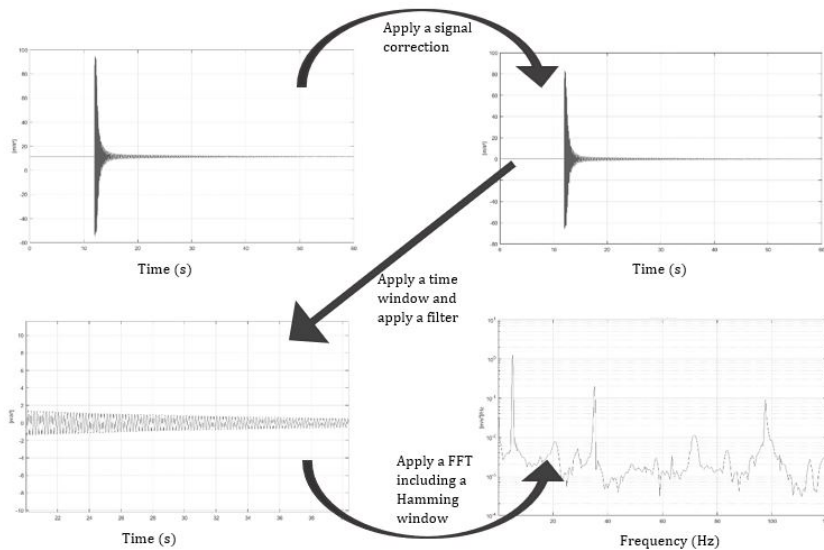


Figure 3.10: Schematic overview of post processing of measurement from impact test. The first step is to reduce the offset of the output signal. The second step is to apply a time window and a low-pass filter frequency. The third step is to apply an FFT with a Hamming window

Table 3.7: Post processing settings for impact test

Setting	Description	Value
Time window	Window for length of measurement in seconds	15s
Low pass filter	Cut off for higher frequency	120Hz
<i>n.f.f.t</i>	Number of Fast Fourier points used for transformation	15000

3.3.2 Forced vibration test

The second part of testing is applying a harmonic load to the steel beam. The harmonic analysis of the experimental test setup is used get insight in the relation between the fatigue life of the experimental setup and the fatigue life of the numerical model. When this relation is obtained, it is possible to predict the fatigue life of the experimental setup according to the numerical model. The harmonic load applied to the experimental test setup is induced by an eccentric motor. It is possible to control the vibration speeds of the motor. The eccentric motor will start to rotate when it is turned on, and as mentioned before, the accelerometers and strain gauges will measure respectively accelerations and strains of the structure. The measurements obtained from these tests are analyzed for the stresses occurring in the structure.

Figure 3.11 shows a picture of the eccentric motor that is used. The eccentric motor is connected to a voltage controlled power supply. The eccentric motor has a speed of 4000RPM in the unloaded condition at 12V. The power supply is connected to the hardware of the measurement system. The harmonic analysis is done for 10 measurements varying from 2V to 11V. The magnitude of the harmonic load depends on the rotation frequency and the magnitude of the eccentric masses. The eccentric masses on the eccentric motor can easily be calculated from the dimensions of the eccentric motor given in Figure 3.11 and Equation 3.3.

$$m = \rho \times t \times \pi r^2 * \frac{1}{2} \qquad 7.85 \times 1.3 \times \pi 1.8^2 \times \frac{1}{2} = 50g \qquad (3.3)$$

Where m is the mass (g), ρ is the density of steel (g/cm^3), t is the thickness of the eccentric mass (cm) and r is the radius of the eccentric mass (cm).

The measurement settings used for the harmonic measurements are given in Table 3.8.

Table 3.8: System settings for forced vibration test

Setting	Description	Value
Measurement length	Measuring time in seconds	60s
Filter frequency	Cut off frequency	500Hz
Sample frequency	How many data points measured per second	1000Hz

Post processing

For the post processing of the harmonic analysis the frequency at which the eccentric motor rotates needs to be considered. This frequency is assumed to correspond with the highest peak in the FFT of the measurement. The harmonic analysis is done for Strain gauge 3 and Strain gauge 4.

In order to reduce the contribution of other frequencies and noise to the stress amplitudes at the frequency of the rotating eccentric motor, a band-pass filter is applied. The band-pass filter is applied for $\pm 20\%$ of the frequency at which the eccentric motor rotates. After the band-pass filter is applied, the signal is analysed with respect to the stress amplitude (σ_a), using Equation 3.4. After the amplitude is found for both strain gauges, it is determined whether signals of the strain gauges are in or out of phase, in order to assume the correct \pm sign to the measured strain.

$$\sigma_a = \frac{\sigma_{max} - \sigma_{min}}{2} \qquad (3.4)$$

In order to be able to compare the occurring strains in the experimental setup with the occurring strains of the numerical model, the measured stresses are converted to strains (ϵ) by the following equation

$$\epsilon = \frac{\sigma}{E} \quad (3.5)$$

Where E is the Young's modulus of the steel beam.



Figure 3.11: The eccentric motor with dimensions used for vibration testing [12]

3.4 Visual representation of setup

This section includes a visual representation of the experimental setup. Figure 3.12 (a) shows the complete setup including the applied sensors. Figure 3.12 (b) presents a front view of the support structure and the top two strain gauges. Figure 3.12 (c) shows the first aluminum block supports which are attached to the beam. Figure 3.12 (d) is a side view of the experimental setup.



(a)



(b)



(c)



(d)

Figure 3.12: A visual representation of the experimental setup where (a) is a front view (b) is the support structure (c) is the aluminum support and (d) is a side view of the experimental test setup

Next to the experimental test setup, a numerical model is created. The numerical model is a representation of the experimental test setup, and is used to mimic the dynamic response of the structure. For this reason parameters of the experimental setup, such as spring stiffness and structural dimensions, are used as input for the numerical model. A modal analysis is done in order to validate the correctness of the numerical model regarding the dynamic response in steady state compared to the results of the modal analysis on the experimental setup. A harmonic analysis is done to find a relation between the fatigue life of the numerical model and the experimental setup.

The numerical model is built in the finite element software ANSYS. In order to enhance model flexibility it is chosen to make use of the ANSYS Parametric Design Language (APDL). This script is used to build, solve and post process the results of the FE model. In this chapter the numerical model and its analysis are explained. Modeling OWT structures by the means of finite element modeling must follow the steps of pre-processing, solution and post-processing. In general the pre-processing includes defining the geometry and material properties of the structure, the solution step includes defining loads, boundary conditions and the calculation itself, and the post-processor includes obtaining the results, which can be visualized and analyzed. The file containing the model is called *Right-ANSYS-model.mac* and will also be used for the optimization methodology explained in Chapter 6.

4.1 Pre-processor

During the pre-processing the geometry and material properties of the structure are defined. The geometry and material properties of the structure are both parametric. The variables for parametrization of the model are written in a different file, which is called upon in the APDL macro code.

4.1.1 Keypoints and lines

The numerical model is made regarding the experimental test setup. Therefore the model is defined by means of beam elements and spring elements. Prior to defining the beam and spring elements, the structure is created by keypoints and lines. These keypoints are generated by a

```

K,1000,x1,0,0,!Keypoint start of the beam
K,2000,x2,0,0, !Keypoint end of the beam

*DO,i,0,n1-1,1 !Keypoints for springs
K,3000+i,d1+i*d2,0,0
K,4000+i,d1+i*d2,y1,0
K,5000+i,d1+i*d2,-y1,0
*ENDDO

*DO,i,0,n2-1,1 !Keypoints for alluminium blocks
K,6000+i,i*d2,0,0
K,7000+i,i*d2,y2,0
K,8000+i,i*d2,-y2,0
*ENDDO

```

Figure 4.1: Generating keypoints in APDL macro code

'*DO'-loop as shown in Figure 4.1. Keypoints are placed at the start and end of the beam, and at the locations of the springs and block supports. Similarly, lines are created between the keypoints by the means of a '*Do'-loop.

4.1.2 Elements and material properties

After the structure is defined, the element sizes are chosen. There are 100 beam elements representing the steel strip in the experimental setup. Therefore the element size of the beam elements is $L/100$. The springs and blocks exist of 1 element. Material properties are assigned to the lines with the **LATT** command.

Beam elements

The elements modelled in the APDL macro code are BEAM188 elements and COMBIN14 elements. The BEAM188 element is a two node beam, which is suitable for analyzing slender and thick beam structures. The BEAM188 element is based on the first-order shear-deformation theory of Timoshenko, which implicates that it takes the effect of bending deformations and shear deformations into account. The beam is modelled as a one-dimensional line element parallel to the X-Z-plane. The beam elements are modelled as linear elastic elements, because the loads that are applied to the beam are all within the linear elastic range of the steel material [40]. The cross-sectional data is provided with the command **SECDATA** and the command **SECTYPE**. The cross-section data and material properties are coded as parameters in the file *parameter.inp*, which can be changed regarding the design of the experimental setup. The *parameter.inp*-file is shown in Figure 4.4. Figure 4.2 shows the cross section of the BEAM188 element with its local coordinate system.

Spring elements

The springs are modelled as COMBIN14 elements. The COMBIN14 element is a spring-damper element with longitudinal and torsional capabilities in 1-D, 2-D and 3-D. In this numerical model the spring-damper is only used as longitudinal compression-tension element, which means that this element neglects torsion and bending displacements. Input data for COMBIN14 elements are a spring constant (k) and damping coefficient (C_v). For a longitudinal spring damper the unit of the spring constant (k) is *Force/Length* and the unit of the damping coefficient is *Force* \times *Time/Length* [40].

The value for the springs constant for the springs is determined regarding the experimental test setup. Damping is not regarded in this numerical model, therefore the damping has not been given a value.

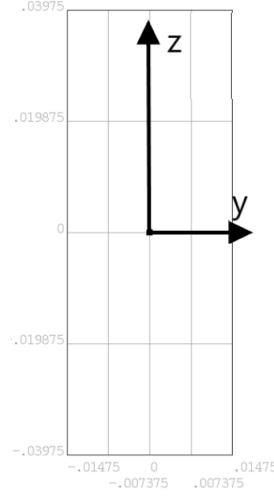


Figure 4.2: Cross section of BEAM188 element with local coordinate system

Aluminum block elements

Ideally the aluminium blocks function as a perfect clamping for the steel strip with an infinite stiffness in the vertical direction. However aluminium is a relatively soft material, the stiffness of aluminium is far from infinite. The steel rods attached to the aluminium blocks are also not perfectly fixed to the aluminium blocks and profiles on the top and bottom of the experimental setup. Therefore the steel rods also cause some imperfection to the supporting of the steel strip. For this reason, the aluminium blocks and steel rods are modelled as one COMBIN14 element. The springs stiffness used for these COMBIN14 elements is determined by the size and the elastic modulus of the aluminium blocks and steel rods. A schematic representation of the determination of the springs stiffness for the COMBIN14 elements is given in Figure 4.3.

The stiffness of the steel rods ($K1$) is calculated following equation 4.1 with A is the stress area, E is the elastic modulus of the steel material and l is the length of the steel rods. The stiffness of the aluminium blocks ($K2$) is calculated by the means of equation 4.2 with A is the area of the block, E is the elastic modulus of the aluminium material and t is the thickness of the block. The total spring stiffness used for the numerical model follows from equation 4.3. The spring stiffness used for the COMBIN14 element is $K = 31.8 * 10^7 N/m$.

$$K1 = \frac{A_{stress} * E}{l} \rightarrow \frac{1.57 * 10^{-4} m^2 * 2.1 * 10^{11} N/m^2}{0.2m} = 16.5 * 10^7 N/m \quad (4.1)$$

$$K2 = \frac{A * E}{t} \rightarrow \frac{4.8 * 10^{-3} m^2 * 70 * 10^9 N/mm^2}{0.04m} = 850 * 10^7 N/m \quad (4.2)$$

$$\frac{1}{K} = \frac{1}{2 * K1} + \frac{1}{K2} \rightarrow \frac{1}{2 * 16.5 * 10^7 N/m} + \frac{1}{850 * 10^7 N/m} = \frac{1}{31.8 * 10^7 N/m} \quad (4.3)$$

4.1.3 Parameters

As mentioned previously the variables for parametrization are written in a *parameter.inp* file. The parameters defined in this file are the material properties and the geometry of the structure. The variables and their values defined in the *parameter.inp* file are given Figure 4.4.

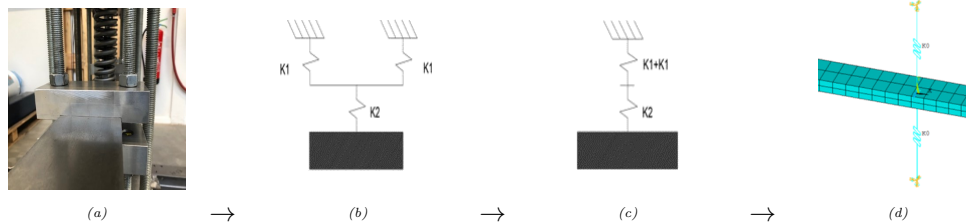


Figure 4.3: (a) Aluminum blocks supporting the steel strip in the experimental test setup; (b) Schematic representation of the aluminum blocks and steel rods; (c) Schematic representation of the calculation for the spring stiffness of the COMBIN14 element; (d) COMBIN14 element in the numerical model

```

!==== Defining parameters ====

T=0.0295 !Thickness of beam (m)
W=0.0795 !Width of beam (m)

L=3.1 !Length of beam (m)
Ls=0.8 !Length of the support

E=2.1e11 !Elastic modulus (N/m^2)
rho=7850 !Density (kg/m^3)
v=0.3 !Poisson ratio

k1=656000 !Stiffness of springs (N/m)
k2=317390000 !Stiffness of alluminium (N/m)

d1=0.2 !Distance between springs and alluminium blocks (m)
d2=0.4 !Distance between alluminium blocks (m)

n1=2 !Number of springs (>0)
n2=1+Ls/d2 !Number of alluminium blocks

x1=-0.3 !Distance at the end of the beam (after support) (m)
x2=2.8 !End of the beam
x3=0 !Location of first alluminium clamping
x4=x3+d2 !Location of second alluminium clamping
x5=x4+d2 !Location of third alluminium clamping
x6=x3+d1 !Location of first spring
x7=x4+d1 !Location of second spring

y1=0.23 !Length of the springs (m)
y2=0.226 !Length of alluminium block support (m)

```

Figure 4.4: parameter.inp file APDL macro code

4.2 Solution

The solution step consist of boundary conditions, loading conditions and analyses. The boundary conditions for the numerical model mainly consists of constraints

The goal of this model is to validate the use of the experimental test setup. For this reason two analyses are defined during the solution step. The first analysis is a modal analysis and the second analysis is a transient analysis.

4.2.1 Boundary conditions

Figure 4.5 shows the boundary conditions which are used for the numerical model as a schematic representation of the experimental model. At the end of each COMBIN14 element the nodes are rigidly constrained. Due to the structural elements which keep the springs in its place, referred to as 'spring supports', these nodes are constrained for displacement in the axial and the transverse direction of the beam. At the locations of the aluminum block supports the nodes are constrained for displacement in the transverse direction. Due to the size of the aluminum block supports, it is assumed that torsional rotations do not occur in those nodes. Therefore torsional constraints are applied to these nodes. The commands used for applying the boundary conditions are shown in

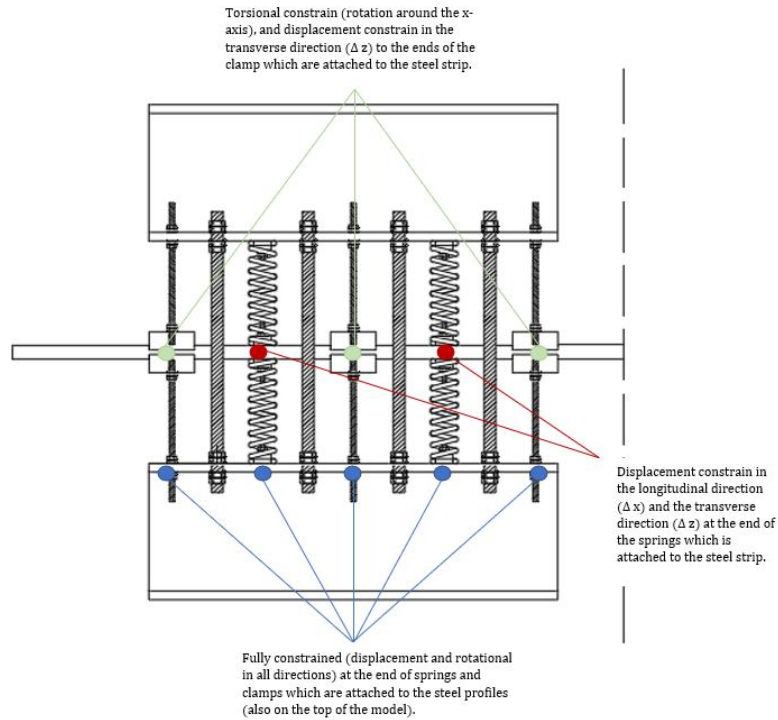


Figure 4.5: Boundary conditions visualised in the experimental setup

Figure 4.6.

4.2.2 Modal analysis

The modal analysis for the numerical model is reported for the first 4 modes of the structure below $1000Hz$. The results of the modal analysis are given in Chapter 5. Figure 4.7 show the commands used for the modal analysis of the numerical model. This analysis is done for all three cases of the state of support structure described in Chapter 3.

```

KSEL,s,loc,y,y1 !Fixed BC's for end of the alluminium block/springs
KSEL,a,loc,y,-y1
KSEL,a,loc,y,y2
KSEL,a,loc,y,-y2
DK,ALL,,,,ALL,,,,,

CMSEL,NONE
*DO,i,0,n1-1,1 !Constrain in the x-,z-direction (for the springs)
KSEL,s,KP,,3000,3000+i
DK,ALL,,,,0,UX,UZ,,,,
*ENDDO

CMSEL,NONE !Constrain in the z,x,rotx-direction (for the alluminium blocks)
*DO,i,0,n2-1,1
KSEL,s,KP,,6000,6000+i
DK,ALL,,,,0,UX,UZ,ROTX,,,
*ENDDO
    
```

Figure 4.6: Commands for the application of boundary conditions


```

/SOL !Solving the system by doing a Modal Analysis
ANTYPE,2

MODEOPT,LANB,4 !How many modes to we want to compare
EQSLV,SPAR
MXPAND,0,,0
LUMPM,0
PSTRES,0

```

Figure 4.7: Commands for the application of modal analysis

```

!==== Harmonic analysis ====
/SOL !Solving the system by doing an harmonic analysis
ANTYPE,HARMIC
hropt, full
hrout, off
outpr, basic, 1
HARFRQ,0,150,
NSUBST,150,
KBC,0

/STATUS,SOLU

outres,all,all

SOLVE

```

Figure 4.8: Commands for the application of harmonic analysis

4.2.3 Harmonic analysis

The harmonic analysis is applied with a unit load for $0Hz - 150Hz$. The commands used for such an analysis are given in Figure 4.8. This analysis is done for all three cases of the state of support structure described in Chapter 3.

4.3 Post-processor

For the modal analysis the natural frequencies are analyzed as well as the mode shapes. The natural frequencies are put into a list and with the ***GET** command these results can be exported to another file. Chapter 6 elaborates further on exporting and analyzing the results for the modal analysis of the numerical model.

The post processing of the harmonic analysis is done for elements at the locations of strain gauge 3 and strain gauge 4 (Figure 3.5). The strains of the top of these elements are analyzed for the same frequency range on which the forced vibration tests are applied to the experimental setup, from $9Hz$ up to $60Hz$. It is important to highlight that when extracting strain results for certain elements, the local axis of the elements is used. This could cause confusion when the local axis is defined differently from the global axis. Figure 4.2 shows the local axis of the beam elements, for this reason the strains of the elements are extracted in the direction of the local y-axis. Figure 4.9 presents an example of strain results for the elements at the locations of strain gauge 3 and strain gauge 4. The strain results for the harmonic analysis are exported to a .txt file, where further analysis can be performed. The commands used for post-processing of the harmonic analysis are presented in Figure 4.10.

As mentioned previously the harmonic analysis is done with a unit load. For this reason the strain results of the elements need to be scaled to the harmonic force applied during the forced vibration testing on the experimental setup. The following equation is used to determine the centrifugal force applied during the forced vibration testing

$$F_c = (f \times 2\pi)^2 \times m \times r \quad (4.4)$$

Where F_c is the centrifugal force (N), f is the applied frequency (Hz), m is the eccentric mass

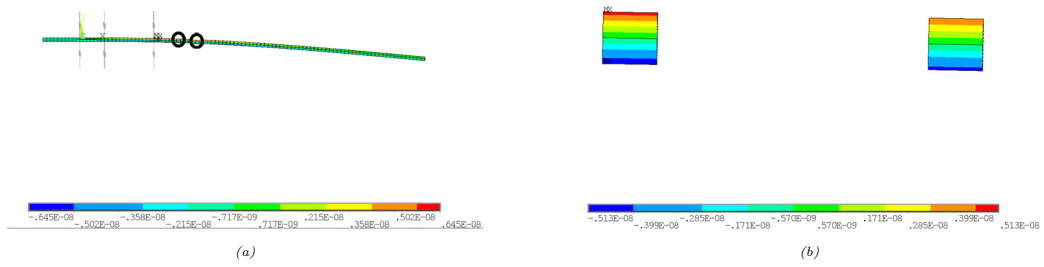


Figure 4.9: Harmonic analysis for strains in (a) numerical model and (b) at location of strain gauge 3 and strain gauge 4 of experimental setup

```

!==== Extract strain results ====
/POST1

CMSEL,NONE
ESEL,S,CENT,x,1.05
ESEL,A,CENT,x,1.24
/REPLOT

*CFOPEN,Strain_results,txt,,
*DO,i,1,150

VAR1=%i%
SET,1,%i%,1,0,, !load a solution step
ETABLE,ESA,sMISC,42 !->EPELbyt = Strain bending around global z-axis and local y-axis

*GET,strain_%i%,ELEM,45,ETAB,ESA
*GET,strain2_%i%,ELEM,51,ETAB,ESA

*VWRITE,VAR1,strain_%i%,strain2_%i%,
(F8.1,'',2X,E13.5,'',2X,E13.5)
*ENDDO

*CFCLOSE
    
```

Figure 4.10: Commands for post-processing of the harmonic analysis

in kg and r is the radius of the rotating eccentric mass in m . The results of these forces are presented in Appendix H.

This chapter presents the results of the modal analysis and the harmonic analysis performed using both the experimental setup and the numerical model.

5.1 Modal analysis

To investigate the dependence of the dynamic response using the stiffness of the support structure a modal analysis is performed using the experimental setup. The modal analysis is done by performing an impact test on the structure. Note that for this impact test the input has not been measured and therefore the amplitude of vibration cannot be measured either. Next to the modal analysis with the experimental setup, a modal analysis using the numerical model of the setup has been conducted as well. At the end of the chapter a comparison between the modal analysis of the experimental setup and the numerical model is provided.

5.1.1 Experimental setup

Figure 5.1, Figure 5.2 and Figure 5.3 show the output signals of accelerations in the frequency domain after the impact test on the experimental setup. Note that the output is presented on a logarithmic scale. The graphs show that the peaks are well separated, three peaks are visible representing the first three natural frequencies, and therefore the Peak Picking method can be applied to find the natural frequencies of the experimental setup. By performing the Peak Picking method the natural frequencies of each state of the support structure is obtained. Case 1 presents the state where three aluminum supports are attached to the beam, Case 2 presents the state where two aluminum supports are attached to the beam and Case 3 presents the state where one aluminum support is attached to the beam. The results of the Peak Picking method are shown in Table 5.1.

Table 5.1: First three natural frequencies of experimental model for different states of support structure

Mode	Case 1	Case 2	Case 3
Mode 1	5.36Hz	3.73Hz	2.63Hz
Mode 2	35.00Hz	23.73Hz	17.20Hz
Mode 3	96.80Hz	68.67Hz	46.40Hz

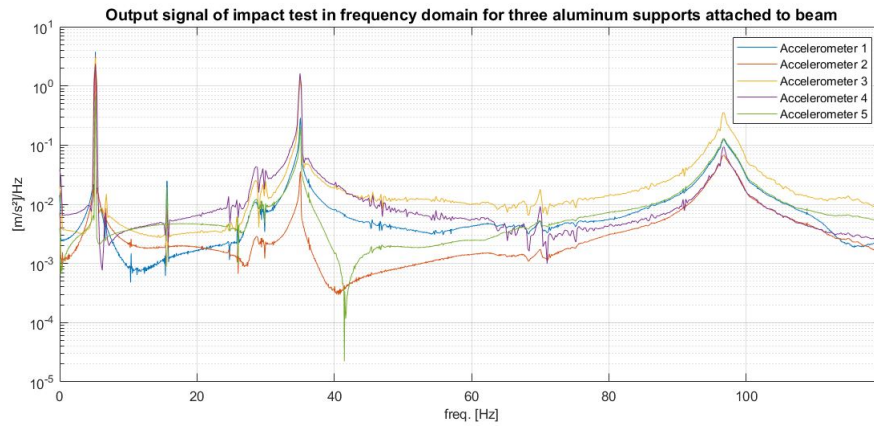


Figure 5.1: Modal analysis Case 1

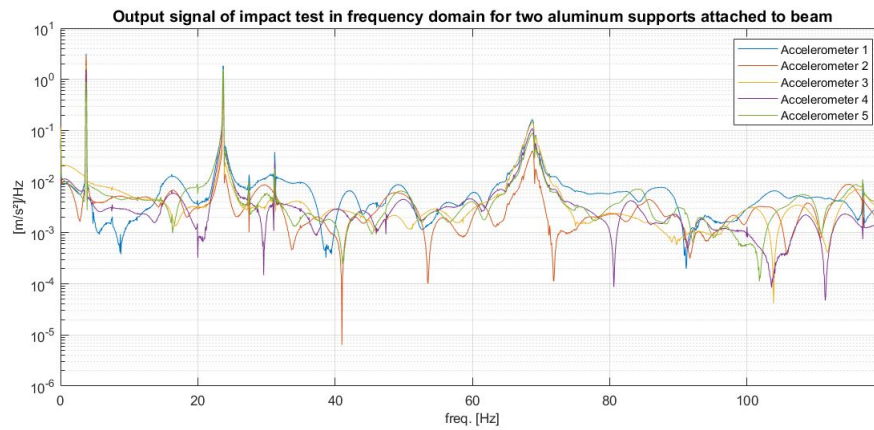


Figure 5.2: Modal analysis Case 2

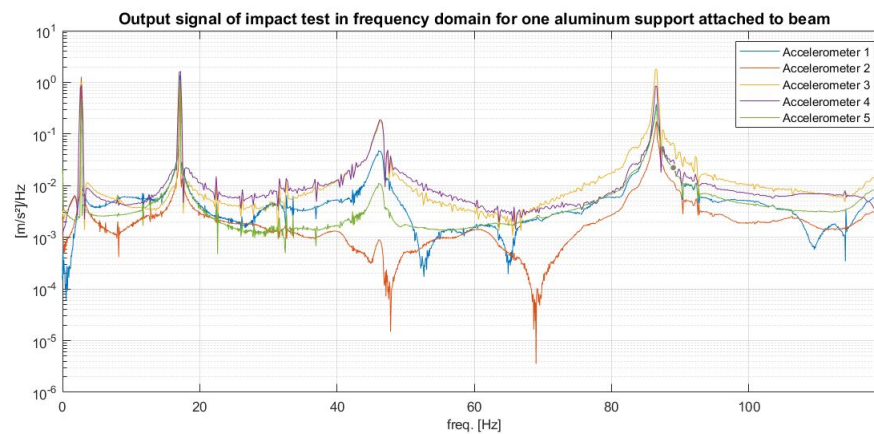


Figure 5.3: Modal analysis Case 3

5.1.2 Numerical model

The following results are obtained by performing a modal analysis with the numerical model developed in ANSYS. Figure 5.4, Figure 5.5 and Figure 5.6 show the modes obtained from a FEA for Case 1, Case 2, and Case 3 of the states of the support structure, respectively. The natural frequencies of the structure for the three different cases of the support structure are presented in Table 5.2.

Table 5.2: First three natural frequencies of numerical model for different states of support structure

Mode	Case 1	Case 2	Case 3
Mode 1	5.53Hz	3.88Hz	2.56Hz
Mode 2	35.24Hz	24.66Hz	16.80Hz
Mode 3	99.62Hz	69.55Hz	45.43Hz

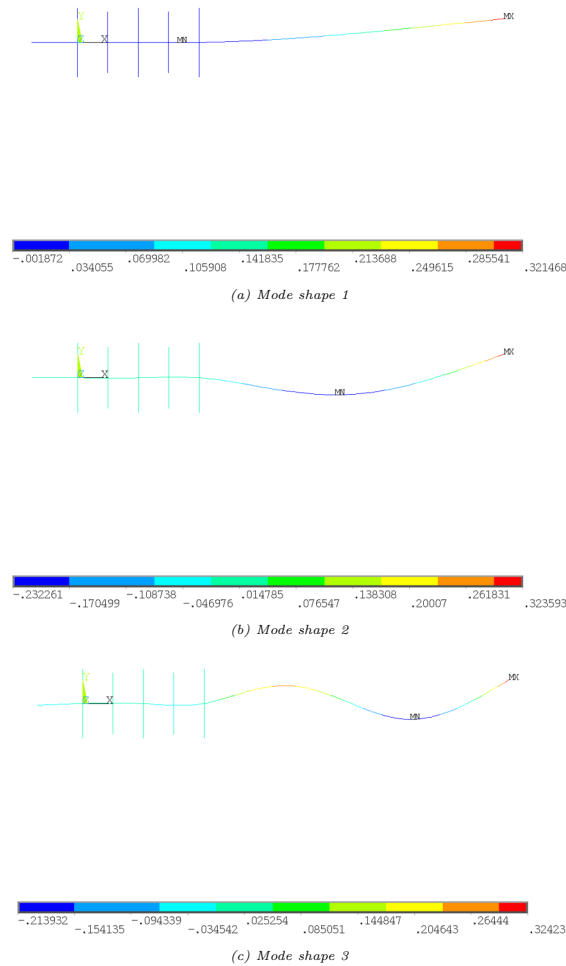


Figure 5.4: Mode shapes for Case 1 of state of the support structure [m/m]

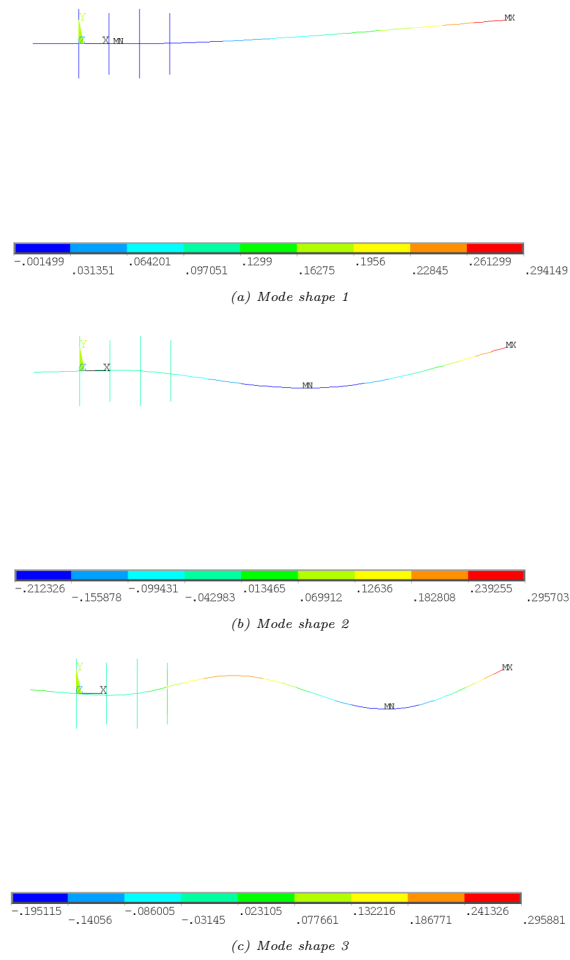


Figure 5.5: Mode shapes for Case 2 of state of the support structure [m/m]

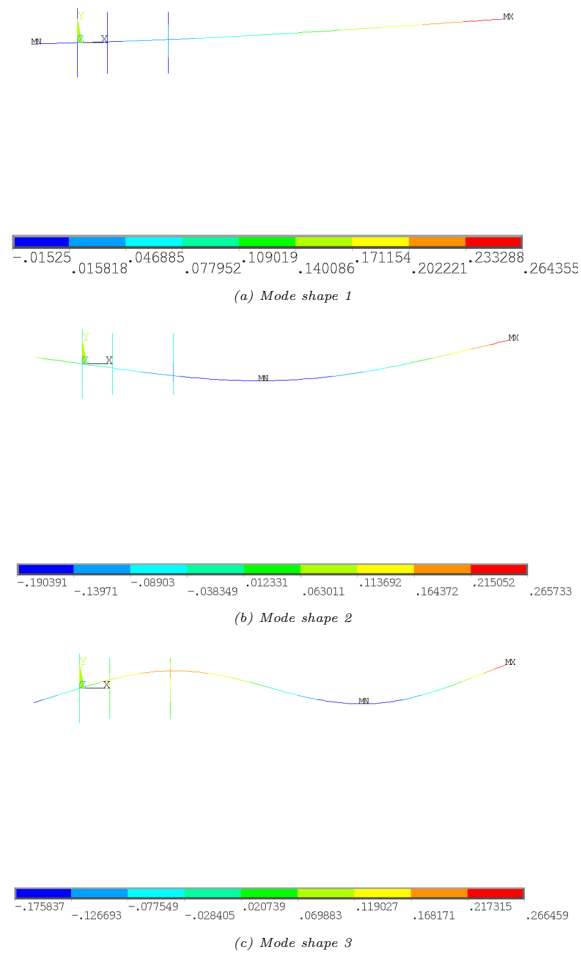


Figure 5.6: Mode shapes for Case 3 of state of the support structure $[m/m]$

5.1.3 Discussion

The output measurements of accelerations presented in the frequency domain clearly show the peaks of the first three natural frequencies of the experimental setup. The results show a decrease in natural frequencies when more aluminum supports are released. In other words the natural frequencies of the structure decrease when the stiffness of the support structure decreases. Figure 5.3, presenting the modal analysis for Case 3, shows a fourth peak at $86.40Hz$. This peak coincides with the fourth mode of the numerical model of Case 3, which determines the fourth natural frequency to be at $88.71Hz$. Thanks to the well presented natural frequencies of the experimental setup after applying a modal analysis, it is possible to compare the natural frequencies with the results of the modal analysis for the numerical model.

A comparison of the experimentally determined results and the numerical results is shown in Table 5.3, Table 5.4 and in Table 5.5 for Case 1, Case 2 and Case 3 respectively. These tables show the error between each mode of each case between the natural frequency of the experimental setup and the numerical model. The error is calculated following the true values of the experimental setup, and therefore obtained by $((numerical - experimental)/experimental) \times 100\%$. In Case 1 and Case 2 the numerical model shows higher natural frequencies than the experimental model. This difference can be explained as follows. It is expected that the aluminum supports do not clamp the beam perfectly, *i.e.*, with infinite stiffness. In that case the supports are not strongly tightened to the steel beam and there might be some space for deflection in the lateral direction of steel beam. In other words, the aluminum supports will have a reduction in supporting stiffness in the lateral direction of the steel beam.

For case 3 the experimentally determined natural frequencies are higher than the natural frequencies of the numerically determined ones. This could be due to the difference in stiffness of the springs attached to the steel beam. Figure 5.6 shows the mode shapes of the corresponding natural frequencies of the numerical model. It can be seen that the second spring has a large deflection in its axial direction. This large deflection might be caused by the fact that the spring stiffness of the springs is not high enough to support the deflections of the steel beam. This results in a lower natural frequency of the model. However, these larger deflections of the springs are not observed in the experimental setup. Therefore it can be concluded that the spring stiffness given to the springs in the numerical model, are lower than the spring stiffness of the springs in the experimental model. This difference in stiffness can be caused for example by a difference in interaction of the springs and the steel beam, or due to the the pre-stress given to the springs in the experimental model.

Despite the structural differences of the experimental setup and the numerical model, causing a difference in natural frequencies, the error remains very small, below 4%. For this reason it is still possible to validate the correctness of the numerical model regarding the steady state response of the experimental model. Therefore it is possible to analyse the state of the support structure of the experimental setup considering only output measurements of accelerations with the numerical model.

Table 5.3: Comparison of modal analysis for Case 1

Mode	Experimental model	Numerical model	Error
Mode 1	$5.36Hz$	$5.53Hz$	3.1%
Mode 2	$35.00Hz$	$35.24Hz$	1%
Mode 3	$96.80Hz$	$99.62Hz$	2.8%

Table 5.4: Comparison of modal analysis for Case 2

Mode	Experimental model	Numerical model	Error
Mode 1	3.73Hz	3.88Hz	3.9%
Mode 2	23.73Hz	24.66Hz	3.8%
Mode 3	68.67Hz	69.55Hz	1.3%

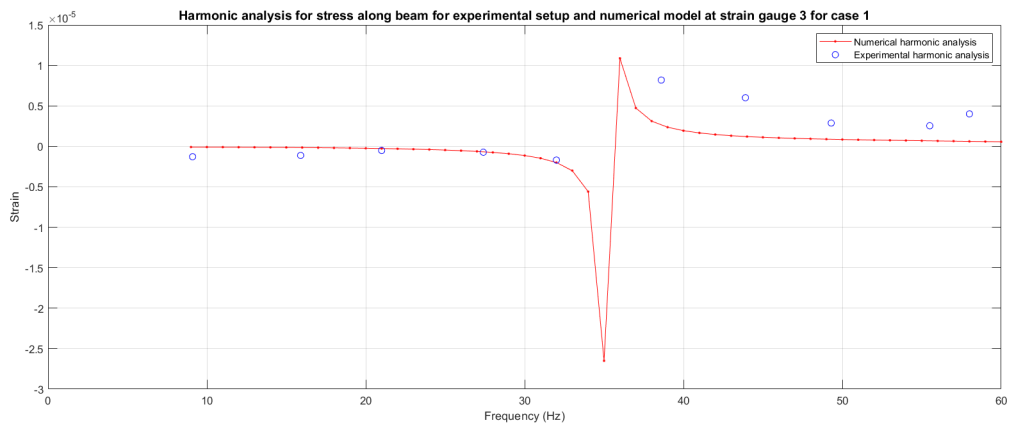
Table 5.5: Comparison of modal analysis for Case 3

Mode	Experimental model	Numerical model	Error
Mode 1	2.63Hz	2.56Hz	-2.7%
Mode 2	17.2Hz	16.80Hz	-2.4%
Mode 3	46.40Hz	45.43Hz	-2.1%

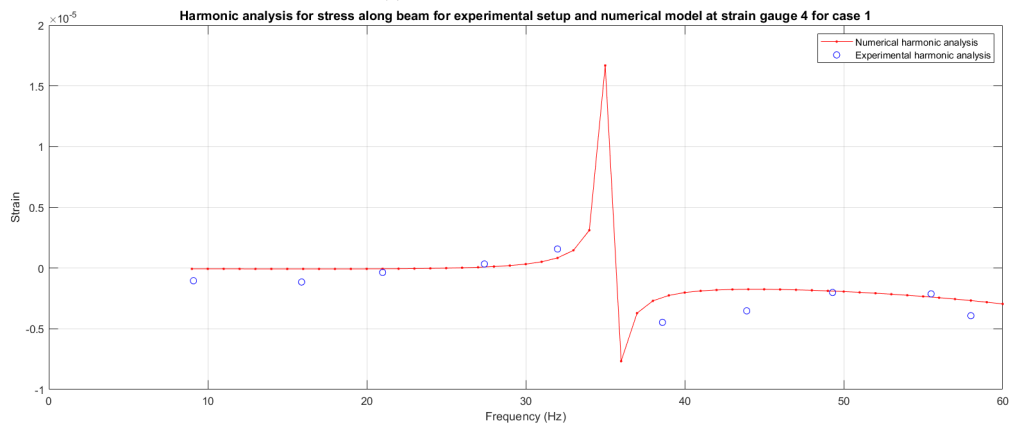
5.2 Harmonic analysis

If the relation between the fatigue life of the experimental setup and the fatigue life of the numerical model can be obtained, it is possible to infer predictions about the fatigue life of the experimental setup from the numerical model. This way the changes in fatigue life of the experimental setup can be continuously updated using the numerical model. To investigate the relation between the fatigue life of the experimental setup and the fatigue life using the numerical model, a harmonic analysis is performed. The harmonic analysis for the experimental setup is done by performing a forced vibration test on the setup. This section provides the results of harmonic analyses done and a comparison is made in order to find a relation between the fatigue life of the experimental setup and the fatigue life of the numerical model.

Figure 5.7, Figure 5.8 and Figure 5.9 show the results of the harmonic analysis in terms of the occurring strains $[m/m]$ due to a harmonic load applied to the structure at different frequencies for respectively Case 1, Case 2 and Case 3 of the state of the support structure. All figures include the harmonic analysis done with the experimental setup combined with the harmonic analysis done using the numerical model. The data of the harmonic analysis for the experimental setup and the numerical model are presented in Appendix H.

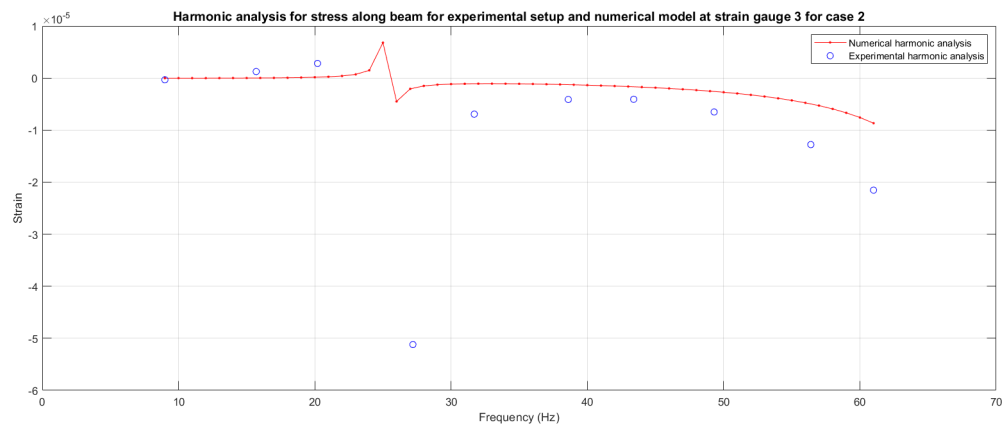


(a) Harmonic analysis strain gauge 3

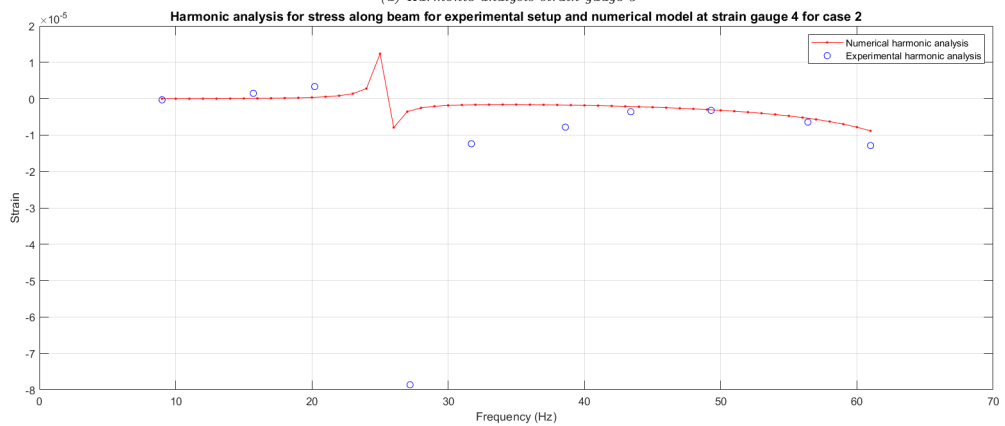


(b) Harmonic analysis strain gauge 4

Figure 5.7: Harmonic analysis on experimental setup and numerical model for Case 1

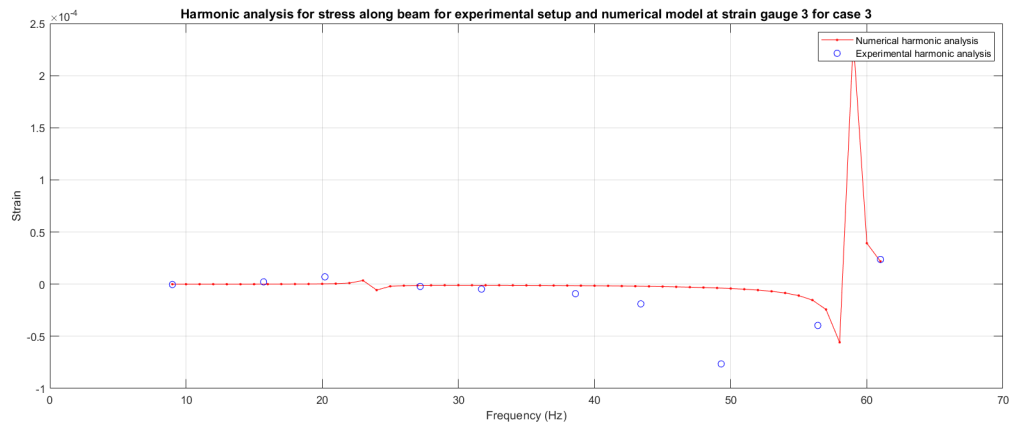


(a) Harmonic analysis strain gauge 3

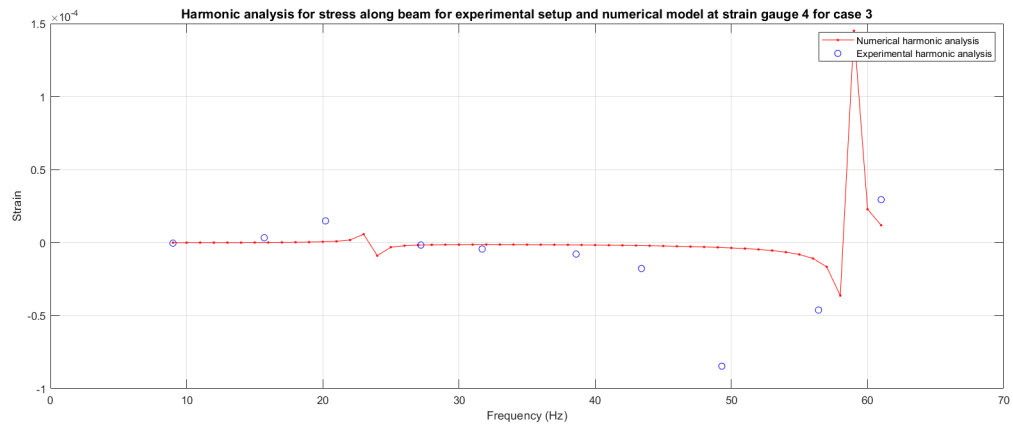


(b) Harmonic analysis strain gauge 4

Figure 5.8: Harmonic analysis on experimental setup and numerical model for Case 2



(a) Harmonic analysis strain gauge 3



(b) Harmonic analysis strain gauge 4

Figure 5.9: Harmonic analysis on experimental setup and numerical model for Case 3

5.2.1 Discussion

From the figures of the results of the harmonic analysis, it can be observed that the data points of the experimental setup and the numerical model coincide. The strains of both the numerical model and the experimental setup are increasing rapidly when the natural frequencies of the structure is approached. The relation between the fatigue life of the experimental setup and the fatigue life of the numerical model is obtained by using the Basquin equation. The Basquin's equation is a description of a linear relation between the applied stress cycles (σ) on the y-axis and the number of cycles to failure (N) on the x-axis. Both variables are plotted on a logarithmic scale and this curve is known as the S-N curve. Section 2.1 shows such a S-N curve which presents the maximum applicable cycles before fatigue failure depending on the stress amplitude or stress range. Deriving the relation between the fatigue life of the experimental setup and the fatigue life of the numerical model is done following Equation 5.1.

$$\begin{aligned}
 N_{num} &= B\sigma_{num}^{-m} \\
 N_{exp} &= B\sigma_{exp}^{-m} \\
 \frac{N_{num}}{N_{exp}} &= \frac{B\sigma_{num}^{-m}}{B\sigma_{exp}^{-m}} \tag{5.1}
 \end{aligned}$$

$$\frac{N_{num}}{N_{exp}} = \left(\frac{\sigma_{num}}{\sigma_{exp}} \right)^{-m}$$

Where stress can be described in terms of strain and Young's modulus ($\sigma = \epsilon * E$). Thus follows Equation 5.2 for the relation between the fatigue life of the experimental setup and the fatigue life of the numerical model considering strain.

$$\frac{N_{num}}{N_{exp}} = \left(\frac{\epsilon_{num}}{\epsilon_{exp}} \right)^{-m} \tag{5.2}$$

Where N_{num} is the amount of applicable cycles before failure for the numerical analysis and N_{exp} are the amount of applicable cycles before failure for the experimental setup.

Table 5.6 shows the results of the harmonic analysis of strain gauge 3 for Case 1. It shows the results of several random picked frequencies in order to assess the relation between the fatigue life of the experimental setup and the fatigue life of the numerical model. The error between the values is calculated following the true values of the experimental setup, and therefore obtained by $((numerical - experimental)/experimental) \times 100\%$.

Table 5.6: Comparison of harmonic analysis of strain gauge 3 for Case 1 in terms of strain (ϵ)

Frequency	Experimental model	Numerical model	Error
9Hz	-1.29×10^{-6}	-8.94×10^{-8}	-93.02%
21Hz	-5.07×10^{-7}	-2.70×10^{-7}	-46.81%
32Hz	-1.70×10^{-6}	-2.00×10^{-6}	18.16%
44Hz	6.01×10^{-6}	1.20×10^{-6}	-79.96%
58Hz	4.01×10^{-6}	6.15×10^{-7}	-84.66%

The results in Table 5.6 shows very large errors between the measured strains of the experimental setup and the determined strains of the numerical model. The observed error can have several causes. For example the results of the harmonic analysis of the experimental setup are not adequate

enough to state a relation between the fatigue life of the numerical model and the fatigue life of the experimental setup. Primarily not enough data points are obtained from the forced vibration testing on the experimental setup. For this reason it is difficult to compare the strains of the experimental setup with the strains of the numerical model at different frequencies. Besides the lack of data points, the measurements are not accurate enough. The harmonic force applied, during the forced vibration test, is too low. This magnitude of harmonic force is not able to cause measurable strains in the experimental setup. The noise measured by the strain gauges might be bigger than the strains measured by the strain gauges. In other words the signal to noise ratio is too low. For this reason the measured data by the strain gauges is unreliable.

What is also observed from the results of the harmonic analysis in Table 5.6, is when the frequency increases the error between the results of the experimental setup and the numerical model also increases. This can also be observed in the figures showing the results of the harmonic analysis. When the natural frequency is passed, for Case 1 at 35Hz, the difference between the data points of the experimental setup and the data points of the numerical model increases. It is expected that this increase in error is caused by the lack of damping in the numerical model. Section ?? proposes a way to incorporate damping into the numerical model. However, currently the support structure in the numerical model is modeled without any damping factors. For these reasons it is not possible to calculate the relation for fatigue life between the numerical model and the experimental setup and more research is needed.

Characterization of support structure

An optimization script is used to characterize the state of the support structure of the beam in the experimental setup using the numerical model. The state of the support structure for the beam is characterized in terms of number of aluminum support, the distance between the aluminum support, the length of the support structure and springs stiffness. The cost function for optimization depends on the difference between the first three frequencies of the experimental model and the first three frequencies of the numerical model. The ability of finding the optimized parameters, and therefore characterizing the state of the support, with only output measurements, contributes to the SHM system of an offshore monopile structure. This contribution includes obtaining insight in the causes of the changing natural frequencies of the monopile structure. If a change in natural frequency is observed, with the help of the optimization methodology, assumptions can be made about the change in soil stiffness around the monopile structure. The new information about the soil stiffness around the structure is useful for example for possible maintenance decisions.

This chapter elaborates on the optimization methodology that is written using Matlab. The complete Matlab files used for the optimization problem are given in Appendix I and the script for the numerical modal is given in Appendix F.

6.1 Cost function

The natural frequencies of the structure are dependent, among other factors, on the stiffness of the springs k , the number of springs n , the length of the support l and the distance between the blocks d . Given certain values of these parameters, the numerical model computes the natural frequencies. Consequently, the problem of identifying the parameters of the support can be formulated as the following optimization problem:

$$\begin{aligned}
 & \min_{k,n,l,d} \quad \|f_{\text{exp}} - f_{\text{num}}(k, n, l, d)\|^2, \\
 & \text{subject to} \quad \underline{k} \leq k \leq \bar{k} \\
 & \quad \quad \quad \underline{l} \leq l \leq \bar{l} \\
 & \quad \quad \quad \underline{d} \leq d \leq \bar{d} \\
 & \quad \quad \quad n \in \{1, \dots, \bar{n}\}
 \end{aligned} \tag{6.1}$$

where f_{exp} are the first 3 natural frequencies measured using the experimental setup, and $f_{\text{num}}(k, n, l, d)$ are the natural frequencies according to the numerical model built in ANSYS.

Note that as the cost function depends on the number of blocks n , which takes integer values, the problem (6.1) is a mixed-integer constrained optimization problem. Consequently the cost function can not be assumed to be continuous or smooth in its parameters, which causes the problem to be hard to solve for any optimization solver in general.

Since the number of blocks are generally of low order in this project, the mixed integer optimization can be avoided at the cost of solving \bar{n} constraint optimization problems of the form

$$\begin{aligned} \min_{k,l,d} \quad & \|f_{\text{exp}} - f_{\text{num}}(k, n, l, d)\|^2, \\ \text{subject to} \quad & \underline{k} \leq k \leq \bar{k} \\ & \underline{l} \leq l \leq \bar{l} \\ & \underline{d} \leq d \leq \bar{d} \end{aligned} \tag{6.2}$$

By doing so, it can be assumed that for each value n the cost function in Problem 6.2 depends smoothly on its input-parameters. On the other hand, the cost function depends on the output of a FE-analysis performed by ANSYS. Consequently, the cost function is a nonlinear function of the parameters and no information regarding the cost function such as a gradient is available. Consequently, the generic optimization solver **fmincon** provided by the Matlab optimization toolbox is used. This solver is able to handle general nonlinear cost functions and constraints. Moreover, this solver is able to approximate the gradient based on data points.

6.2 ANSYS and Matlab scripting

The script that runs the optimization is called *Optimization-script-ANSYS.m*. It is necessary to primarily identify the first three natural frequencies obtained from the experimental model. These frequencies are defined in the array *freqref*.

```
freqref = [2.4 ; 16.6 ; 46.2];
```

After defining *freqref*, an initial point is given to the generic optimization solver and the boundary conditions of the optimization problem are defined. The boundary conditions are given in Problem 6.2. Starting from a given initial point, Matlab will change the parameters k, n, l and d with a function written in the *ParameterANSYS.m* file. This file opens the *parameter.inp* file and will overwrite the parameters for the spring stiffness, number of aluminum supports, length of the support structure and distance between the aluminum supports.

When the parameters are adjusted in the *parameter.inp* file, ANSYS is executed in batch mode, using the command as shown below.

```
SET KMP_STACKSIZE=4096K & "C:\Program Files\ANSYS Inc\v211\ANSYS\bin\winx64\ANSYS211.exe"  
-b -i Right_ANSYS_model.mac -o PRE.txt
```

The command shown above launches the file *Right-ANSYS-model.mac* in ANSYS. This file is described in detail in Chapter 4. When the *Right-ANSYS-model.mac* has run, the first three natural frequencies of the numerical model can be extracted from the *Respons.m* file. This file is made by importing the content from the *Export.mac* file. The *Export.mac* file contains several **GET* functions to extract the results of the first three natural frequencies from the modal analysis done in the *Right-ANSYS-model.mac* file.

```

!Export resonance frequencies to txt

*GET,f1,MODE,1,FREQ
*GET,f2,MODE,2,FREQ
*GET,f3,MODE,3,FREQ

/OUTPUT, 'C:\Users\20202632\OneDrive -
TU Eindhoven\Documenten\TUE\Master SED\Afstuderen\Matlab\Optimization\RESPONS', 'm',
*VWRITE,f1,f2,f3,
(F)

```

When the results of the first three frequencies of the numerical model are exported to the Matlab file *Respons.m*, it is possible to analyze Problem 6.1. The script below shows the commands used for the evaluation of the norm, given in Equation 6.2, between the first three natural frequencies of the experimental model (f_{exp}) and the first three frequencies of the numerical model (f_{num}). The evaluation of the norm is done according to the cost function given in Equation 6.2. The function calculates the norm for a given point and estimates the gradient for this point. The evaluation continues in the direction for which the norm decreases. When there a decreasing direction for the norm can not be found, the evaluation will stop and the minimum value for the norm, given in Equation 6.2, is found.

$$\|f_{exp} - f_{num}\|^2 \quad (6.3)$$

```

%initialize point
x0 = [0.5; 0.8; 65600];

%set boundary conditions for the parameters
% dmin =< dblocks <= dmax
% lmin =< lsupport <= lmax
dmin = 0.1;
dmax = 0.9;
lmin = 0.4;
lmax = 0.9;
stiffmin = 64000;
stiffmax = 66000;
minblocks = 1;
maxblocks = 3;

x = zeros(3,maxblocks);
fval = zeros(1,maxblocks);

for i=minblocks:1:maxblocks
%Stop searching if there does not exist a feasible point.
if i*dmin >= lmax
    fprintf('\n There does not exist a feasible point anymore \n')
    break
end
%parameters=(distance between blocks, lenght support)
fun=@(par) norm(freqref-ANSYS(par(1),par(2),par(3),i));

%Add constraints parameters such that ANSYS works properly (i*d-1<=0)
A = [ i -1 0];
b = 0;

%print for which number of blocks the algorithm is searching an optimum
fprintf('\n the algorithm looks for optimum with %d blocks \n',i);

%minimize difference of the model response with respect to measurement, as
%a function of inputs
[x(:,i),fval(i)] = fmincon(fun,x0,A,b,[],[],[dmin;lmin;stiffmin],[dmax;lmax;stiffmax]);
end

```

The output of the optimization script is a characterization of the support structure in term of springs stiffness, number of aluminum supports, length of the support structure and distance between the aluminum supports. This characterization is obtained from only output acceleration and strain measurements. A schematic flowchart of the optimization problem described in this chapter is given in Figure 6.1.

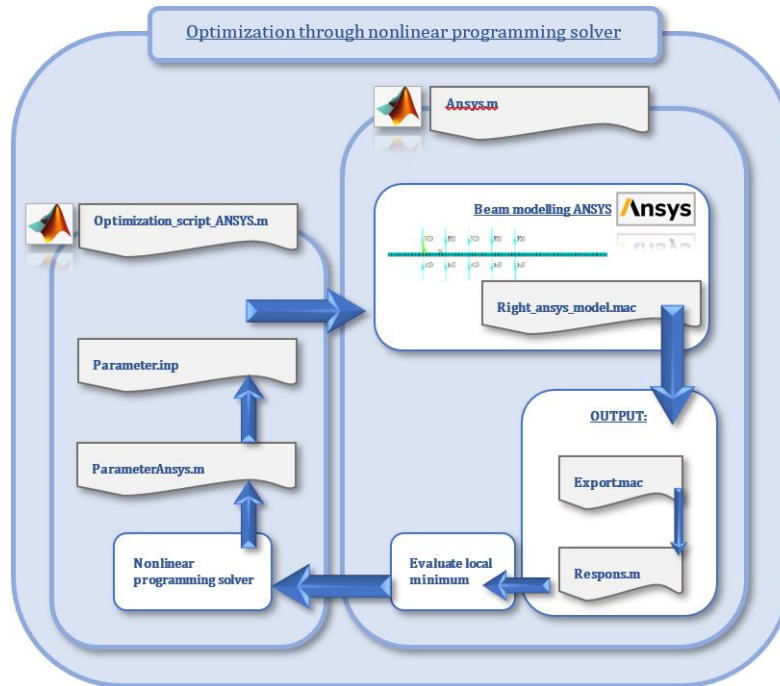


Figure 6.1: Flowchart of the optimization problem

6.3 Validation

To verify how well the optimization script performs, a numerical experiment was performed where the input $freqref$ is generated by a test setup of which the parameters are known. In this case the optimization algorithm can be said to perform well if the output of the algorithm, *i.e.*, the predicted parameters, are close to the true values.

To test the algorithm, the natural frequencies of the setup in Case 3 are chosen as an input. For Case 3 only one aluminum block is attached to the beam, the distance between the blocks remains at $0.4m$, the springs have a spring stiffness of $65600N/mm^2$, and the length of the support is $0.8m$. These parameters are also shown in Table 6.1. The input for the optimization script are the first three natural frequencies of Case 3 as measured during the modal analysis, which are

1. First natural frequency: $2.63Hz$
2. Second natural frequency: $17.20Hz$
3. Third natural frequency: $46.40Hz$

and thus we set

```
freqref = [2.63 ; 17.20 ; 46.40];
```

The boundary conditions are chosen as follows

$$\begin{aligned} \underline{k} &= 64000, & \bar{k} &= 66000 \\ \underline{d} &= 0.1, & \bar{d} &= 0.9 \\ \underline{l} &= 0.4, & \bar{l} &= 0.9 \\ n &\in \{1, 2, 3\} \end{aligned}$$

For these constraints and input we obtain the following output of the optimization script:

```

the optimal distance is 0.39 m
the optimal length of support is 0.77 m
the optimal stiffness is 65733.2
the amount of blocks is 1
    
```

The parameters of the support structure for Case 3 of the experimental setup and the optimized parameters for the support structure as output of the optimization script are presented in Table 6.1.

Table 6.1: Parameters for the support structure of the input and output of the optimization script

Parameter	Case 3 parameters	Numerical results	Error
n	1	1	0%
d	0.40 m	0.45 m	2.5%
k	65600 N/m	65733.2 N/m	0.2%
l	0.80 m	0.78 m	2.4%

Note that the difference between the numerical values of the parameters and the true values is at most 2.5%. Recall that the difference between the experimentally determined natural frequencies and the numerically determined natural frequencies was at most 4%. Hence, a relative error in the estimated parameters of 4% at most was to be expected. Therefore we can conclude that the optimization algorithm performs well.

It remains a future direction of research to instigate how well the algorithm performs if the constraints are loosened and the search space is enlarged. This was not investigated in this research as running the optimization script was very time consuming due to the fact that in each step of the optimization an FE analysis has to be performed. A potential consequence of enlarging the search space of the algorithm could be that it will return a local minimum which is not close to the true values. As the cost function is dependent on the output of an FE analysis, the optimization algorithm has no information on the gradient and thus has to approximate the gradient based on data points, which makes it difficult to determine whether a solution is a local or a global solution. In particular since the cost function is nonlinear in its arguments. Consequently, the algorithm can not determine whether the produced solution is a local or a global optimum.

Another direction of research would be to find a solver which can handle a mixed integer optimization problem. As this was overcome in this research by solving n regular optimization problems, the algorithm works for low orders of n . However, in real case scenarios a higher order n need to be taken into account to approximate the continuity of the change in soil stiffness. Hence it necessary to save computational time by using a better solver for the problem considered.

Conclusions and future research

7.1 Conclusions

In this research project the relation between a change in soil stiffness and the dynamic response in steady state of offshore monopile foundations was investigated, in order to contribute to the Structural Health Monitoring framework of offshore wind turbines. To that extent, an experimental setup representative of planar geometry and loading conditions was designed where the soil-structure interaction is assessed by means of spring and aluminum block supports. To investigate to what extent the parameters of the support can be estimated based on output measurements such as accelerations and strains, a numerical model was also developed.

It was shown, by means of a modal analysis after doing an impact test using the experimental setup, that as the stiffness of the support decreases, also the natural frequencies of the setup decrease. The same phenomenon was observed by a modal analysis using the numerical model. Moreover, the difference between the natural frequencies of the structure determined after the modal analysis determined experimentally and numerically was only 4%. Consequently, the numerical model is considered to approximate the dynamic response behavior of the experimental setup sufficiently well to infer data on the experimental parameters from the numerical model.

The harmonic analysis has shown promising results for finding a relation between the fatigue life of the numerical model and the fatigue life of the experimental setup. However, further research needs to be done in order to create a reliable relation regarding the fatigue life. The next section provides recommendations for future research.

As the experimental and numerical determined natural frequencies are sufficiently close to another, an algorithm is suggested to determine the parameters of the support. This algorithm solves an optimization problem, where the cost function is the norm of the difference between the experimental and numerical natural frequencies. The algorithm aims to minimize this norm over the parameters of the support required in the numerical model such as the amount of aluminum block supports, the distance between the blocks, the stiffness of the springs and the length of the support. The validation of the algorithm solving the optimization problem results in the methodology for characterizing the stiffness of the support in the experimental setup. This methodology contributes to the development of a Structural Health Monitoring framework for the fatigue assessment for a monopile of an offshore wind turbine.

7.2 Future Research

Based on the results obtained in this research, the following recommendations are made for future research. The main contribution of this research is the identification of the influence of soil stiffness reduction on the natural frequencies and a method to estimate the stiffness parameters of the support. Consequently, two natural directions of research follow.

First, it remains an open question what the influence of this reduction in soil stiffness is on the fatigue life. Although a first attempt to investigate this influence on the fatigue life was made by performing a harmonic analysis, a more thorough investigation is recommended where damping is incorporated in the numerical model. Damping can be incorporated to the numerical model by analyzing the damping coefficient of the experimental setup, using the results of the measurements of the impact test that are done. The decay rate in acceleration of the accelerometers is equal to the damping coefficient of the experimental test setup.

In order to have more significant stresses in the structure, and therefore increasing the signal to noise ratio, it is recommended to increase the harmonic amplitude in the forced vibration test, using the experimental setup. The harmonic amplitude can easily be increased by increasing the eccentric masses on the eccentric motor.

Secondly, the estimation method proposed in this research assumes that the natural frequencies of the structure are measured and known. In other words, the natural frequencies are obtained from the structure in steady state. However, it is more difficult to obtain these natural frequencies from output measurements for an offshore wind turbine in operation. Figure 7.1 shows an output signal of accelerations in the frequency domain during forced vibration testing on the experimental setup. This figure shows many peaks in the output signal and therefore the difficulty of finding the correct natural frequencies of the structure. An offshore wind turbine in operation is a time-variant system, and to be able to apply a modal analysis, the system has to be transferred to a time-invariant system. Such a transformation can be made by applying Liapunov-Floquet transformation [41]. However more research is needed to apply a modal analysis on a time-variant system. Therefore it is recommended to extend this research to infer the natural frequencies from operational data.

Finally, the research conducted in this project was done in a 2D setup. In order to obtain a thorough understanding of the structure soil interaction of operational offshore wind turbines, it is necessary to generalize all results to a setup in 3D.

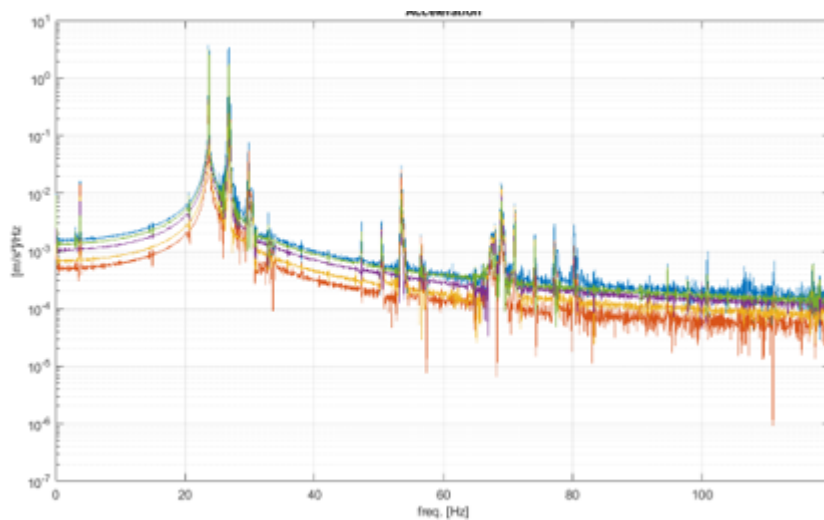


Figure 7.1: An example of an output signal of accelerations in the frequency domain during forced vibration testing on the experimental setup

Bibliography

- [1] G. Nikitas, Nathan J. Vimalan, and S. Bhattacharya. An innovative cyclic loading device to study long term performance of offshore wind turbines. *Soil Dynamics and Earthquake Engineering*, 82:154–160, 3 2016. xi, 2, 3, 19
- [2] J. Schijve. *Fatigue of Structures and Materials*. Springer, 2nd edition, 2008. xi, 2, 7, 8
- [3] Johan Maljaars, M Matija Lukic, and F Frans Soetens. Comparison between the Eurocode for Fatigue of Steel Structures, EN 1993-1-9, and the Eurocode for Fatigue of Aluminium Structures, EN 1999-1-3. *Procedia Engineering*, 66:34–48, 1 2013. xi, 8, 9
- [4] DNV. Fatigue design of offshore steel structures. Technical Report DNV-RP-C203, 9 2019. xi, 8, 9
- [5] Lu-Qing Yu, Li-Zhong Wang, Zhen Guo, S. Bhattacharya, G. Nikitas, Ling-Ling Li, and Yue-Long Xing. Long-term dynamic behavior of monopile supported offshore wind turbines in sand. *Theoretical and Applied Mechanics Letters*, 5(2):80–84, 3 2015. xi, 10, 11
- [6] S. Schafhirt, A. Page, G.R. Eiksund, and M. Muskulus. Influence of Soil Parameters on Fatigue Lifetime of Offshore Wind Turbines with Monopile Support Structure. *Energy Procedia*, 94:347–356, 1 2016. xi, 1, 11, 12
- [7] A. Hassanirad and S. Mohammadi. Applied and Theoretical Cantilever Beam Free Vibration Analysis. *World Academy of Science*, 1 2012. xi, xv, 12, 13
- [8] Free Vibration of a Cantilever Beam (Continuous System). xi, 14
- [9] Encardio Rite. [Updated] Strain Gauge: Principle, Types, Features and Applications - Encardio Rite, 1 2023. xi, 17
- [10] Rajiv. Low Pass, High Pass and Band Pass Filters; Simple Explanation, 7 2022. xi, 18
- [11] Increasing Sampling Frequency to Avoid Aliasing. xi, 19, 20
- [12] BestTong DC 12V-24V 8000RPM 775 Brushed Vibration Motor DOUBLE-HEAD High Torque Electric Vibrating Motors with 2 Iron Rotating Mass - - Amazon.com. xii, 31
- [13] ATV Springs. Catalogus standaard technische veren - Verenfabriek, 9 2020. xii, 80
- [14] J Wiemann and K Lesny. Design aspects of monopiles in German offshore wind farms. *Frontiers in Offshore Geotechnics*, 8 2005. xv, 10, 11
- [15] Offshore Wind Outlook 2019 – Analysis, 2019. 1

-
- [16] M. Henkel, W. Weijtjens, and C. Devriendt. Fatigue Stress Estimation for Submerged and Sub-soil Welds of Offshore Wind Turbines on Monopiles Using Modal Expansion. 11 2021. 1
- [17] M. Damgaard, L.V. Andersen, and L.B. Ibsen. Dynamic response sensitivity of an offshore wind turbine for varying subsoil conditions. *Ocean Engineering*, 101:227–234, 4 2015. 1, 2, 11
- [18] Offshore123. 2.2. Monopile Design Monopile Design Basis - Design Parameters and Assumptions for monopile foundations, 12 2021. 2
- [19] Modal Parameter Identification — EMEA — Brüel & Kjær, 11 2022. 2, 16, 20
- [20] S. Aasen, A.M. Page, K.S. Skau, and T.A. Nygaard. Effect of foundation modelling on fatigue lifetime of a monopile-based offshore wind turbine. 4 2017. 3, 11
- [21] Eindhoven University of Technology. Fatigue and Fracture - Introduction to Fatigue. Technical report, 11 2021. 7, 8
- [22] B.C. O’Kelly and M. Arshad. Offshore wind turbine foundations – analysis and design. *Offshore Wind Farms*, pages 589–610, 2016. 10
- [23] Peter Avitabile. Experimental modal analysis : A simple non-mathematical presentation. *Sound and Vibration*, 35(1):20–31, 1 2001. 12, 17
- [24] B. Adavardkar and A. Admuthe. Modal Analysis of Cantilever Beam Using Analytical and Finite Element Method. *Journal of Emerging Technologies and Innovative Research (JETIR)*, 8(6), 2021. 12
- [25] Akash Gaur and Priyanka Dhurvey. Comparative Study of Beam Theories on the Effect of Span-Depth Ratio for Symmetric and Un-symmetric Loadings. *IOP conference series*, 936(1):012047, 9 2020. 14
- [26] Modal Analysis Summary — Ansys Innovation Courses, 1 2022. 14
- [27] Intro to Modal Analysis — Ansys Innovation Courses, 1 2022. 14
- [28] Governing Equations for Modal Analysis — Ansys Courses, 1 2022. 15
- [29] Kate Brush. finite element analysis (FEA), 11 2019. 15
- [30] Eigenvalue Problem in Modal Analysis — Ansys Courses, 1 2022. 15
- [31] Jacek Grosel, Wojciech Sawicki, and Wojciech Pakos. Application of Classical and Operational Modal Analysis for Examination of Engineering Structures. *Procedia Engineering*, 91:136–141, 2014. 15, 16
- [32] A beginner’s guide to accelerometers. 16
- [33] Wei-Xin Ren and Zhou-Hong Zong. Output-only modal parameter identification of civil engineering structures. *Structural Engineering and Mechanics*, 17(3.4):429–444, 3 2004. 17
- [34] Rune Brincker, Lingmi Zhang, and Palle Andersen. Modal identification of output-only systems using frequency domain decomposition. *Smart Materials and Structures*, 10(3):441–445, 6 2001. 17
- [35] Michael Cerna and Audrey Harvey. The Fundamentals of FFT-Based Signal Analysis and Measurement. *National Instruments*, 1 2000. 17
- [36] Brian Schwarz and Mark P. Richardson. Experimental modal analysis. *Applied Structural and Mechanical Vibrations*, 11 1999. 18, 19
- [37] What is aliasing? What causes it? How to avoid it? - WolfSound. 19
- [38] Davide Leonetti. Introduction to Structural Health Monitoring. 20

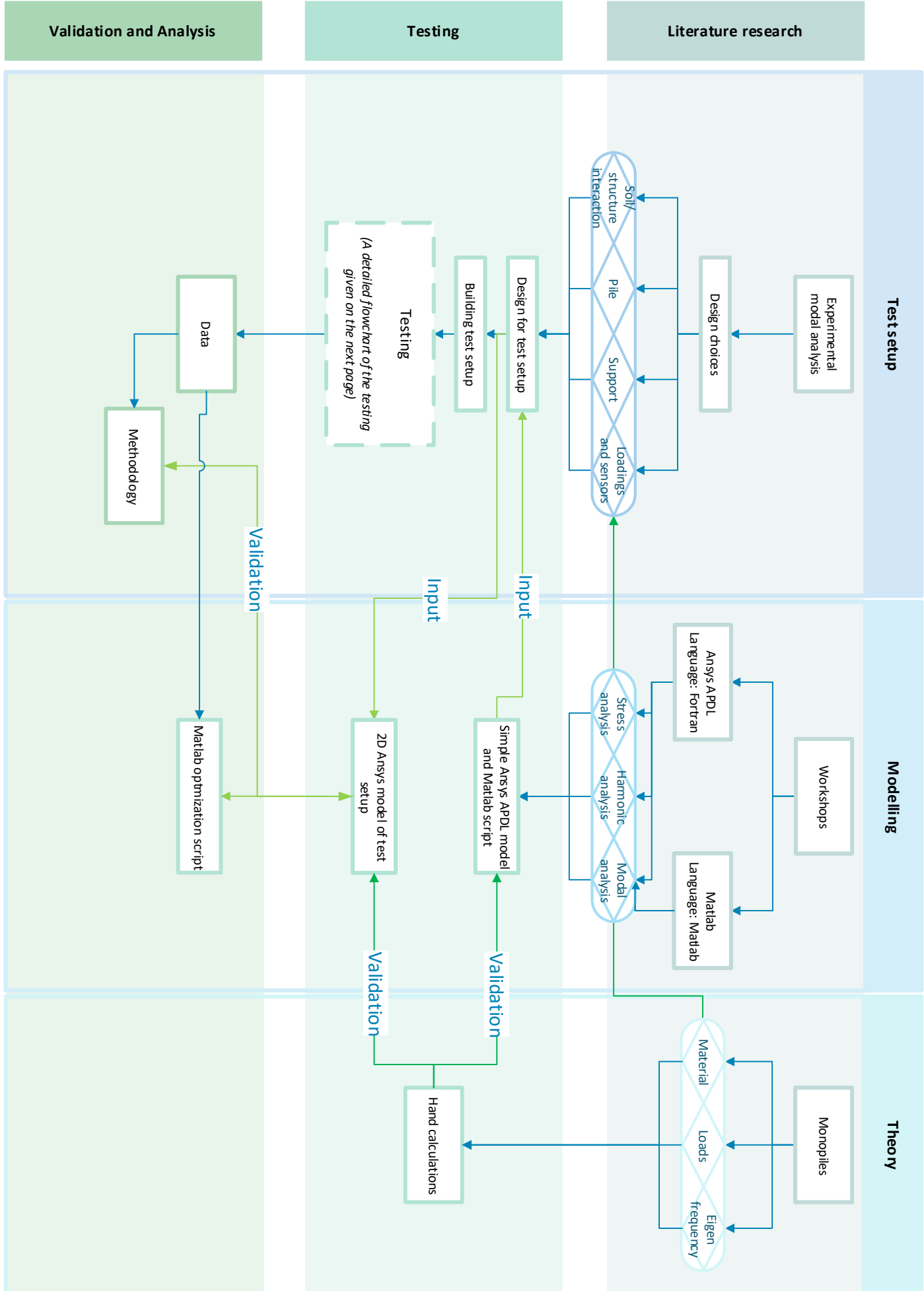
- [39] Total Materia - Articles. 24, 77
- [40] inc Ansys. *ANSYS mechanical APDL command reference*. 13 edition, 2008. 34
- [41] Dmitri Tcherniak and Gunner Chr. Larsen. Application of OMA to an Operating Wind Turbine: now including Vibration Data from the Blades. *5th International Operational Modal Analysis Conference*, 1 2013. 60
- [42] EurocodeApplied Team. Table of material properties for structural steel S235, S275, S355, S420. 77

APPENDIX A

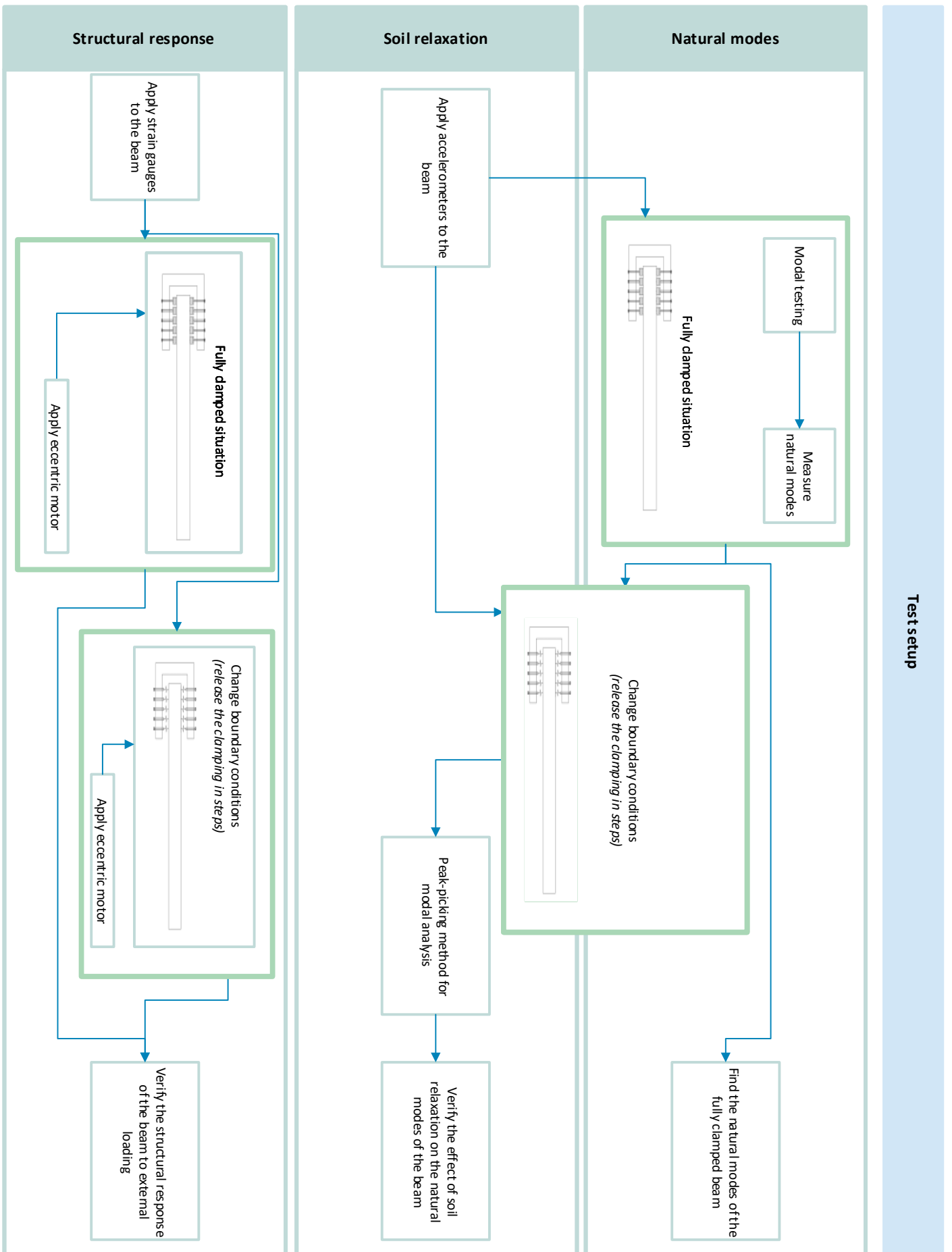
Flowchart

This appendix presents a detailed flowchart about the activities done for this research project.

Flowchart of actions for graduation project
Yonne Jaeger



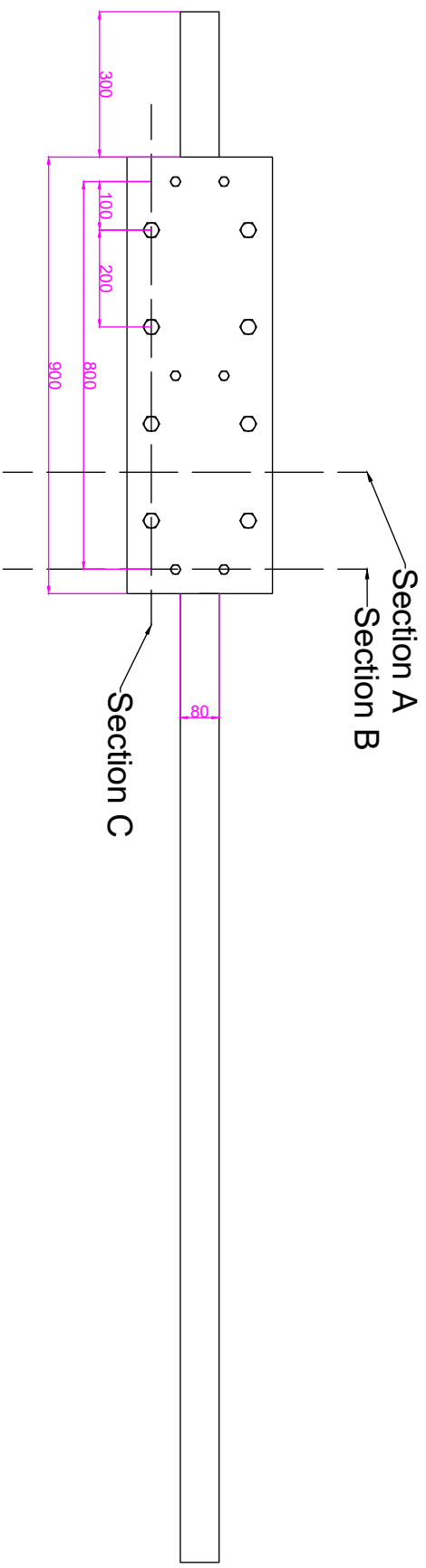
Testing



APPENDIX B

Drawings of Experimental test setup

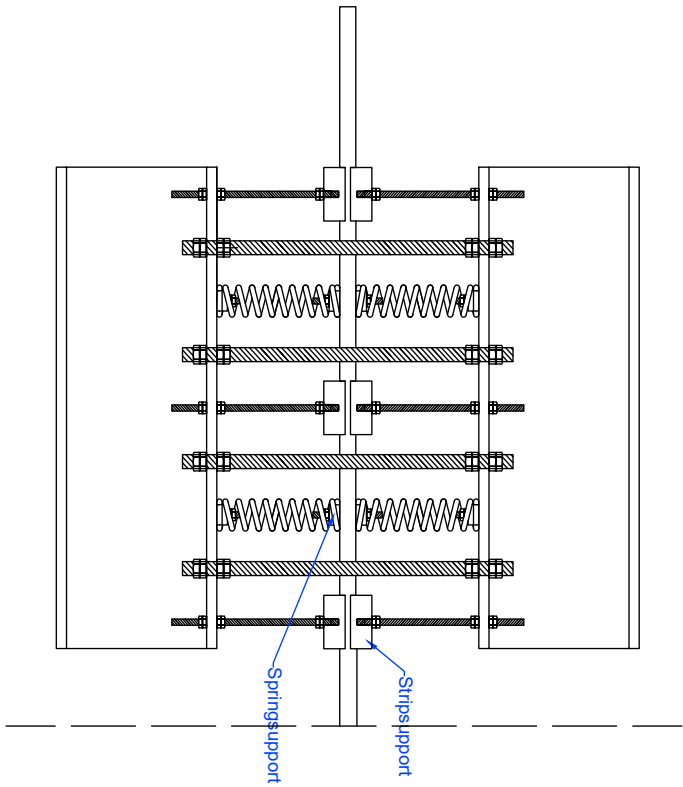
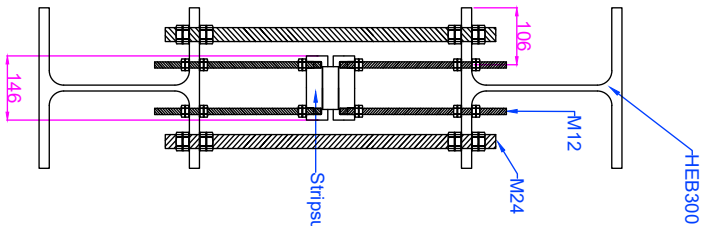
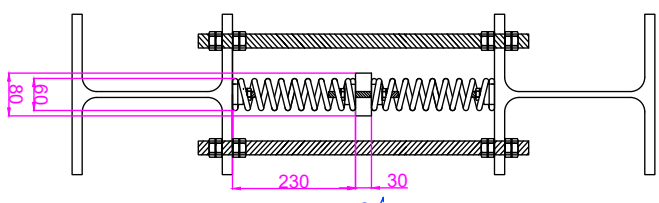
This appendix includes scaled drawings of layout of the experimental setup. The drawings include dimensions and details of the layout of the experimental setup.



Section A

Section B

Section C



PROJECT NAME: Graduation Project	
DRAWING TITLE: Small scale test setup of an offshore monopile structure	
DRAWN BY: Y. Joeger	DATE: 06/02/2023
Institute: TU/e Structural Engineering and Design	
CONTACT NO. EMAIL: y.c.joeger@student.tue.nl	
PROJECT NO.:	SHEET NO.:
SCALE: 1:10	SHEET SIZE: A3
DRAWING NO.:	SHEET NO.:
REVISION:	
DATE:	

Numerical Justification of Experimental Setup

It is important to note that extensive descriptions of modeling in ANSYS APDL is written in Chapter 4. In order to find the best compromise between the natural frequencies and the sizes of the elements for the test setup, a preliminary numerical model is developed. Based on the natural frequencies of the model and the stresses along the beam elements, the size of the steel strip used in the experimental setup is chosen. The preliminary model is also used to find a suitable spring constant for the springs used in the experimental setup. The numerical model is built in ANSYS APDL, a finite element software.

For simplicity the structure is modeled as a cantilever beam. The numerical model exists of two different elements, beam elements and spring elements. The beam is modeled as BEAM188 elements and the spring elements are modeled as COMBIN14 elements. A detailed clarification on the elements in the numerical model is given in Chapter 4. The applied boundary conditions in the numerical model with respect to the experimental setup is shown in Figure C.1.

C.1 Boundary conditions

As previously mentioned a cantilever beam is modeled. The beam is supported by rigid supports and springs. The rigid supports are modeled as rigid boundary conditions, rotations around all axis (x -, y - and z -axis) and displacements in all directions (Δx , Δy , Δz) are prohibited. The locations of these rigid boundary conditions are equal to the locations of the aluminum clamps in the experimental setup. The ends of the modeled spring elements also have rigid boundary conditions. All boundary conditions of the support structure are shown in Figure C.1

Other boundary conditions that are applied are the boundary conditions to make the model respond only in a 2D plane. This means that along the BEAM188 elements displacement in the z -direction (Δz) and rotations along the x - and y -axis are constraint.

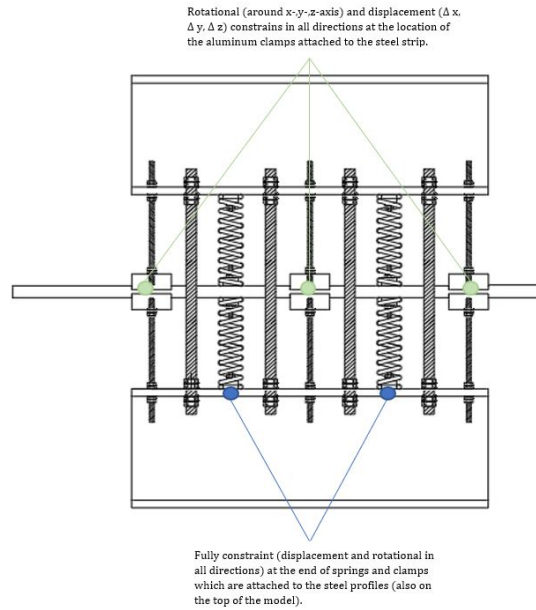


Figure C.1: Location of rigid boundary conditions shown by the means of the experimental test setup section

C.2 Springs

A suitable spring constant is found by considering the displacements of the springs and the influence on the cantilever beam. When the spring constant which is too low, the compression displacement will be too high. In other words, the springs do not contribute to the stiffness of the support. However when the spring constant is too high, the springs will act as simple supports to the structure, in a similar way the aluminum blocks do. The two exaggerated situations are shown in Figure C.2. This figure shows the deflection (δy) of the beam when it is supported by one aluminum block and two springs (Case 3) in the third mode.

With the applied boundary conditions and a correct spring constant it is possible to extract preliminary results of the structure by doing a modal analysis on the structure. A modal analysis is used to extract the natural frequencies of the structure. It is favorable that the natural frequencies lay between $0Hz - 100Hz$.

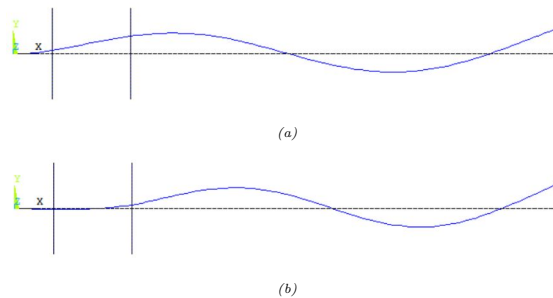
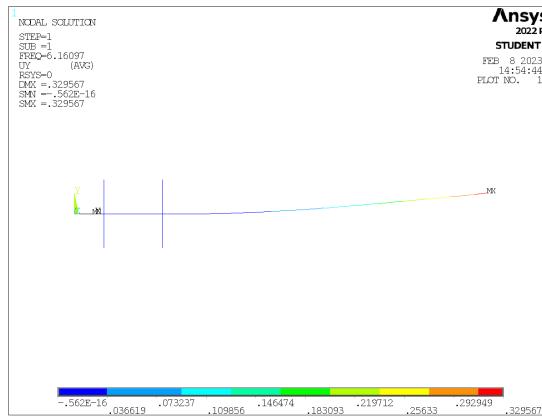


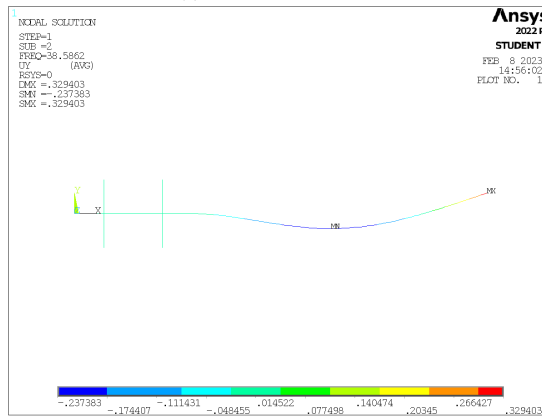
Figure C.2: (a) Deflection of the beam in the third mode when a spring constant of $0N/m$ is applied and (b) the deflection of the beam in the third mode when a spring constant of $1000000N/m$

C.3 Results of modal analysis

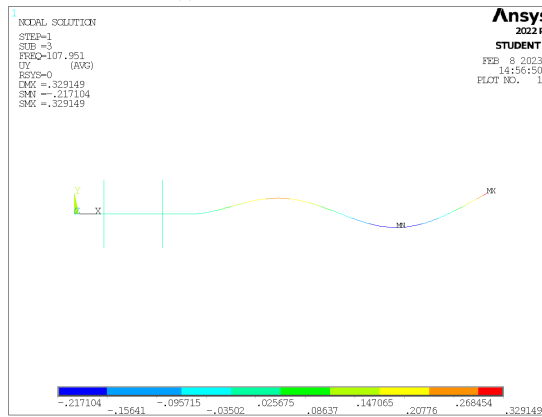
For the case with all aluminum supports attached to the steel beam, the first three modes are the following:



(a) Mode shape 1 at 6.16 Hz



(b) Mode shape 2 at 38.58 Hz



(c) Mode shape 3 at 107.95 Hz

C.4 Preliminary numerical analysis script

```

/PREP7

!material properties
ET,1,BEAM188
ET,2,COMBIN14

KEYOPT,2,1,0
KEYOPT,2,2,2
KEYOPT,2,3,0

R,1,656000,0, , , ,
RMORE,0,

MPTEMP,,,,,,,,
MPTEMP,1,0
MPDATA,DENS,1,,7850
MPDATA,EX,1,,2.1e11
MPDATA,PRXY,1,,0.3
SECTYPE, 1, BEAM, RECT, , 0
SECOFFSET, CENT
SECDATA,0.0295,0.0795,0,0,0,0,0,0,0,0,0

K,1,0,0,0,
K,2,2.8,0,0,
K,3,0.2,0,0,
K,4,0.4,0,0,
K,5,0.6,0,0,
K,6,0.8,0,0,

K,7,0.2,0.23,0,
K,8,0.6,0.23,0,

K,9,0.2,-0.23,0,
K,10,0.6,-0.23,0,

LSTR,      1,      3
LSTR,      3,      4
LSTR,      4,      5
LSTR,      5,      6
LSTR,      6,      2

L, 7, 3
L, 9, 3
L,      8,      5
L,      10,      5

!Assigning element types to springs
FLST,5,4,4,ORDE,2
FITEM,5,6
FITEM,5,-9
CM,_Y,LINE
LSEL, , , ,P51X
CM,_Y1,LINE
CMSEL,S,_Y

CMSEL,S,_Y1
LATT,1,1,2, , , ,1
CMSEL,S,_Y
CMDELE,_Y
CMDELE,_Y1

FLST,5,4,4,ORDE,2
FITEM,5,6
FITEM,5,-9
CM,_Y,LINE
LSEL, , , ,P51X
CM,_Y1,LINE
CMSEL,,_Y

LESIZE,_Y1, , ,1, , , ,0
    
```

```

FLST,5,5,4,ORDE,2
FITEM,5,1
FITEM,5,-5
CM,_Y,LINE
LSEL, , , ,P51X
CM,_Y1,LINE
CMSEL,S,_Y

!Assign element to the beam and mesh size
CMSEL,S,_Y1
LATT,1,1,1, , , ,1
CMSEL,S,_Y
CMDELE,_Y
CMDELE,_Y1

FLST,5,5,4,ORDE,2
FITEM,5,1
FITEM,5,-5
CM,_Y,LINE
LSEL, , , ,P51X
CM,_Y1,LINE
CMSEL,,_Y

LESIZE,_Y1,0.028, , , , , ,0

FLST,2,9,4,ORDE,2
FITEM,2,1
FITEM,2,-9

!MESHING
LMESH,P51X

!BC for springs
FLST,2,4,3,ORDE,2
FITEM,2,7
FITEM,2,-10
!*
/GO
DK,P51X, , , ,0,ALL, , , , ,

!For the beam
FLST,2,109,1,ORDE,6
FITEM,2,1
FITEM,2,-105
FITEM,2,112
FITEM,2,119
FITEM,2,126
FITEM,2,133
!*
/GO
D,P51X, , , , , ,UZ,ROTX,ROTY, ,

FLST,2,3,3,ORDE,3
FITEM,2,1
FITEM,2,4
FITEM,2,6
!*
/GO
DK,P51X, , , ,0,ALL, , , , ,

!Solver for modal analysis

/SOL
ANTYPE,2

MODOPT,LANB,20
EQSLV,SPAR
MXPAND,0, , ,0
LUMPMP,0
PSTRES,0

MODOPT,LANB,20,0,10000, ,OFF

/SOLU

/output,result,lis
SOLVE
FINISH
/output
/POST1
SET,LIST

```

APPENDIX D

Hand calculations

The stability of the experimental setup is checked by the means of the following hand calculations. The maximum harmonic load which can be applied to the end of the steel beam is calculated in section D.2. Material properties of the steel beam are given in Table 3.1 in Chapter 3.

D.1 Stability of experimental setup

This section presents the hand calculations done for the experimental setup. These calculations concern the static state of the structure, only the self-weight is considered in this load-case.

Weight of the steel strip:

$$\begin{aligned} mass(kg) &= \rho * b * h * L \\ &= 7850 * 0.08 * 0.03 * 2 = 37.7kg \end{aligned}$$

Equally divided q-load due to self-weight:

$$\begin{aligned} q(N/m) &= \frac{m * g}{L} \\ &= \frac{37.7 * 9.81}{2} = 184.9N/m \end{aligned}$$

Reaction forces in support:

$$\begin{aligned} R_{support}(N) &= q * L \\ &= 184.9 * 2 = 369.8N \\ M_{support}(Nm) &= \frac{1}{2} * q * L^2 \\ &= \frac{1}{2} * 184.9 * 2^2 = 369.8Nm \end{aligned}$$

Deflection due to self-weight:

$$\begin{aligned} I(mm^4) &= \frac{1}{12} * b * h^3 \\ &= \frac{1}{12} * 80 * 30^3 = 180000mm^4 \\ \omega_{self-weight}(mm) &= \frac{q * L^4}{8 * E * I} \\ &= \frac{184.9 * 10^{-3} * (2 * 10^3)^4}{2 * 2.1 * 10^5 * 180000} = 9.8mm \end{aligned}$$

Stress distribution in section at the support:

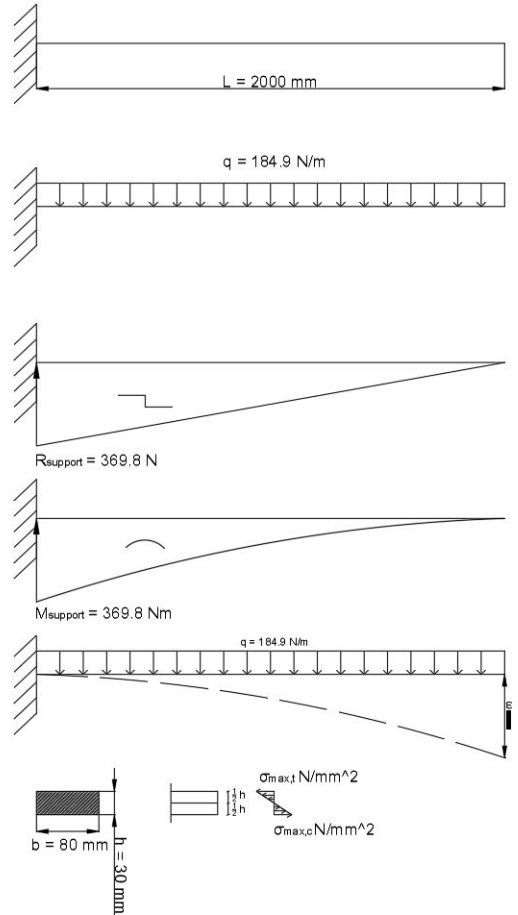
$$\begin{aligned} \sigma_{max}(N/mm^2) &= \frac{M_{support} * \frac{1}{2} * h}{I} \\ &= \frac{369.8 * 10^3 * \frac{1}{2} * 30}{180000} = 30.8N/mm^2 \end{aligned}$$

Check maximum stress

We make use of a safety factor for static loading ($\gamma = 1.15$)

$$\begin{aligned} \sigma_{allowable}(N/mm^2) &= \frac{\sigma_{tensile}}{\gamma} \\ &= \frac{235}{1.15} = 200N/mm^2 \end{aligned}$$

$$\begin{aligned} \sigma_{allowable} &\geq \sigma_{max} \\ 200N/mm^2 &> 30.8N/mm^2 \text{ Check correct} \end{aligned}$$



D.2 Harmonic load

The following rule of thumb is used: The fatigue limit is roughly around 40% of the fatigue limit [39]. The tensile strength of S235 steel is $360N/mm^2$ [42].

Fatigue limit

$$\begin{aligned} \text{fatigue limit } (N/mm^2) &= 0.40 * \sigma_{tensile} \\ &= 0.40 * 360 = 144N/mm^2 \end{aligned}$$

Tensile strength for additional dynamic loading:

$$\begin{aligned} \sigma_{max,dynamic} (N/mm^2) &= \sigma_{max,tensile} - \sigma_{max,static} \\ &= 144 - 30.8 = 113.2N/mm^2 \end{aligned}$$

Maximum weight of additional dynamic loading:

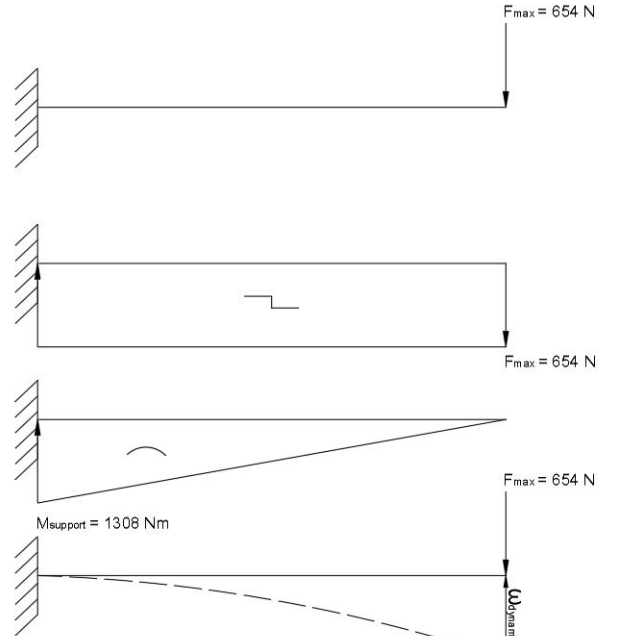
$$\begin{aligned} M_{support} (Nm) &= \frac{\sigma_{max,dynamic} * I}{\frac{1}{2} * h} \\ &= \frac{113.2 * 180000}{\frac{1}{2} * 30} * 10^{-3} = 1358.4Nm \\ F_{max,dynamic} (N) &= \frac{M_{support}}{L} \\ &= \frac{1358.4}{2} = 679.2N \\ \text{mass} (kg) &= \frac{F_{max,dynamic}}{a} \\ &= \frac{679.2}{9.81} = 69.2kg \end{aligned}$$

Deflection due to maximum dynamic mass:

$$\begin{aligned} \omega_{dynamic} (mm) &= \frac{F_{max,dynamic} * L^3}{3 * E * I} \\ &= \frac{679.2 * (2 * 10^3)^3}{3 * 2.1 * 10^5 * 180000} = 47.9mm \end{aligned}$$

Total deflection ($\omega_{self-weight} + \omega_{dynamic}$):

$$\begin{aligned} \omega_{tot} (mm) &= \omega_{self-weight} + \omega_{dynamic} \\ &= 9.8 + 47.9 = 57.7mm \end{aligned}$$



D.3 Loads on support

Total force (F) on support:

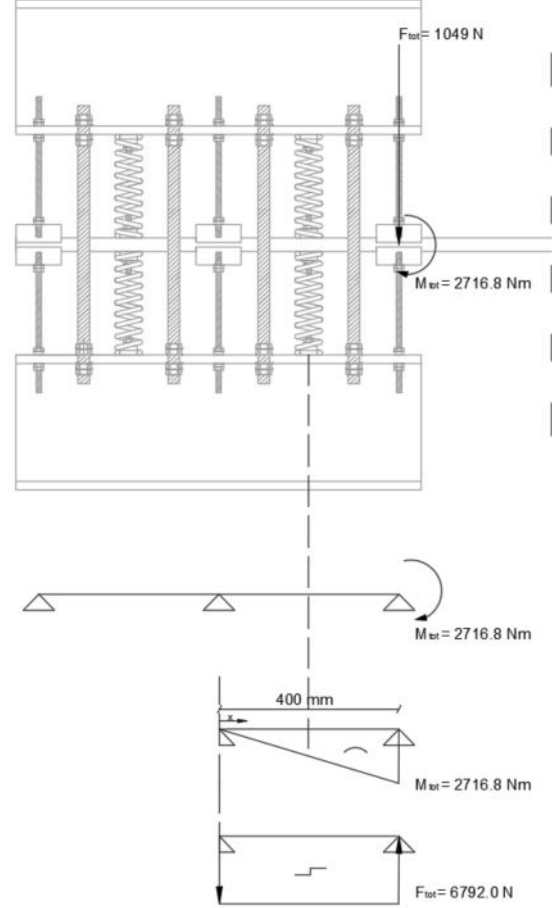
$$\begin{aligned} F_{tot}(N) &= q * L + F_{max,dynamic} \\ &= 184.9 * 2 + 679.2 = 1049(N) \end{aligned}$$

Total moment (Nm) on support:

$$\begin{aligned} M_{tot}(Nm) &= M_{support,self-weight} + M_{support,dynamic} \\ &= 369.8 + 1358.4 = 2716.8Nm \end{aligned}$$

Force (N) on spring

$$\begin{aligned} F_{spring}(N) &= \frac{M_{tot}}{x} \\ &= \frac{2716.8}{400 * 10^{-3}} = 6792(N) \end{aligned}$$



D.4 Analytical Modal Analysis

The theory described in Chapter 2 for analytical modal analysis is used to find the first three natural frequencies of a cantilever beam with the same dimensions of the steel beam used in the experimental test setup. The results of the mode shapes of the cantilever beam are shown in Figure 3.7. The natural frequencies found for the analytical and numerical analysis are shown in Table D.1. This table also shows the error between the analytical and numerical analysis, which is as expected, close to 0.

Table D.1: Comparison between first three natural frequencies based on analytical and numerical calculations

Analytical Hz	Numerical Hz	Error
6.16	6.16	0%
38.62	38.58	0.01%
108.12	107.95	0.01%

APPENDIX E

Spring specifications

This appendix shows a table with all the specifications of the springs used in the experimental setup. The table is obtained from ATV-Springs. It is important to note that the actual spring constant, measured with the Schenk electromechanical machine, deviates from the spring constant listed by the sponsor ATV-springs.

Product informatie:

Specificatie	Waarde
as (maximale as maat)	38.8
bus (minimale bus maat)	61.5
c (veerconstante in n/mm)	65.20
d (draaddikte)	10.00
di (inwendige diameter)	40.00
dm (diameter hart op hart)	50.00
du (uitwendige diameter)	60.00
eindafwerking	Aangelegd, Geslepen
fc (maximale veerconstante)	6194.0
fn (hoogst toelaatbare kracht)	5073.4
lc (bloklengte)	135.0
ln (kleinste indruk lengte)	152.2
lo (lengte ongespannen)	230.0
materiaal specificatie en	EN 10270-1
materiaal type	Verenstaal
nt (totale aantal windingen)	14.0
nw (totale werkzame windingen)	12.5
sc	95.0
sn (grootste toelaatbare veerweg in mm)	77.8
spoed	17.9
werkstofnummer	1.1200
wikkelrichting	Rechtsom

Figure E.1: Spring specifications from ATV-Springs [13]

APPENDIX F

FE-model script

This chapter includes the script for the numerical model. The model exists of two different files and different analysis. The files and analysis are presented separately.

F.1 Numerical model script

The solution step of this model depends on the required analysis. The script for the modal analysis is given in Section F.3, and the script required for the harmonic analysis is given in Section F.4.

```

FINISH
/CLEAR,START

/inp,parameter,inp

/PREP7

!==== Element type and Material data ====
ET,1,BEAM188
ET,2,COMBIN14
ET,3,COMBIN14

KEYOPT,2,1,0
KEYOPT,2,2,2
KEYOPT,2,3,0

KEYOPT,3,1,0
KEYOPT,3,2,2
KEYOPT,3,3,0

R,1,k1,0, , , ,
RMORE,0,

R,2,k2,0,0, , ,0,
RMORE,0,

MPTEMP,,,,,,,,
MPTEMP,1,0
MPDATA,DENS,1,,rho
MPDATA,EX,1,,E
MPDATA,PRXY,1,,v
SECTYPE, 1, BEAM, RECT, , 0
SECOFFSET, CENT
SECDATA,T,W,0,0,0,0,0,0,0,0,0,0

!==== Geometry of the model, Element assignment and Meshing ====

K,1000,x1,0,0,!Keypoint start of the beam
K,2000,x2,0,0, !Keypoint end of the beam

*DO,i,0,n1-1,1 !Keypoints for springs
K,3000+i,d1+i*d2,0,0
K,4000+i,d1+i*d2,y1,0
K,5000+i,d1+i*d2,-y1,0
*ENDDO

*DO,i,0,n2-1,1 !Keypoints for alluminium blocks
K,6000+i,i*d2,0,0
K,7000+i,i*d2,y2,0
K,8000+i,i*d2,-y2,0
*ENDDO

L,1000,6000
L,6000,3000 !Assume we start with an alluminium block and the spring will be next

*IF,n1-1,LT,n2-1,THEN,!Beam
*DO,i,0,n1-1,1
L,3000+i,6000+i
*ENDDO
*DO,i,0,n1-1,1
L,3000+i,6000+1+i
*ENDDO
L,6000+(n2-1),2000

*ELSEIF,n1-1,EQ,n2-1
*DO,i,0,n2-1,1
L,3000+i,6000+i
*ENDDO
*DO,i,0,n2-2,1
L,3000+i,6000+1+i
*ENDDO
L,3000+(n1-1),2000

```

```

*ELSEIF,n1-1,GT,n2-1
*DO,i,0,n2-1,1
L,3000+i,6000+i
*ENDDO
*DO,i,0,n2-2,1
L,3000+i,6000+1+i
*ENDDO
*DO,i,0,n1-n2-1,1
L,3000+(n2-1),3000+n2+i
*ENDDO
L,3000+(n1-1),2000
*ENDIF

CM,Beam,line
ALLSEL
LATT,1,,1,, , , ,1 !Beam element
LESIZE,Beam,L/100,, , , , ,1 !Mesh size of the beam

*DO,i,0,n1-1,1 !Springs
L,3000+i,4000+i
L,3000+i,5000+i
*ENDDO

ALLSEL
CMSEL,u,Beam !Unselect the beam
CM,Springs,line
LATT,1,1,2,, , ,1 !Spring elements
LESIZE,Springs,1,, , , , ,1 !Mesh size of the spring

*DO,i,0,n2-1,1 !Alluminium supports
L,6000+i,7000+i
L,6000+i,8000+i
*ENDDO

ALLSEL
CMSEL,u,Beam
CMSEL,u,Springs
CM,Alluminium,line
LATT,1,2,3,, , ,1 !Alluminium blocks elements
LESIZE,Alluminium,1,, , , , ,1 !Mesh size alluminium blocks

ALLSEL
LMESH,ALL !Mesh all

!==== Boundary conditions ====

KSEL,s,loc,y,y1 !Fixed BC's for end of the alluminium block/springs
KSEL,a,loc,y,-y1
KSEL,a,loc,y,y2
KSEL,a,loc,y,-y2
DK,ALL,,,,,ALL,,,,,

CMSEL,NONE
*DO,i,0,n1-1,1 !Constrain in the x-,z-direction (for the springs)
KSEL,s,KP,,3000,3000+i
DK,ALL,,,,,0,UX,UZ,,,,,
*ENDDO

CMSEL,NONE !Constrain in the z-direction (for the alluminium blocks)
*DO,i,0,n2-1,1
KSEL,s,KP,,6000,6000+i
DK,ALL,,,,,0,UX,UZ,ROT,,,,,
*ENDDO

CMSEL,NONE !Boundary conditions to filter out the modes in the different directions, keep it a 2D problem
NSEL,s,loc,y,0
D,ALL,,,,,0,,UZ,,,,,

ALLSEL

```

F.2 Script for parameters

```

!==== Defining parameters ====

T=0.0295 !Thickness of beam (m)
W=0.0795 !Width of beam (m)

L=3.1 !Length of beam (m)
Ls=0.8 !Length of the support

E=2.1e11 !Elastic modulus (N/m^2)
rho=7850 !Density (kg/m^3)
v=0.3 !Poisson ratio

k1=65600 !Stiffness of springs (N/m)
k2=317390000 !Stiffness of alluminium (N/m)

d1=0.2 !Distance between springs and alluminium blocks (m)
d2=0.4

n1=2 !Number of springs (>0)
n2=3 !Number of blocks

x1=-0.3 !Distance at the end of the beam (after support) (m)
x2=2.8 !End of the beam
x3=0 !Location of first alluminium clamping
x4=x3+d2 !Location of second alluminium clamping
x5=x4+d2 !Location of third alluminium clamping
x6=x3+d1 !Location of first spring
x7=x4+d1 !Location of second spring

y1=0.20 !Length of the springs (m)
y2=0.226 !Length of alluminium block support (m)

```

F.3 Modal analysis script

```

!==== Modal analysis ====

/SOL !Solving the system by doing a Modal Analysis
ANTYPE,2

MODOPT,LANB,4 !How many modes to we want to compare
EQSLV,SPAR
MXPAND,0,,0
LUMPMP,0
PSTRES,0

MODOPT,LANB,10,0,10000,,OFF

/SOLU

/output,result,lis
SOLVE
FINISH
/output
/POST1
SET,LIST

/OUTPUT, 'C:\Users\20202632\OneDrive - TU Eindhoven\Documenten\TUE\Master SED
\Afstuderen\Matlab\Optimization\POST', 'txt'
/INPUT, 'EXPORT', 'mac', 'C:\Users\20202632\OneDrive -
TUEindhoven\Documenten\TUE\MasterSED\Afstuderen\Matlab\Optimization\'

```

F.4 Harmonic analysis script

```
!==== Harmonic analysis ====
/SOL !Solving the system by doing an harmonic analysis
ANTYPE,HARMIC
hropt, full
hrout, off
outpr, basic, 1
HARFRQ,0,150,
NSUBST,150,
KBC,0

/STATUS,SOLU

outres,all,all

SOLVE

!==== Show elements ====
/DIST, 1 ,1.082226,1
/REP,FAST
/DIST, 1 ,1.082226,1
/REP,FAST
!*
/SHRINK,0
/ESHAPE,1.0
/EFACET,1
/RATIO,1,1,1
/CFORMAT,32,0
/REPLOT
!==== Extract strain results ====
/POST1

CMSEL, NONE
ESEL, s, CENT, x, 1.05
ESEL, a, CENT, x, 1.24
/REPLOT

*CFOPEN, Strain_results, txt, , ,
*DO, i, 1, 150

VAR1=%i%
SET, 1, %i%, 1, 0, , , !load a solution step
ETABLE, ESA, sMISC, 42 !->EPELbyt = Strain bending around global z-axis and local y-axis

*GET, strain_%i%, ELEM, 45, ETAB, ESA
*GET, strain2_%i%, ELEM, 51, ETAB, ESA

*VWRITE, VAR1, strain_%i%, strain2_%i%,
(F8.1, ', ', 2X, E13.5, ', ', 2X, E13.5)
*ENDDO

*CFCLOSE
```


APPENDIX G

Post processing of output signals

G.1 Three aluminum supports attached to the beam

The output signal of all acceleration sensors are shown in Figure G.1. As explained in Chapter 3 the post processing of the acceleration output signals is done by first applying a correction to the signal, in order to reduce the offset. The result of this operation is shown in Figure G.2. A time frame of 15 seconds is chosen to continue with post processing of the signal. This time window starts at 15 seconds and ends at 30 seconds, this is shown in Figure G.3. After the applied time window the transformation between the time domain to the frequency domain is made by the means of an FFT with a Hamming window. The number of data points for the FFT is 15000. The result of this operation is shown in Figure G.4.

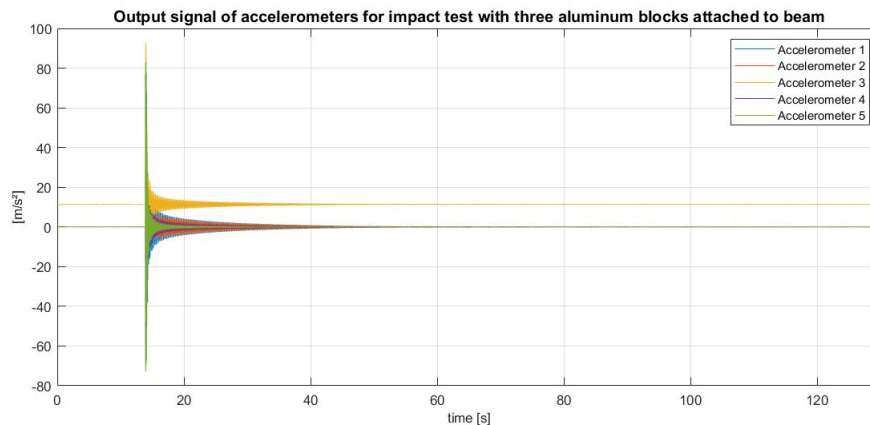


Figure G.1: Output signal of accelerometers during impact test with three aluminum blocks attached to the steel beam

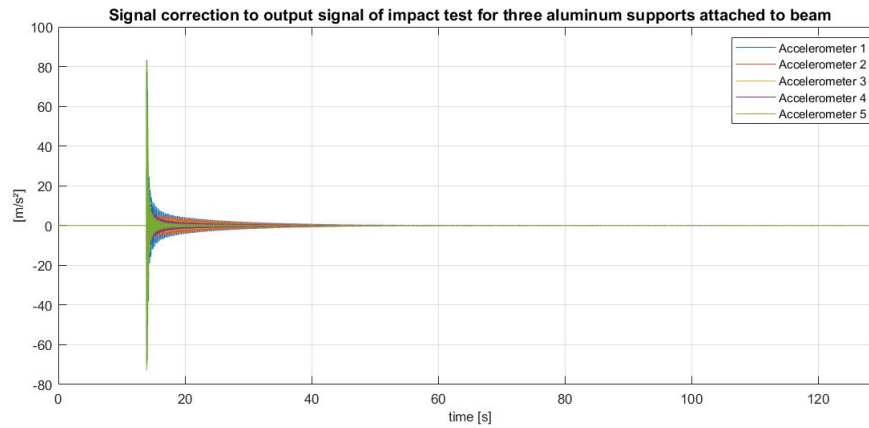


Figure G.2: Signal correction for output signal of impact test for three aluminum supports attached to steel beam

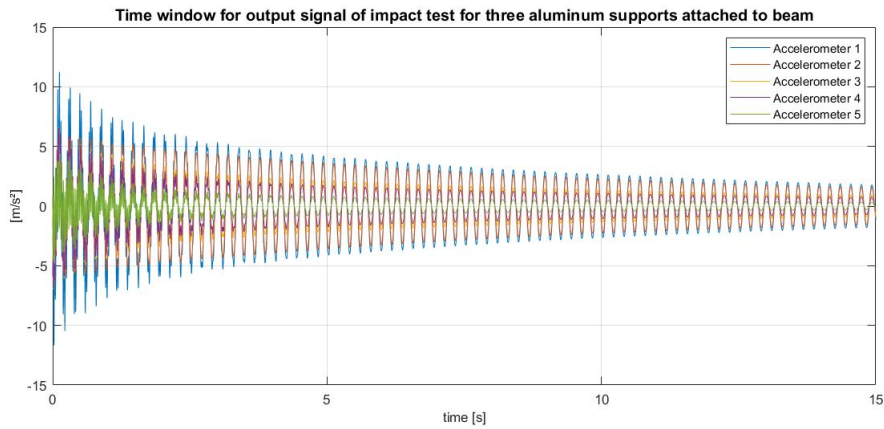


Figure G.3: Application of a time window on output signal for impact test for three aluminum supports attached to steel beam

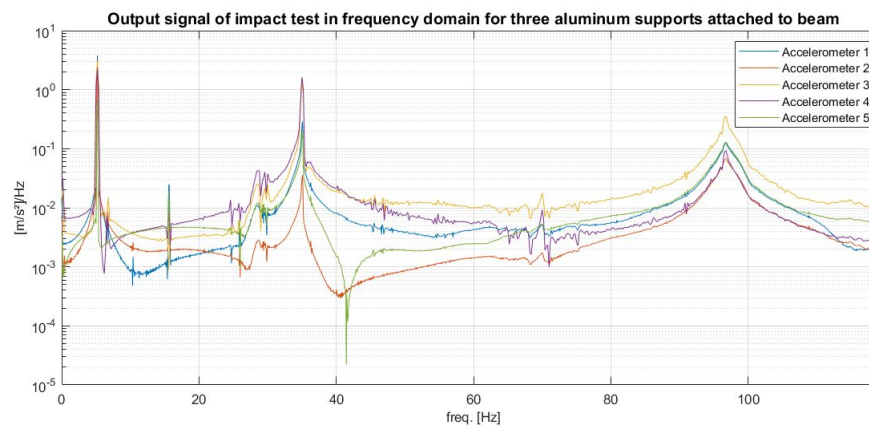


Figure G.4: Output signal in frequency domain for three aluminum supports attached to steel beam

G.2 Two aluminum supports attached to the beam

The output signal of all acceleration sensors are shown in Figure G.5. As explained in Chapter 3 the post processing of the acceleration output signals is done by first applying a correction to the signal, in order to reduce the offset. The result of this operation is shown in Figure G.6. A time frame of 15 seconds is chosen to continue with post processing of the signal. This time window starts at 15 seconds and ends at 30 seconds, this is shown in Figure G.7. After the applied time window the transformation between the time domain to the frequency domain is made by the means of an FFT with a Hamming window. The number of data points for the FFT is 15000. The result of this operation is shown in Figure G.8.

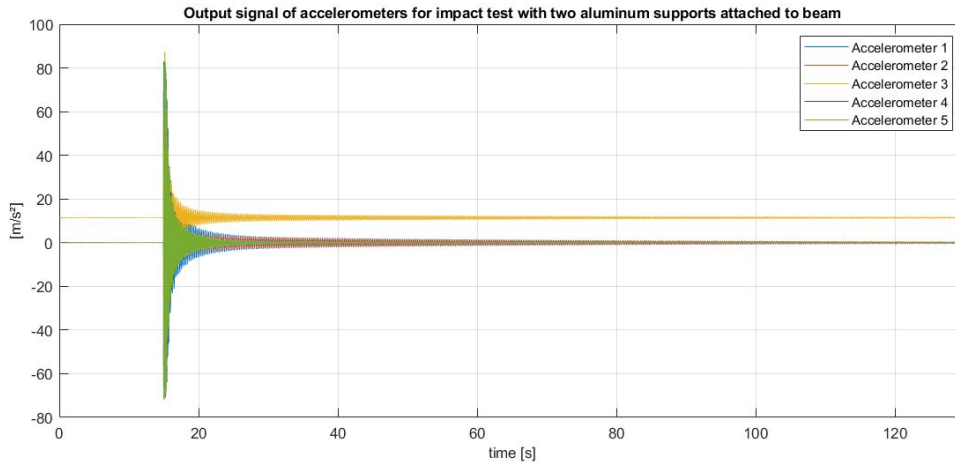


Figure G.5: Output signal of accelerometers during impact test with two aluminum blocks attached to the steel beam

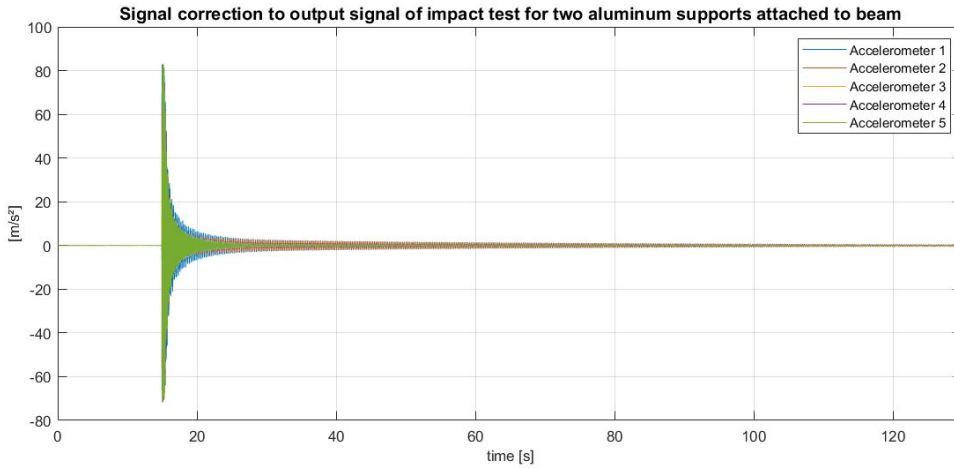


Figure G.6: Signal correction for output signal of impact test for two aluminum supports attached to steel beam

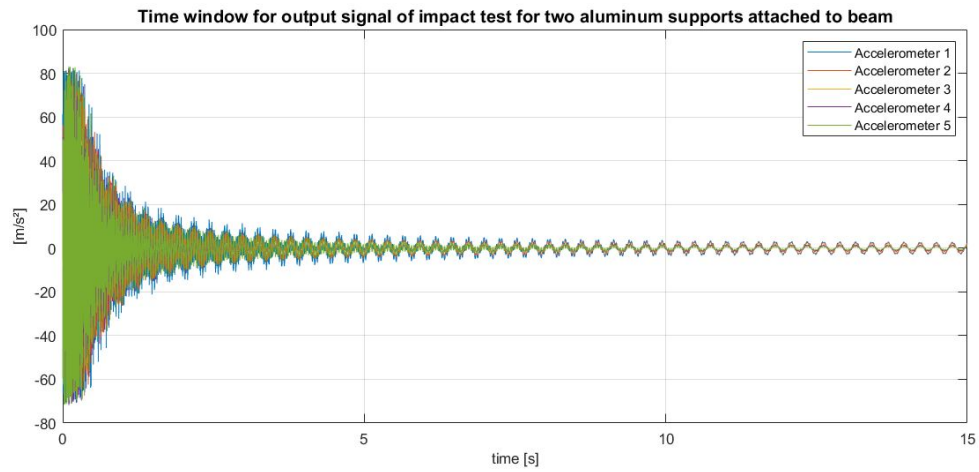


Figure G.7: Application of a time window on output signal for impact test for two aluminum supports attached to steel beam

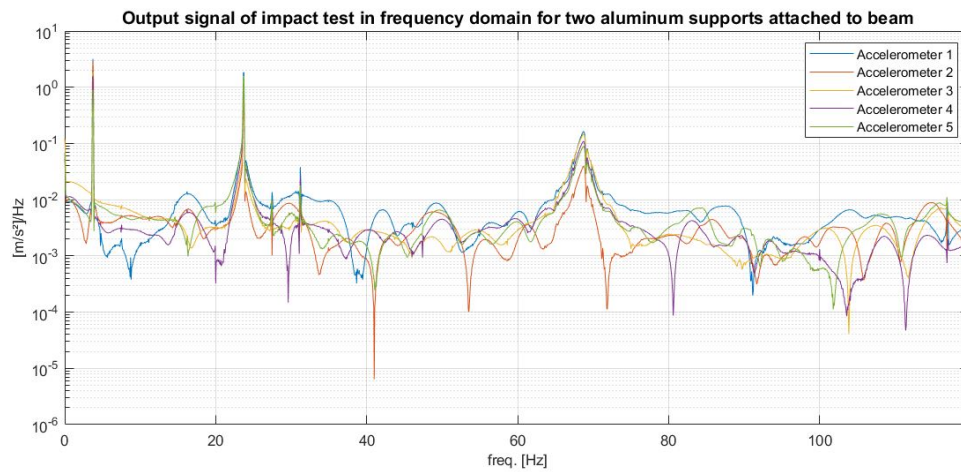


Figure G.8: Output signal in frequency domain for two aluminum supports attached to steel beam

G.3 One aluminum support attached to the beam

The output signal of all acceleration sensors are shown in Figure G.9. As explained in Chapter 3 the post processing of the acceleration output signals is done by first applying a correction to the signal, in order to reduce the offset. The result of this operation is shown in Figure G.10. A time frame of 15 seconds is chosen to continue with post processing of the signal. This time window starts at 15 seconds and ends at 30 seconds, this is shown in Figure G.11. After the applied time window the transformation between the time domain to the frequency domain is made by the means of an FFT with a Hamming window. The number of data points for the FFT is 15000. The result of this operation is shown in Figure G.12.

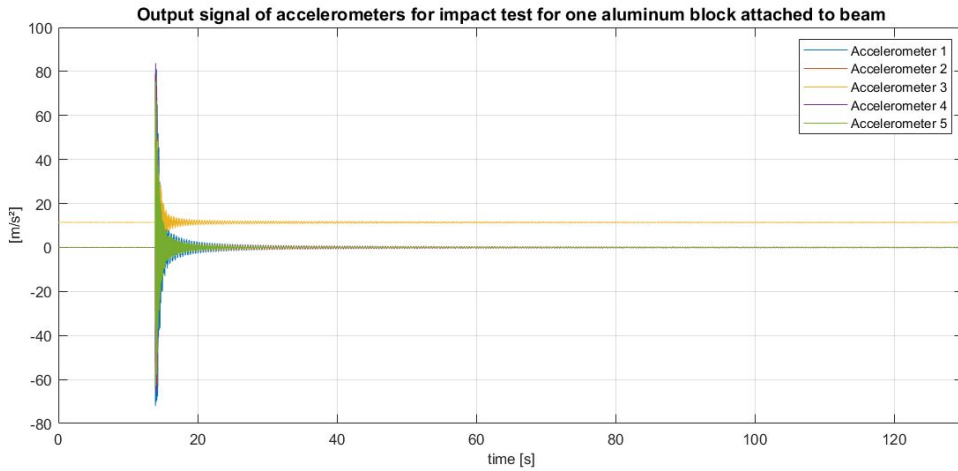


Figure G.9: Output signal of accelerometers during impact test with one aluminum blocks attached to the steel beam

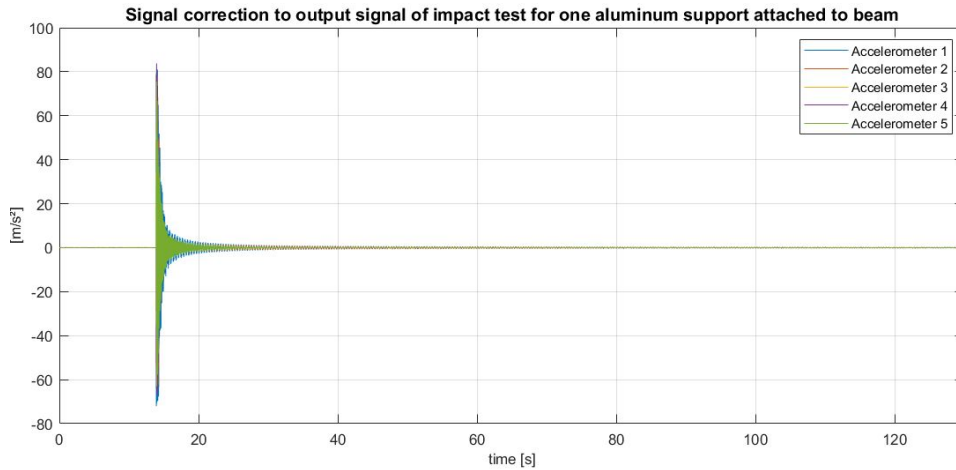


Figure G.10: Signal correction for output signal of impact test for one aluminum supports attached to steel beam

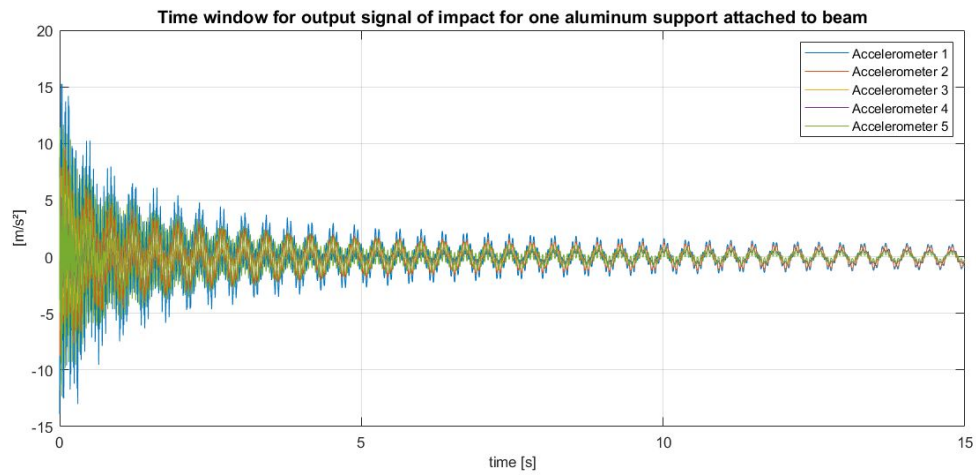


Figure G.11: Application of a time window on output signal for impact test for one aluminum supports attached to steel beam

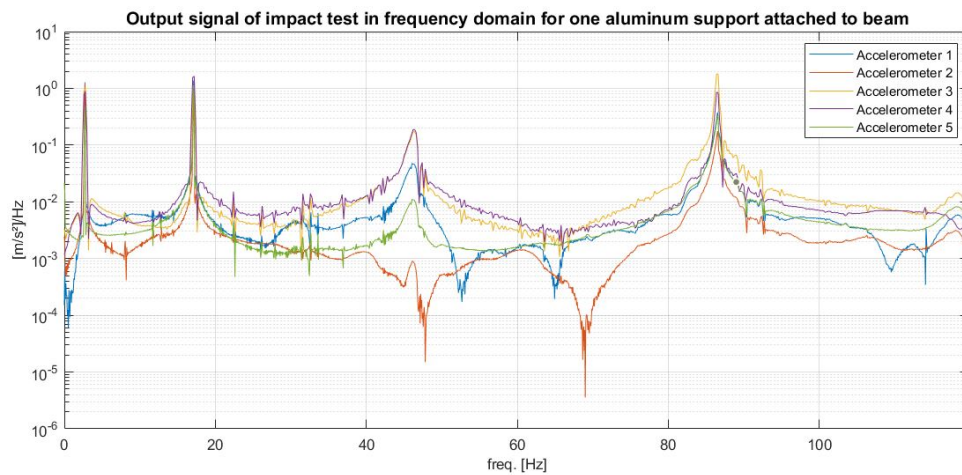


Figure G.12: Output signal in frequency domain for one aluminum supports attached to steel beam

APPENDIX H

Harmonic analysis data

This appendix presents all data obtained from the harmonic analysis for the experimental setup and the numerical model.

H.1 Experimental setup

Table H.1: Output measurement of stresses for forced vibration testing for case 1

Voltage (V)	Frequency (Hz)	Strain 3 (ϵ)	Strain 4 (ϵ)
2	9.1	-1.29E-06	-1.04E-06
3	15.9	-1.12E-06	-1.15E-06
4	21	-5.07E-07	-3.58E-07
5	27.4	-7.28E-07	3.33E-07
6	32	-1.70E-06	1.57E-06
7	38.6	8.19E-06	-4.47E-06
8	43.9	6.01E-06	-3.52E-06
9	49.3	2.88E-06	-2.01E-06
10	55.5	2.54E-06	-2.12E-06
11	58	4.01E-06	-3.92E-06

Table H.2: Output measurement of stresses for forced vibration testing for case 2

Voltage (V)	Frequency (Hz)	Strain 3 (ϵ)	Strain 4 (ϵ)
2	9	-3.43E-07	-3.01E-07
3	15.7	1.25E-06	1.49E-06
4	20.2	2.80E-06	3.34E-06
5	27.2	-5.12E-05	-7.86E-05
6	31.7	-6.94E-06	-1.24E-05
7	38.6	-4.12E-06	-7.81E-06
8	43.4	-4.09E-06	-3.58E-06
9	49.3	-6.52E-06	-3.20E-06
10	56.4	-1.28E-05	-6.43E-06
11	61	-2.15E-05	-1.29E-05

Table H.3: Output measurement of stresses for forced vibration testing for case 3

Voltage (V)	Frequency (Hz)	Strain 3 (ϵ)	Strain 4 (ϵ)
2	9	-3.44E-07	-3.67E-07
3	15.7	2.17E-06	3.34E-06
4	20.2	7.04E-06	1.49E-05
5	27.2	-2.18E-06	-1.66E-06
6	31.7	-4.73E-06	-4.35E-06
7	38.6	-9.10E-06	-7.82E-06
8	43.4	-1.89E-05	-1.77E-05
9	49.3	-7.65E-05	-8.46E-05
10	56.4	-3.96E-05	-4.62E-05
11	61	2.37E-05	2.94E-05

H.2 Numerical model

Table H.4: Harmonic analysis for numerical model for case 1

Frequency (Hz)	Centrifugal force (N)	Strain 3 (ϵ)	Strain 4 (ϵ)
9	2.877977	-8.94E-08	-6.58E-08
10	3.553058	-9.21E-08	-6.49E-08
11	4.2992	-9.77E-08	-6.55E-08
12	5.116403	-1.05E-07	-6.68E-08
13	6.004667	-1.15E-07	-6.84E-08
14	6.963993	-1.26E-07	-6.99E-08
15	7.99438	-1.39E-07	-7.13E-08
16	9.095827	-1.54E-07	-7.21E-08
17	10.26834	-1.71E-07	-7.24E-08
18	11.51191	-1.91E-07	-7.18E-08
19	12.82654	-2.13E-07	-7.00E-08
20	14.21223	-2.39E-07	-6.68E-08
21	15.66898	-2.70E-07	-6.16E-08
22	17.1968	-3.06E-07	-5.38E-08
23	18.79567	-3.48E-07	-4.28E-08
24	20.46561	-3.98E-07	-2.73E-08
25	22.20661	-4.60E-07	-5.92E-09
26	24.01867	-5.35E-07	2.36E-08
27	25.90179	-6.29E-07	6.44E-08
28	27.85597	-7.51E-07	1.22E-07
29	29.88121	-9.13E-07	2.04E-07
30	31.97752	-1.14E-06	3.25E-07
31	34.14488	-1.47E-06	5.15E-07
32	36.38331	-2.00E-06	8.35E-07
33	38.6928	-3.01E-06	1.46E-06
34	41.07335	-5.60E-06	3.11E-06
35	43.52496	-2.65E-05	1.67E-05

Frequency (Hz)	Centrifugal force (N)	Strain 3 (ϵ)	Strain 4 (ϵ)
36	46.04763	1.09E-05	-7.67E-06
37	48.64136	4.73E-06	-3.71E-06
38	51.30615	3.11E-06	-2.70E-06
39	54.04201	2.36E-06	-2.25E-06
40	56.84892	1.93E-06	-2.02E-06
41	59.7269	1.66E-06	-1.88E-06
42	62.67594	1.46E-06	-1.80E-06
43	65.69603	1.32E-06	-1.76E-06
44	68.78719	1.20E-06	-1.75E-06
45	71.94942	1.11E-06	-1.75E-06
46	75.1827	1.04E-06	-1.76E-06
47	78.48704	9.82E-07	-1.79E-06
48	81.86245	9.30E-07	-1.83E-06
49	85.30891	8.85E-07	-1.88E-06
50	88.82644	8.45E-07	-1.94E-06
51	92.41503	8.10E-07	-2.00E-06
52	96.07468	7.78E-07	-2.07E-06
53	99.80539	7.48E-07	-2.15E-06
54	103.6072	7.19E-07	-2.24E-06
55	107.48	6.92E-07	-2.34E-06
56	111.4239	6.66E-07	-2.44E-06
57	115.4388	6.41E-07	-2.55E-06
58	119.5249	6.15E-07	-2.68E-06
59	123.6819	5.90E-07	-2.81E-06
60	127.9101	5.63E-07	-2.95E-06

Table H.5: Harmonic analysis for numerical model for case 2

Frequency (Hz)	Centrifugal force (N)	Strain 3 (ϵ)	Strain 4 (ϵ)
9	2.877977	-2.52E-08	-1.27E-08
10	3.553058	-2.47E-08	-8.59E-09
11	4.2992	-2.34E-08	-2.84E-09
12	5.116403	-2.12E-08	5.18E-09
13	6.004667	-1.76E-08	1.62E-08
14	6.963993	-1.20E-08	3.13E-08
15	7.99438	-3.71E-09	5.17E-08
16	9.095827	8.43E-09	7.96E-08
17	10.26834	2.60E-08	1.18E-07
18	11.51191	5.16E-08	1.71E-07
19	12.82654	8.93E-08	2.47E-07
20	14.21223	1.46E-07	3.58E-07
21	15.66898	2.37E-07	5.31E-07
22	17.1968	3.93E-07	8.21E-07
23	18.79567	6.97E-07	1.38E-06
24	20.46561	1.48E-06	2.80E-06
25	22.20661	6.80E-06	1.24E-05
26	24.01867	-4.50E-06	-7.91E-06
27	25.90179	-2.08E-06	-3.55E-06
28	27.85597	-1.52E-06	-2.52E-06
29	29.88121	-1.29E-06	-2.08E-06
30	31.97752	-1.17E-06	-1.85E-06
31	34.14488	-1.11E-06	-1.72E-06
32	36.38331	-1.09E-06	-1.65E-06
33	38.6928	-1.08E-06	-1.61E-06
34	41.07335	-1.09E-06	-1.60E-06
35	43.52496	-1.12E-06	-1.61E-06

Frequency (Hz)	Centrifugal force (N)	Strain 3 (ϵ)	Strain 4 (ϵ)
36	46.04763	-1.15E-06	-1.63E-06
37	48.64136	-1.19E-06	-1.67E-06
38	51.30615	-1.24E-06	-1.71E-06
39	54.04201	-1.30E-06	-1.77E-06
40	56.84892	-1.37E-06	-1.84E-06
41	59.7269	-1.45E-06	-1.91E-06
42	62.67594	-1.54E-06	-2.00E-06
43	65.69603	-1.64E-06	-2.10E-06
44	68.78719	-1.75E-06	-2.21E-06
45	71.94942	-1.87E-06	-2.33E-06
46	75.1827	-2.01E-06	-2.47E-06
47	78.48704	-2.16E-06	-2.62E-06
48	81.86245	-2.33E-06	-2.80E-06
49	85.30891	-2.52E-06	-2.98E-06
50	88.82644	-2.73E-06	-3.20E-06
51	92.41503	-2.97E-06	-3.43E-06
52	96.07468	-3.24E-06	-3.70E-06
53	99.80539	-3.55E-06	-4.00E-06
54	103.6072	-3.90E-06	-4.34E-06
55	107.48	-4.30E-06	-4.73E-06
56	111.4239	-4.77E-06	-5.17E-06
57	115.4388	-5.30E-06	-5.68E-06
58	119.5249	-5.94E-06	-6.28E-06
59	123.6819	-6.69E-06	-6.99E-06
60	127.9101	-7.58E-06	-7.82E-06
61	132.2093	-8.68E-06	-8.84E-06

Table H.6: Harmonic analysis for numerical model for case 3

Frequency (Hz)	Centrifugal force (N)	Strain 3 (ϵ)	Strain 4 (ϵ)
9	2.877977	-2.23E-08	-9.95E-09
10	3.553058	-2.09E-08	-5.02E-09
11	4.2992	-1.85E-08	1.95E-09
12	5.116403	-1.47E-08	1.17E-08
13	6.004667	-8.78E-09	2.54E-08
14	6.963993	1.14E-10	4.43E-08
15	7.99438	1.33E-08	7.05E-08
16	9.095827	3.27E-08	1.07E-07
17	10.26834	6.16E-08	1.60E-07
18	11.51191	1.06E-07	2.38E-07
19	12.82654	1.75E-07	3.57E-07
20	14.21223	2.93E-07	5.55E-07
21	15.66898	5.15E-07	9.22E-07
22	17.1968	1.05E-06	1.79E-06
23	18.79567	3.52E-06	5.77E-06
24	20.46561	-5.67E-06	-8.97E-06
25	22.20661	-2.03E-06	-3.11E-06
26	24.01867	-1.42E-06	-2.11E-06
27	25.90179	-1.18E-06	-1.71E-06
28	27.85597	-1.07E-06	-1.51E-06
29	29.88121	-1.01E-06	-1.40E-06
30	31.97752	-9.92E-07	-1.34E-06
31	34.14488	-9.92E-07	-1.31E-06
32	36.38331	-1.01E-06	-1.31E-06
33	38.6928	-1.03E-06	-1.31E-06
34	41.07335	-1.07E-06	-1.34E-06
35	43.52496	-1.12E-06	-1.37E-06

Frequency (Hz)	Centrifugal force (N)	Strain 3 (ϵ)	Strain 4 (ϵ)
36	46.04763	-1.18E-06	-1.41E-06
37	48.64136	-1.25E-06	-1.46E-06
38	51.30615	-1.33E-06	-1.53E-06
39	54.04201	-1.42E-06	-1.60E-06
40	56.84892	-1.52E-06	-1.68E-06
41	59.7269	-1.64E-06	-1.78E-06
42	62.67594	-1.78E-06	-1.89E-06
43	65.69603	-1.94E-06	-2.01E-06
44	68.78719	-2.12E-06	-2.15E-06
45	71.94942	-2.33E-06	-2.31E-06
46	75.1827	-2.58E-06	-2.50E-06
47	78.48704	-2.87E-06	-2.71E-06
48	81.86245	-3.22E-06	-2.97E-06
49	85.30891	-3.64E-06	-3.27E-06
50	88.82644	-4.16E-06	-3.64E-06
51	92.41503	-4.82E-06	-4.10E-06
52	96.07468	-5.68E-06	-4.68E-06
53	99.80539	-6.83E-06	-5.45E-06
54	103.6072	-8.47E-06	-6.53E-06
55	107.48	-1.10E-05	-8.15E-06
56	111.4239	-1.52E-05	-1.09E-05
57	115.4388	-2.43E-05	-1.66E-05
58	119.5249	-5.58E-05	-3.63E-05
59	123.6819	2.35E-04	1.45E-04
60	127.9101	3.92E-05	2.28E-05
61	132.2093	2.18E-05	1.19E-05

APPENDIX I

MatLab script

This appendix presents the Matlab scripts used to develop the optimization script presented in Chapter 6. All files are presented separately.

I.1 Optimization-script-ANSYS.m

```

tic
%For the current settings, the runtime is 10 minutes (so just 1 block, and
%the given boundary conditions for fmincon)
%function handle (to tell matlab what is a variable and what is a
%parameter: x is a variable)
freqref = [2.63 ; 17.20 ; 46.40];

%initialize point
x0 = [0.5; 0.8; 65600];

%set boundary conditions for the parameters
% dmin =< dblocks <= dmax
% lmin =< lsupport <= lmax
dmin = 0.3;
dmax = 0.5;
lmin = 0.7;
lmax = 0.9;
stiffmin = 65600;
stiffmax = 65700;
minblocks = 1;
maxblocks = 3;

x = zeros(3,maxblocks);
fval = zeros(1,maxblocks);

for i=minblocks:1:maxblocks
%Stop searching if there does not exist a feasible point.
    if i*dmin >= lmax
        fprintf('\n There does not exist a feasible point anymore \n')
        break
    end
%parameters=(distance between blocks, lenght support)
fun=@(par) norm(freqref-Ansys(par(1),par(2),par(3),i));

%Add constraints parameters such that Ansys works properly (i*d-l<=0)
A = [ i -1 0];
b = 0;

%print for which number of blocks the algorithm is searching an optimum
fprintf('\n the algorithm looks for optimum with %d blocks \n',i);

%minimize difference of the model response with respect to measurement, as
%a function of inputs
[x(:,i),fval(i)] = fmincon(fun,x0,A,b,[],[],[dmin;lmin;stiffmin],[dmax;lmax;stiffmax]);
end

[minerror position] = min(fval);
xmin = x(:,position);
optblocks = minblocks +(position-1);

fprintf(' the optimal distance is %.3f m
\n the optimal lenght of support is %.3f m
\n the optimal stiffness is %.1f
\n the amount of blocks is %d
\n the corresponding error is %.3f
\n',xmin(1),xmin(2),xmin(3),optblocks,sqrt(fval(i)));

toc

```


I.2 ParameterAnsys.m

```

function []=parametersAnsys(distance, nrblocks,lsupport,springstiffness)
%%
% This functions overwrites the 'Right_ansys_model.mac' file such that the
% distance between the blocks, the nr of blocks, the length of the support
% and the springstiffness in the file are given by input of this function.

%In order to do this, it first reads an already existing .mac file. If the
%lines where the parameters in this file are different than assumed in this
%function, things will go wrong.

%%
fid = fopen('parameter.inp','r');
i = 1;
tline = fgetl(fid);
A{i} = tline;
while ischar(tline)
    i = i+1;
    tline = fgetl(fid);
    A{i} = tline;
end
fclose(fid);
% Change cell A
formatSpec = 'k1=%f !Stiffness of springs (N/m)';
formatSpec0 = 'Ls=%f !Length of the support';
formatSpec1 = 'd2=%f';
formatSpec2 = 'n2=%d !Number of blocks';

A{13} = sprintf(formatSpec, springstiffness);
A{7} = sprintf(formatSpec0, lsupport);
A{17} = sprintf(formatSpec1,distance);
A{20} = sprintf(formatSpec2,nrblocks);
% Write cell A into txt

fid = fopen('parameter.inp', 'w');
for i = 1:numel(A)
    if A{i+1} == -1
        fprintf(fid,'%s', A{i});
        break
    else
        fprintf(fid,'%s\n', A{i});
    end
end
end
end

```

I.3 Ansys.m

```

function [freqAnsys]=Ansys(distance, lsupport,springstiffness, nrblocks)
%%
% This function lets Ansys run with the distance, length of the support,
% spring stiffness and the nr of blocks given as an input.

% The functin parametersAnsys writes the parameters in the inputfile for
% Ansys.
%%

%compute the number of blocks that fit on within the length of the support
%nrblocks = floor(lsupport/distance);

%write input to an input file
parametersAnsys(distance,nrblocks,lsupport,springstiffness);

%run ansys (read the file, make calculation, write output file with value)
dos('LAUNCH.BAT');

freqAnsys=table2array(importRESPONS);

end

```

I.4 LAUNCH.BAT

```
!Run ansys within Matlab
SET KMP_STACKSIZE=4096K & "C:\Program Files\ANSYS Inc\v211\ansys\bin\winx64\ANSYS211.exe"
-b -i Right_ansys_model.mac -o PRE.txt
```

I.5 Export.mac

```
!Export resonance frequencies to txt

*GET,f1,MODE,1,FREQ
*GET,f2,MODE,2,FREQ
*GET,f3,MODE,3,FREQ

/OUTPUT, 'C:\Users\20202632\OneDrive - TU Eindhoven\Documenten\TUE\Master SED\Afstuderen
\Matlab\Optimization\RESPONS', 'm',
*VWRITE,f1,f2,f3,
(F)

/OUTPUT, 'C:\Users\20202632\OneDrive - TU Eindhoven\Documenten\TUE\Master SED\Afstuderen
\Matlab\Optimization\POST', 'txt'
```